43564

PERMISSION TO MICROFILM — AUTORISATION DE MICROFILMER

● Please print, or type — Écrire en lettres moulées ou dactylographier

Full Name of Author — Nom complet de l'auteur

Adam Szyjewicz

Date of Birth — Date de naissance
March 1, 1951

Country of Birth — Lieu de naissance
Poland

Permanent Address — Résidence fixe

Dept. of Physics, Univ of Saskatchewan, Saskatoon, Sask
S7N 0W0

Title of Thesis — Titre de la thèse

A Relativistic Calculation of Proton-Proton Bremsstrahlung

University — Université

University of Alberta

Degree for which thesis was presented — Grade pour lequel cette thèse fut présentée
Ph.d

Year this degree conferred — Année d'obtention de ce grade
1979

Name of Supervisor — Nom du directeur de thèse
Dr. A. N. Kamal

Date
Nov. 22, 1979

Signature
Adam

NL-91 (4/77)

NOTICE

AVIS

The quality of this microfiche is heavily dependent upon the quality of the original thesis submitted for microfilming. Every effort has been made to ensure the highest quality of reproduction possible.

If pages are missing, contact the university which granted the degree.

Some pages may have indistinct print especially if the original pages were typed with a poor typewriter ribbon or if the university sent us a poor photocopy.

Previously copyrighted materials (journal articles, published tests, etc.) are not filmed.

Reproduction in full or in part of this film is governed by the Canadian Copyright Act, R.S.C. 1970, c. C-30. Please read the authorization forms which accompany this thesis.

La qualité de cette microfiche dépend grandement de la qualité de la thèse soumise au microfilmage. Nous avons tout fait pour assurer une qualité supérieure de reproduction.

S'il manque des pages, veuillez communiquer avec l'université qui a conféré le grade.

La qualité d'impression de certaines pages peut laisser à désirer, surtout si les pages originales ont été dactylographiées à l'aide d'un ruban usé ou si l'université nous a fait parvenir une photocopie de mauvaise qualité.

Les documents qui font déjà l'objet d'un droit d'auteur (articles de revue, examens publiés, etc.) ne sont pas microfilmés.

La reproduction, même partielle, de ce microfilm est soumise à la Loi canadienne sur le droit d'auteur, SRC 1970, c. C-30. Veuillez prendre connaissance des formules d'autorisation qui accompagnent cette thèse.

THE UNIVERSITY OF ALBERTA

A RELATIVISTIC CALCULATION OF

PROTON-PROTON BREMSSTRAHLUNG

by

(C) ADAM SZYJEWICZ

A THESIS

SUBMITTED TO THE FACULTY OF GRADUATED STUDIES AND RESEARCH

IN PARTIAL FULFILMENT OF THE REQUIREMENTS FOR THE DEGREE

OF DOCTOR OF PHILOSOPHY

DEPARTMENT OF PHYSICS

EDMONTON, ALBERTA

FALL, 1979

THE UNIVERSITY OF ALBERTA

FACULTY OF GRADUATE STUDIES AND RESEARCH

The undersigned certify that they have read, and
recommend to the Faculty of Graduate Studies and Research,
for acceptance, a thesis entitled "Relativistic Calculation of
Proton-Proton Bremsstrahlung" by Adam Szyjewicz in partial
fulfilment of the requirements for the degree of Doctor of
Philosophy in Theoretical Physics.

....
Supervisor

....

....

....

....

Date... 11 oct 1979 ....

....
External Examiner

ABSTRACT

A calculation of proton-proton bremsstrahlung is presented that is fully relativistic and gauge invariant. The external-emission part of the amplitude consists of a sum of Born one-boson-exchange terms. Elastic cross-section data are used as input, to constrain the soft-photon behaviour in accordance with the Burnett-Kroll theorem. The problems associated with the non-unitarized one-boson-exchange model are discussed in detail. Internal-emission contributions from ω radiative decay and Δ excitation with π and ρ exchange are added coherently. Computed cross sections are compared with experiments with incident-beam energies 99 MeV and above. The ω radiative-decay contribution is found to be small but not negligible ($\leq 10\%$) for the TRIUMF experiment, and may have to be considered in a careful comparison between potential-model calculations and the experiment. A large discrepancy with the asymmetric-geometry data from the Orsay experiment is noted, similar to that found previously in potential-model calculations. The Δ excitation contributions are included in a comparison with the data from the 730 MeV UCLA experiment.

ACKNOWLEDGMENTS

TABLE OF CONTENTS

LIST OF TABLES

INTRODUCTION

There has been a great deal of work done in the field of nucleon-nucleon bremsstrahlung ($N+N \rightarrow N+N+\gamma$) since the paper of Ashkin and Marshak, published in 1949 [1]. Interest in this reaction stems mainly from the possibility of learning something about the off-shell behaviour of the N-N force. In particular, it is hoped that the reaction can serve as an off-shell testing ground for the various N-N potentials and other models used in the treatment of N-N scattering. Other reactions involving two nucleons and at least one other particle (e.g. pion production) might also serve this purpose, however the case where the third particle is a photon seems to be the simplest, since it avoids the complications of three strongly interacting particles.

We should note that the correct off-shell N-N interaction is important to our understanding of the properties of nuclear matter and of other many-body systems involving nucleons.

The first extensive calculation of proton-proton bremsstrahlung (henceforth abbreviated as $pp\gamma$) was done by Sobel and Cromer [2] in 1963. Soon thereafter, the first experiments were done at Harvard* by Gottschalk, Shlaer, and Wang [4] with 158 MeV incident protons, at Manitoba by Warner [5] with $T_{lab} = 48$ MeV, and at Rochester by Rothe, Koehler, and Thorndike [6] with $T_{lab} = 204$ MeV incident protons.

---

*Bremsstrahlung from collisions of protons on complex nuclei was first observed in 1952 by Wilson [3], who attributed the γ rays to n-p bremsstrahlung. Here we are mainly concerned with bremsstrahlung from protons on targets of free protons.

In the Harvard and Manitoba experiments the directions and energies of the two final-state protons were measured, while the photon was undetected*; such an arrangement is now commonly referred to as Harvard geometry**. Since the $NN\gamma$ system has 5 degrees of freedom - 9 momentum components minus 4 energy-momentum constraints - Harvard geometry once overdetermines each event. In the Rochester experiment, on the other hand, the directions of all three final-state particles and the energies of the protons were measured, thus overdetermining each event three times. Nevertheless the experiments are difficult because of large backgrounds and low counting rates - the $pp\gamma$ cross section is typically 10^{-4} times the p-p elastic cross section.

There have been several experiments performed since the pioneering ones mentioned above. Jovanovich [8] has classified the experiments as first or second generation; the former measure the angles of the protons through collimation in proton telescopes, while the latter use coordinate-measuring proton detectors such as wire chambers, allowing a larger region of phase space to be simultaneously observed. An important problem in the analysis of the data is the correction for finite solid-angle acceptance (the acceptance window) of the detectors. This is less of a problem in the second generation experiments since the acceptance window can be arbitrarily set in the computer program

---

*The Harvard group used a Čerenkov counter, but only to confirm the presence of the bremsstrahlung photons.

**The term "Harvard geometry" is used in a more restrictive sense by some authors. Our usage of this term is the same as that of Liou [7].

when the data are analyzed.

Besides the Rochester experiment there have been three other second generation experiments: the 42 MeV measurements at Manitoba $[9]$ and 200 MeV at Triumf $[10]$, both in the Harvard geometry, and the 730 MeV measurement at UCLA* $[11]$ in the Rochester geometry.

The data from Harvard geometry experiments are usually presented in the form of distributions $d\sigma/d\Omega_3 d\Omega_4 d\theta_\gamma$ $(\mu b/sr^2-r)$ vs θ_γ (where the polar axis is along the incident beam and the subscripts 3, 4, γ refer to the scattered protons and the photon), and integrated cross sections $d\sigma/d\Omega_3 d\Omega_4$ $(\mu b/sr^2)$. The Rochester group presented its data in the form $d\sigma/d\Omega_{cm} d\Omega_\gamma dk$, where $d\Omega_{cm}$ is the solid-angle element of $\vec{p}_3 - \vec{p}_4$ and k is the photon energy - all quantities being given in the center-of-momentum frame. The 730 MeV UCLA data are reported in the lab frame as spectra $d\sigma/d\Omega_3 d\Omega_\gamma dk$ in k.

For a more detailed discussion of the experiments performed so far the reader is referred to two review articles: one by Halbert $[12]$ covers the period up to 1971, the other by Jovanovich $[8]$ covers the period since then till 1978. Table 1.1, compiled from these two papers, is a listing of the $pp\gamma$ experiments performed up to now with beam energy 99 MeV and above.

---

*In this experiment the directions of all three final-state particles and the energy of one of the protons is measured; each event is thus twice overdetermined.

Beam Energy (MeV)	Institution	Publication Dates (first – last)	Ref.
99	McGill Univ.	68 – 70	48
156	Orsay	72	54
158	Harvard Univ.	65 – 67	4
200	TRIUMF	77	10
204	Univ. of Rochester	66 – 67	6
730	UCLA	77	11

Table 1.1 ppγ experiments with beam energy 99 MeV and above (from refs. 8 and 12).

1.1 Potential Model

Most of the calculations have been done in the framework of the potential model. It is hoped that differences in the cross sections predicted with various N-N potentials will be larger than experimental errors, thus allowing us to rule out some of these potentials. Unfortunately, in spite of the number of experiments and calculations this condition has never been sufficiently satisfied. The reasons are a combination of the following factors: 1. experiments have been performed in kinematic regions where model dependence is small; 2. uncertainties due to finite solid-angle detector acceptance; 3. large experimental errors; 4. uncertainties in the predicted cross sections due to the neglect of some corrections, such as relativistic effects, coulomb effect, rescattering terms, gauge terms, meson currents, etc. Another problem is that the existing N-N potentials, such as the Hamada-Johnston [67], Reid [68], Bryan-Scott [69], etc., are not really equivalent on the energy shell. These on-shell differences must somehow be taken into account before purely off-shell differences can be extracted. A common method for this correction (used for example in ref. 13 and 14) has been to consider the ratio of

the cross-section computed with a given potential to the cross-section computed with the same potential in the on-shell approximation (discussed below).

The formulation and pioneering calculations of ppγ using potentials were done by Sobel and Cromer [2]. The formalism starts with the distorted-wave Born-approximation (DWBA) amplitude

$$T_{fi} = \langle \psi_f^{(-)} | V^{(em)} | \psi_i^{(+)} \rangle \tag{1.1}$$

where $\psi^{(+)}(\psi^{(-)})$ is the exact outgoing (incoming) wave function with the nuclear potential, V_N, alone*. V^{em} is usually taken as

$$V^{(em)}(\vec{p},\vec{\sigma}) = e\vec{\epsilon}\cdot\vec{p} + i\frac{\mu}{2}\vec{\sigma}\cdot(\vec{\epsilon}\times\vec{k}) \tag{1.2}$$

where e, μ, and p is the charge, magnetic moment, and momentum of the proton, and $\vec{\epsilon}$ and $\vec{k}$ is the polarization and momentum of the photon. Gauge terms arising from the replacement $\vec{p}\rightarrow\vec{p}-e\vec{A}$ in V_N (whether V_N is implicitly momentum dependent as from orbital angular momentum terms, or explicitly as is the case of the Bryan-Scott potential) have been neglected. Relativistic corrections to V^{em} have been considered by Liou et al [15, 16]. The amplitude then, is given to first order in the electromagnetic interaction and to all Born orders in the strong interaction.

The matrix element (1.1) can be rewritten as

$$T_{fi} = V_{fn}^{(em)} G_n^{(+)} t_{ni} + t_{fn} G_n^{(+)} V_{ni}^{(em)}$$
$$+ \sum_m t_{fn} G_n^{(+)} V_{nm}^{(em)} G_m^{(+)} t_{mi} \tag{1.3}$$

___

*The Coulomb potential - in the case of ppγ - has been neglected in most calculations; it has been considered by Signell and Marker [18] and by Heller and Rich [17].

where $G^{(\pm)} = (E - H_0 \pm i\epsilon)^{-1}$ is the free propagator and $t_{ni} = \langle \phi_n | V_N | \Psi_i^{(\pm)} \rangle$ is the off-energy-shell two-nucleon matrix element. The first term in (1.3) represents nuclear scattering followed by photon emission, the second term represents photon emission followed by nuclear scattering, and the third term is the rescattering (or double scattering) term. These processes are diagrammed in fig. 1. The rescattering term has been included by V.R. Brown [19], Drechsel and Maximon [20], and by Heller and Rich [17].

The multitude of published similar potential-model calculations is partly a result of some serious discrepancies in the early calculations. The cross section predicted by Sobel and Cromer [2] was about four times the experimental value at 158 MeV measured by Gottshalk et al [4a], and ten times the experimental value at 48 MeV measured by Warner [5]. The calculation was done in the lab frame (and in the transverse gauge, $\vec{\epsilon} \cdot \vec{k} = 0$) and neglected the rescattering term. Another calculation was done by Duck and Pearce [21] based on the Sobel and Cromer formulation and using the Tabakin potential [70]. Again the rescattering term was neglected and the transverse gauge was used, but this time the amplitudes were evaluated in the CM frame. The results agreed with experiment at 158 MeV but were small by a factor of three at 50 MeV. Subsequently an error was discovered in the Sobel and Cromer equations. Now the Duck and Pearce calculation agreed qualitatively with both experiments, while the Sobel and Cromer cross sections were approximately correct at 158 MeV but were still a factor of 6 too large at

48 MeV. Also there were problems with Sobel and Cromer's differential cross sections $d\sigma/d\Omega_3 d\Omega_4 d\theta_\gamma$ at 158 MeV; at 48 MeV they predicted a dipole distribution (although Warner did not obtain differential cross sections from his experiment).

This discrepancy was resolved by Signell [22] who derived an analytic expression for the differential cross section, $d\sigma/d\Omega_3 d\Omega_4 d\theta_\gamma$ in the very low incident-energy limit (scattering-length limit). He found in the CM frame an electric-quadrupole contribution from the single scattering terms, while the rescattering term was negligible. In the lab frame, on the other hand, the single scattering terms have a large electric-dipole component but this is cancelled by a large rescattering term. This cancellation takes place in all Born orders (except, of course, the lowest, where the rescattering term does not contribute). In the lab frame then, the rescattering term is large even at low energies, and must be included. Subsequent potential-model calculations were all done in the CM frame.*

1.2 Model-Independent Calculations

Another method of obtaining bremsstrahlung cross sections is to make an approximation such that only the on-shell nucleon-nucleon scattering amplitudes are used. This is what is meant by "model independence": although the on-shell amplitudes may be obtained from a model, the radiative amplitude is to

---

*It is interesting to note that before this error (neglect of the rescattering term in the lab frame) was known, an early UCLA experimental group of Slaus et al [23] measured distributions in θ_γ which, they stated, were in agreement in shape with the lab-frame calculation; i.e., their distributions appear to have the incorrect dipole shape.

some approximation, uniquely specified. . Model-independent calculations are useful for exploring kinematic regions and for checking model calculations. The approximations that have been used are of two types: the two-energy approximation and the soft-photon approximation. We discuss each in turn.

Two-Energy On-Shell Approximation

One of the important results of Sobel and Cromer's analysis $/\overline{2}4\overline{/}$ is the angular-momentum expansion of the off-shell nuclear matrix element, $t_{ni} = \langle \phi_n | V_N | \psi_i^{(+)} \rangle$, in terms of the phase shifts and what they called the "quasiphase parameters". This is entirely analogous to the phase-shift expansion, of Stapp, Ypsilantis, and Metropolis, for the elastic scattering matrix elements. For the uncoupled states* the expansions are

$$t_{ni} = \sum_L (2L+1) \, P_L(\cos\theta) \, e^{i\,\delta_L(p_i)} \, \Delta_L(p_n, p_i) \qquad (1.4a)$$

$$t_{fn} = \sum_L (2L+1) \, P_L(\cos\theta) \, e^{i\,\delta_L(p_f)} \, \Delta_L(p_n, p_f) \qquad (1.4b)$$

Here the matrix element t_{ni} (t_{fn}) is written in the initial (final) nucleon-nucleon CM frame, P_i, P_f, P_n are the CM nucleon momenta, $\delta_L(p)$ is the phase shift,

$$\Delta_L(p_n, p_i) = -m \int_0^\infty j_L(p_n, r) \, V_N(r) \, u_L(p_i, r) \, r \, dr \qquad (1.5)$$

is the quasiphase, and $u_L(p, r)$ is the radial wavefunction with

---

*To avoid the complications of nucleon spins, in these introductory remarks, the coupled states are not considered. The equations including the coupled states and other details are given in the paper by Sobel $/\overline{2}4\overline{/}$.

the usual asymptotic condition:

$$u_L(p,r) \xrightarrow[r \to \infty]{} \sin\left(pr - \frac{L\pi}{2} + \delta_L(p)\right)$$

On the energy shell $p_n = p_i$ in t_{ni} and $p_n = p_f$ in t_{fn}, and the quasiphase is simply

$$\Delta_L(p,p) = \sin \delta_L(p) \qquad\qquad (1.6)$$

Within the framework of the potential model the problem then is to evaluate the integrals (1.5) for the quasiphases. Since the model dependence is all in the quasiphases, it can be investigated by comparing quasiphases evaluated with different potentials, although any model dependence found in this way must be considered as preliminary, since the total matrix element may involve cancellations. Often the quasiphases are divided by their on-shell values (1.6) before the comparison is made, in order to remove on-shell differences. The results are that at incident lab energies less than about 100 MeV the model dependence is small and not likely to be seen in the present experiments.

The two-energy on-shell approximation consists of the replacement of the quasiphases by their on-shell values (the rescattering term being ignored). The nuclear matrix elements, t_{ni} and t_{fn}, then involve only the phase shifts at the momenta p_i and p_f respectively. This approximation has been studied by Signell and Marker [18, 22, 25]. They found it to be accurate at small incident energies, even at small proton exit angles where the photon energies are largest, with the error rising rapidly with increasing incident energies. For example, at 20 MeV and proton exit angles $\theta = 35°$ (coplanar, symmetric

Harvard geometry) they found the error in $d\sigma/d\Omega_3\,d\Omega_4$ to be less than 1%, rising to 10% at 61.7 MeV $\theta = 30°$ and about 15% at 99 MeV $\theta = 30°$. These results discourage us from looking for off-shell effects in experiments performed at low energies.

Finally it should be mentioned that the two-energy approximation is useful for examining the effect of the on-shell differences among the potentials and for correcting for these differences.

Soft-Photon Approximation

The second type of model-independent calculation, the soft-photon approximation, is based on Low's theorem $/26/$. For photons of low energy k, the radiative amplitude has a 1/k singularity (resulting in the well known "infrared catastrophe") and can be expanded in powers of k as

$$T = \frac{T_{-1}}{k} + T_0 + T_1 k + O(k^2).$$ (1.7)

Low's theorem states that the leading two terms in this expansion, T_{-1} and T_0, depend only on the non-radiative amplitudes. The first term, T_{-1}, is proportional to the on-shell amplitude, while T_0 is proportional to the derivatives of this amplitude (with respect to the two invariants of the non-radiative process). The essential part of this theorem, that T_0 is model-independent as well as T_{-1}, is a consequence of gauge invariance. The explicit expressions for the coefficients T_{-1}, T_0 were derived for N-N scattering, by Nyman $/27/$. Nyman's elastic amplitudes are given at the Mandelstam variables $s = [(p_1+p_2)^2 + (p_3+p_4)^2]/2$ and $t = [(p_3-p_1)^2 + (p_4-p_2)^2]/2$. The choice of the on-shell

point has been shown by Fearing $[28]$ to affect the radiative

amplitude only in $O(k)$ or higher*, as long as this on-shell point

has the correct limit as k approaches zero.

In discussing bremsstrahlung it is useful to distinguish

between the external-radiation processes - nucleon-pole terms with

the photon being emitted from an external nucleon line (the single

scattering terms of fig. 1), and internal-radiation processes -

all the others. The latter type are represented in fig 2., and

include the rescattering terms of fig. 1, meson-current terms,

and isobar excitation terms.

With Nyman's choice of the on-shell point, the leading term

in the expansion (1.7) is solely due to external radiation and

is gauge invariant by itself, the 1/k singularity being due to

the nucleon propagator in the radiating leg. The second term, $\tilde{T}_\sigma$,

contains a part from the external processes, which by itself is not

gauge invariant, and a part from internal processes. This internal

part is independent of k^μ and makes the second term gauge invariant

as well.

In the soft-photon approximation the two leading terms in

the k expansion are obtained from the elastic-scattering amp-

litudes while higher-order terms are irrelevant. The cal-

culations were first done by Nyman $[27]$ who used a numerical

representation for the amplitudes to obtain the cross section.

The method has the advantage over the two-energy approximation

of Signell in that it is gauge invariant and fully relativistic,

---

*More precisely, the first two terms in the expansion (1.7) may
individually change with the on-shell point, but their sum must
change only in $O(k)$ or higher.

and is therefore more useful for the higher energy experiments $(T_{lab} > 100$ MeV) which are of most interest to us.

Squaring (1.7) gives the following expansion for $|T|^2$:

$$|T|^2 = \frac{|T_{-1}|^2}{k^2} + \frac{2 Re(T_{-1} T_0^*)}{k} + \left[|T_0|^2 + 2 Re(T_{-1} T_1^*) \right] + O(k) \quad (1.8)$$

The calculation of the first two terms is greatly simplified by a theorem of Burnett and Kroll [29]. They showed (for fermion-boson scattering) that for unpolarized cross sections (i.e. fermion spins unspecified) the leading term is proportional to the non-radiative cross section and the second term is proportionalto the derivatives of the non-radiative cross section. The explicit formula for N-N scattering was derived by Fearing [30], who also obtained a generalization of the Burnett-Kroll theorem for polarized cross sections (i.e. nucleon spins being specified)[28].

The complete model-independent calculation requires the inclusion of the $|T_0|^2$ term in (1.8) as well as the two leading terms discussed above. In certain kinematic regions neglect of this term may even result in negative "cross sections". The importance of the various model-independent terms depends on the incident energy, as discussed by Fearing [31]. We shall return to this later.

1.3 Relativistic Boson-Exchange Model

In this thesis we have computed the $pp\gamma$ cross sections directly from relativistic perturbation theory; the strong interaction was generated by exchanges of mesons. In com-

parison, the potential model has the advantage of treating the strong interaction to all orders but suffers the disadvantage of being non relativistic - and one expects sizable relativistic corrections even at 158 MeV incident lab energy. Furthermore, none of the potential-model calculations is gauge invariant, since, as mentioned before, gauge terms from the momentum-dependent parts of the potential are neglected.

The present calculation is along similar lines to that of Baier, Kühnelt, and Urban [32]. It has the advantage over the potential method of being fully relativistic, gauge invariant and automatically includes processes such as that in fig. 3, which contain a virtual antibaryon in the intermediate state. It also suffers from a serious disadvantage: the strong interaction can only be handled easily in lowest order, inclusion of processes of higher order in the strong interaction is impractical with this method. Unfortunately this difficulty does not appear to have been fully appreciated by Baier et al, with the result that their model fails to conform to the Low's theorem calculation in soft-photon regions; such an agreement is mandatory for all models. This difficulty, and the method we used to handle it, is discussed later in detail.

We have also studied contributions from isobar excitation and meson currents.

CHAPTER 2

KINEMATICS AND PHASE-SPACE CONSIDERATIONS

2.1 Kinematics

We shall write the $pp\gamma$ reaction symbolically as $1 + 2 \to 3 + 4 + \gamma$ where particles 1 and 2 are the beam and target protons respectively, particles 3 and 4 are the scattered protons and γ is the emitted photon. For convenience the photon will also be denoted as particle 5. Define a coordinate system in the lab frame with the z axis along the beam and the **x-z** plane in the horizontal plane. In this system the incident and target protons have energies and momenta $E_1 = m + T_{lab}, \quad \vec{p}_1 = [T_{lab}(2m + T_{lab})]^{1/2} \hat{z},$ $E_2 = m, \quad \vec{p}_2 = 0$. We consider only events in which the two final-state protons emerge on opposite sides of the y-z plane; the proton with a positive x component of momentum is labelled as particle 3, that with a negative x component of momentum as particle 4. In terms of spherical coordinates we have

$$\vec{p}_i = p_i (\sin\theta_i \cos\varphi_i \, \hat{x} + \sin\theta_i \sin\varphi_i \, \hat{y} + \cos\theta_i \hat{z}) \quad i = 3, 4, 5 \quad (2.1)$$

For non-coplanar events the momenta are sometimes given in terms of the Harvard angles $\bar{\theta}_i$, $\bar{\varphi}_i$, defined as follows: $\bar{\theta}_i$ is the angle between the projection of $\vec{p}_i$ onto the horizontal plane and the beam axis, $\bar{\varphi}_i$ is the angle of $\vec{p}_i$ out of the horizontal plane. Normally $\bar{\theta}_\gamma$ is allowed to span the full circle, i.e. $0 \le \bar{\theta}_\gamma \le 2\pi$, with $0 < \bar{\theta}_\gamma < \pi$ for k_x positive; while $\bar{\theta}_3$, $\bar{\theta}_4$ are restricted by the labeling convention to half circles, i.e. $0 \le \bar{\theta}_3, \bar{\theta}_4 \le \pi$. (see fig. 4).

In terms of the Harvard angles the momenta are

$$\vec{P_3} = P_3 \left(\sin\bar{\theta}_3 \cos\bar{\varphi}_3 \, \hat{x} + \sin\bar{\varphi}_3 \, \hat{y} + \cos\bar{\theta}_3 \cos\bar{\varphi}_3 \, \hat{z} \right)$$

$$\vec{P_4} = P_4 \left(-\sin\bar{\theta}_4 \cos\bar{\varphi}_4 \, \hat{x} + \sin\bar{\varphi}_4 \, \hat{y} + \cos\bar{\theta}_4 \cos\bar{\varphi}_4 \, \hat{z} \right) \qquad (2.2)$$

$$\vec{k} = k \left(\sin\bar{\theta}_\gamma \cos\bar{\varphi}_\gamma \, \hat{x} - \sin\bar{\varphi}_\gamma \, \hat{y} + \cos\bar{\theta}_\gamma \cos\bar{\varphi}_\gamma \, \hat{z} \right)$$

The transformation from spherical to Harvard angles can be obtained by equating the components of (2.1) and (2.2). For k we have

$$\sin\bar{\theta}_\gamma \cos\bar{\varphi}_\gamma = \sin\theta_\gamma \cos\varphi_\gamma \qquad (2.3x)$$

$$\sin\bar{\varphi}_\gamma = -\sin\theta_\gamma \sin\varphi_\gamma \qquad (2.3y)$$

$$\cos\bar{\theta}_\gamma \cos\bar{\varphi}_\gamma = \cos\theta_\gamma \qquad (2.3z)$$

therefore

$$\bar{\varphi}_\gamma = \sin^{-1}\left(-\sin\theta_\gamma \sin\varphi_\gamma\right) \qquad -\frac{\pi}{2} \leq \bar{\varphi}_\gamma \leq \frac{\pi}{2}$$

$\bar{\theta}_\gamma = $ polar angle of the vector.

$$(x_1, x_2) = (\cos\theta_\gamma, \sin\theta_\gamma \cos\varphi_\gamma); \qquad (2.4)$$

i.e., $\quad \bar{\theta}_\gamma = \tan^{-1}\left(\tan\theta_\gamma \cos\varphi_\gamma\right)$

taken in the appropriate branch.

Similarly

$$\bar{\varphi}_3 = \sin^{-1}\left(\sin\theta_3 \sin\varphi_3\right) \qquad -\frac{\pi}{2} \leq \bar{\varphi}_3 \leq \frac{\pi}{2}$$

$$\bar{\theta}_3 = \tan^{-1}\left(\tan\theta_3 \cos\theta_3\right) \qquad 0 \leq \bar{\theta}_3 \leq \frac{\pi}{2} \qquad (2.5)$$

and

$$\bar{\varphi}_4 = \sin^{-1}\left(\sin\theta_4 \sin\varphi_4\right) \qquad -\frac{\pi}{2} \leq \bar{\varphi}_4 \leq \frac{\pi}{2}$$

$$\bar{\theta}_4 = \tan^{-1}\left(-\tan\theta_4 \cos\varphi_4\right) \qquad 0 \leq \bar{\theta}_4 \leq \frac{\pi}{2} \qquad (2.6)$$

As a measure of noncoplanarity Gottschalk et al [4] defined the angle $\overline{\Phi} = \frac{1}{2}(\overline{\varphi_3} + \overline{\varphi_4})$; on the other hand Drechsel and Maximon [20], who used spherical coordinates defined the angle $\Phi = \frac{1}{2}[\varphi_3 + (\pi - \varphi_4)]$. When $\theta_3 = \theta_4 = \theta$ these two angles can be simply related as follows: rotate the coordinate system about the beam axis so that $\varphi_3 = \pi - \varphi_4$. Then $\Phi = \varphi_3 = \pi - \varphi_4$ and $\overline{\Phi} = \overline{\varphi_3} = \overline{\varphi_4}$ and from (2.5) we have

$$\sin \overline{\Phi} = \sin \theta \, \sin \Phi \qquad (2.7)$$

Since the quantities involved are invariant under rotation about the beam axis, this equation holds even when $\varphi_3 \neq \pi - \varphi_4$

For a fixed θ_γ the noncoplanarity, $\overline{\Phi}$, has a maximum value allowed by kinematics, $\Phi_{max}(\theta_r)$. When θ_r is unrestricted the noncoplanarity has a maximum, Φ_{max}, at a certain gamma-ray momentum $\vec{k_0}$ with angles $\theta_r = \theta_0$, $\varphi_r = \varphi_0$ – the "limiting gamma ray".

We shall now consider the energy-momentum equations explicitly. In the lab system they are

$$\vec{P_3} + \vec{P_4} + \vec{k} = \vec{P_1} \qquad (2.8)$$

$$E_3 + E_4 + k = E_{tot} \qquad (2.9)$$

where $E_{3,4} = \sqrt{P_{3,4}^2 + m^2}$

$$E_{tot} = 2m + T_{lab}$$

For convenience, in what follows we shall consider the coordinate system defined so that $\varphi_3 = \pi - \varphi_4 = \Phi$. The components of (2.8) in the x, y, z directions respectively are.

$$(p_3 \sin \theta_3 - p_4 \sin \theta_4) \cos \Phi + k \sin \theta_r \cos \varphi_r = 0 \qquad (2.10)$$

$$(p_3 \sin \theta_3 + p_4 \sin \theta_4) \sin \overline{\Phi} + k \sin \theta_r \sin \varphi_r = 0 \qquad (2.11)$$

$$p_3 \cos \theta_3 + p_4 \cos \theta_4 + k \cos \theta_\gamma = p_1 \qquad (2.12)$$

Squaring (2.7) and (2.8) and eliminating φ_γ we get

$$(p_3 \sin \theta_3 - p_4 \sin \theta_4)^2 = k^2 \sin^2 \theta_\gamma - 4 p_3 p_4 \sin \theta_3 \sin \theta_4 \sin^2 \tfrac{\phi}{2} \qquad (2.13)$$

Eqs. (2.9) and (2.12) can be solved for $p_4 = p_4(p_3, \theta_\gamma)$; the result (see appendix A) is

$$p_4 = \begin{cases} -\dfrac{(A^2 - m^2 \cos^2 \theta_\gamma)}{2A \cos \theta_4} & \text{when } \cos^2 \theta_\gamma = \cos^2 \theta_4 \\[2ex] \dfrac{-A \cos \theta_4 + \cos \theta_\gamma \left[A^2 + m^2 (\cos^2 \theta_4 - \cos^2 \theta_\gamma) \right]^{1/2}}{\cos^2 \theta_4 - \cos^2 \theta_\gamma} & \text{when } \cos^2 \theta_\gamma \neq \cos^2 \theta_4 \end{cases} \qquad (2.14)$$

where $A = (E_{tot} - E_3) \cos \theta_\gamma - (p_1 - p_3 \cos \theta_3)$.

Eqs. (2.13), (2.14) and (2.9) can now be combined to give ϕ as a function of p_3 and θ_γ. We have maximized this function numerically with respect to p_3 and θ_γ to obtain $\overline{\phi}_{max}$ and at fixed θ_γ with respect to p_3 to obtain $\overline{\phi}_{max}(\theta_\gamma)$. Table 2.1 shows $\overline{\phi}_{max}$ and the angles θ_γ, φ_γ of the limiting gamma ray for several energies and angles θ_3, θ_4.

When the directions of the final-state protons are specified, the locus of points satisfying the kinematic equations (2.8) and (2.9) depends on one other parameter, which can be taken as the photon's polar angle θ_γ. Since this parameter is periodic, the locii are closed curves; these are normally displayed in the T_4 - T_3 plane. Such plots are commonly used by experimentalists, and their properties are well known*. For

---

*See for example the review paper by Halbert [12].

T_{lab} (MeV)	θ_3	θ_4	Φ_{max}	θ_0	φ_0
66	30	30	6.12	72.4	-90
157	30	30	9.27	63.4	-90
157	40	40	2.41	60.0	-90
200	12	12	46.27	63.0	-90
200	16.3	16.3	30.12	62.7	-90
200	10	18	37.80	62.6	-84.7
200	25	25	15.43	61.4	-90
200	30	30	10.38	60.3	-90
200	35	35	6.25	58.7	-90
200	40	40	2.57	56.3	-90
400	20	20	31.96	52.6	-90

Table 2.1   Maximum noncoplanarity Φ_{max} for several energies, T_{lab}, and angles θ_3, θ_4. θ_0 and φ_0 are the spherical angles of the limiting gamma ray. Labelling is such that $90° < \varphi_4 < 270°$, $-90° < \varphi_3 < 90°$; $\pi - \varphi_4 = \varphi_3$. All angles are in degrees.

example the locii of constant k are the lines $T_3 + T_4 = T_{lab} - k$, hence the $T_4 - T_3$ plots are convenient for locating regions with maximum photon energy. In appendix B we show, for coplanar geometry, that the closed curves are approximately elliptical when $P_1/m \left[\sin(\theta_3 + \theta_4) \right]^{-1} \ll 1$; the ellipses distort even at low energies when $\theta_3 + \theta_4$ is made small.

2.2 Cross-Section Formulas

The (invariant) T matrix is defined by

$$S_{fi} = \delta_{fi} + i (2\pi)^4 \delta^{(4)}(p_3 + p_4 + k - p_1 - p_2)$$

$$\times \left[\frac{1}{(2\pi)^{3/2}} \right]^5 \left[\frac{m^4}{E_1 E_2 E_3 \, 2 |\vec{k}|} \right]^{1/2} T_{fi} \qquad (2.15)$$

According to the prescription given by Bjorken and Drell [33] the differential cross section is

$$d\sigma = \frac{m^4}{(2\pi)^5 |\vec{v}_1 - \vec{v}_2| E_1 E_2} |T_{fi}|^2 \frac{\delta^{(4)}(p_f - p_i) \, d^3 p_3 \, d^3 p_4 \, d^3 k}{2 |\vec{k}| E_3 E_4} \qquad (2.16)$$

where
$$p_f^\mu = (p_3 + p_4 + k)^\mu$$

and
$$p_i^\mu = (p_1 + p_2)^\mu$$

$\vec{v}_1$ and $\vec{v}_2$ are the velocities of the beam and target proton respectively. Eq. (2.16) is the starting point for deriving the expressions for the various phase-space factors we shall require.

Rochester Cross Section

From (2.16) we get

$$d\sigma / d\Omega_3 \, d\Omega_r \, dk = \frac{m^4}{(2\pi)^5 |\vec{v}_1 - \vec{v}_2| E_1 E_2} \int \frac{p_3^2 \, dp_3}{E_3} \int \frac{d^3 p_4}{E_4}$$

$$\times \frac{k^2}{2k} \frac{1}{4} \sum_{spins} |T|^2 \, \delta(E_3 + E_4 + k - E_{tot}) \, \delta^{(3)}(\vec{p}_3 + \vec{p}_4 + \vec{k} - \vec{p}_i) \qquad (2.17)$$

where $\frac{1}{4}\sum_{spins} |T|^2$ represents the sum of $|T_{f_i}|^2$ over final-state

proton spins and photon polarization and the average over

initial-state proton spins. The second delta function in (2.17)

determines $\vec{p}_4$ as

$$\vec{p}_4 = \vec{p}_i - \vec{k} - \vec{p}_3$$

and

$$E_4 = [(\vec{p}_i - \vec{k} - p_3)^2 + m^2]^{1/2} \tag{2.18}$$

$$= [(\vec{p}_i - \vec{k})^2 + p_3^2 - 2 p_3 |\vec{p}_i - \vec{k}| \cos\alpha + m^2]^{1/2}$$

where α is the angle between $\vec{p}_3$ and $\vec{p}_i - \vec{k}$.

We now need to evaluate

$$\int \delta(f(p_3)) \, dp_3$$

with

$$f(p_3) = E_3 + E_4 - k - E_{tot} \tag{2.19}$$

With $E_3 = (p_3^2 + m^2)^{1/2}$ and E_4 given by (2.18) we get

$$df/dp_3 = p_3/E_3 + (p_4 - |\vec{p}_i - \vec{k}| \cos\alpha)/E_4$$

and

$$\int \delta(f(p_3)) \, dp_3 = \int \frac{\delta(f)}{\left|\frac{df}{dp_3}\right|} \, df = \frac{1}{\left|\frac{df}{dp_3}\right|_{f(p_3)=0}}$$

$$= \frac{p_3 E_3 E_4}{\left| p_3^2 (E_3 + E_4) - \vec{p}_3 \cdot (\vec{p}_i - \vec{k}) E_3 \right|} \tag{2.20}$$

It is understood that p_3 is a zero of (2.19).

Putting these results back into (2.17) we obtain

$$\frac{d\sigma}{d\Omega_3 \, d\Omega_\gamma \, dk} = \frac{m^4}{2(2\pi)^5 |\vec{v}_1 - \vec{v}_2| E_1 E_2} \frac{k \, p_3^2 \, \frac{1}{4}\sum_{spins} |T|^2}{\left| p_3^2 (E_3 + E_4) - \vec{p}_3 \cdot (\vec{p}_i - \vec{k}) E_3 \right|} \tag{2.21}$$

The quantity in the denominator in (2.21) can be rewritten

simply in terms of $\vec{p}_4$ as follows:

$$\left| p_3^2 (E_3 + E_4) - \vec{p}_3 \cdot (\vec{p}_i - \vec{k})E_3 \right| = \left| p_3^2 (E_3 + E_4) - \vec{p}_3 \cdot (\vec{p}_3 + \vec{p}_4)E_3 \right| \tag{2.22}$$

$$= \left| p_3^2 E_4 - \vec{p}_3 \cdot \vec{p}_4 E_3 \right|$$

In the lab frame
$$\left.\begin{aligned}
\vec{v}_2 &= 0 \\
\vec{p}_i &= \vec{p}_1 \\
E_2 &= m \\
\vec{v}_1 &= \vec{p}_1 / E_1
\end{aligned}\right\} \tag{2.23}$$

and (2.21) with (2.22) reads

$$\left.\frac{d\sigma}{d\Omega_3 \, d\Omega_r \, dk}\right|_{lab} = \frac{m^3}{2(2\pi)^5 p_1} \frac{k \, p_3^3}{\left| p_3^2 E_4 - \vec{p}_3 \cdot \vec{p}_4 E_3 \right|} \frac{1}{4}\sum_{spins} |T|^2 \tag{2.24}$$

In the center-of-momentum frame
$$\left.\begin{aligned}
\vec{v}_1 &= -\vec{v}_2 = \vec{p}_1 / E_1 \\
E_1 &= E_2 \\
\vec{p}_C &= 0
\end{aligned}\right\} \tag{2.25}$$

and (2.21) reads

$$\left.\frac{d\sigma}{d\Omega_3 \, d\Omega_s \, dk}\right|_{cm} = \frac{m^4}{4(2\pi)^5 p_1 E_1} \frac{k \, p_3^3 \frac{1}{4}\sum_{spins} |T|^2}{\left| p_3^2 (E_3 + E_4) + \vec{p}_3 \cdot \vec{k} \, E_3 \right|} \tag{2.26}$$

In the experiment of Rothe, Koehler, and Thorndike [6] the differential cross sections were given not in terms of θ_3, φ_3, but θ_q, φ_q, the spherical angles of the vector $\vec{q} = \vec{p}_3 - \vec{p}_4$ (in the CM frame). In this case the cross section is [27b].

$$\left.\frac{d\sigma}{d\Omega_q \, d\Omega_r \, dk}\right|_{cm} = \frac{m^2 E_1}{8(2\pi)^5 p_1} \frac{k \, q^3 \frac{1}{4}\sum_{spins} |T|^2}{\left| q^2 (E_3 + E_4) - 2\vec{k} \cdot \vec{q} (E_3 - E_4) \right|} \tag{2.27}$$

Using the coordinates of $\vec{q}$ instead of $\vec{p}_3$ has the advantage that in the soft-photon limit θ_q becomes the usual CM elastic-scattering angle θ_{CM}.

Note that for soft photons the phase-space factors in (2.24), (2.26), (2.27) can be expanded as a power series in k with the leading term of O(k).

Harvard Cross Section

From (2.15) we have in the lab frame

$$\frac{d\sigma}{d\Omega_3\, d\Omega_4\, d\theta_\gamma} = \frac{m^3 \sin\theta_\gamma}{2(2\pi)^5 p_1} \int \delta^{(4)}(p_f - p_i)\, |T_{fi}|^2 \frac{p_3^2\, dp_3\, p_4^2\, dp_4}{E_3\, E_4}\, k\, dk\, d\varphi_\gamma \qquad (2.28)$$

This phase-space integral is evaluated by Drechsel and Maximon [20]; the result is

$$\frac{d\sigma}{d\Omega_3\, d\Omega_4\, d\theta_\gamma} = \frac{m^3}{2(2\pi)^3 p_1} \frac{p_3^2\, p_4^2\, k \sin\theta_\gamma}{E_3\, E_4\, |N|}\, \frac{1}{4}\sum_{spins} |T|^2 \qquad (2.29)$$

where
$$N = (p_4 \sin\theta_4 - p_3 \sin\theta_3)\cos\theta_\gamma\, (\sin(\theta_3 + \theta_4) - v_3 \sin\theta_4 - v_4 \sin\theta_3)$$
$$- k\, (v_3 \sin\theta_4 - v_4 \sin\theta_3) \sin^2\theta_\gamma$$
$$+ 2\sin\theta_3 \sin\theta_4 \sin^2\Phi\, [p_3 \cos\theta_3 - p_4 \cos\theta_4 - (v_3 p_3 - v_4 p_4)\cos\theta_\gamma]$$

It is understood here that the coordinate system is defined so that $\varphi_3 = \pi - \varphi_4 = \Phi$. The phase-space factor in (2.29) is singular when $\Phi = \Phi_{max}(\theta_\gamma)$. This is easy to see for symmetric events, $\theta_3 = \theta_4 = \theta$: $\Phi = \Phi_{max}(\theta_\gamma)$ when $\varphi_\gamma = \frac{3}{2}\pi$, implying (from the symmetry) that $p_3 = p_4$ and hence that N vanishes. Furthermore when $\theta_\gamma = 0$ or π only coplanar events are allowed, hence $\Phi_{max}(0) = \Phi_{max}(\pi) = 0$. For events with $0 < \Phi < \Phi_{max}$ there are no solutions to the kinematics when θ_γ is such that $\Phi_{max}(\theta_\gamma) < \Phi$. For example consider the situation $T_{lab} = 200$ MeV, $\theta_3 = \theta_4 = 16.3°$, $\Phi = 5°$. Fig. 5 is a plot of

$\oint_{max}(\theta_r)$ and shows that $\oint_{max}(\theta_r) = \oint$ at $\theta_r \simeq 6°$ and at $\theta_r \simeq 163°$, hence there are no solutions for $\theta_r < 6°$ and for $\theta_r > 163°$. Because of these two problems — singularily of phase-space factor at the kinematic limits and restricted range of θ_r — Gottschalk et al defined a different angle, ψ_r, that avoids the problems and reduces to θ_r in the coplanar geometry. ψ_r is defined in terms of the limiting gamma ray

$$\vec{k_o} = k_o \sin\theta_o \cos\varphi_o \hat{x} + k_o \sin\theta_o \sin\varphi_o \hat{y} + k_o \cos\theta_o \hat{z} \quad (2.30)$$

in the following way: consider the vector

$$\vec{k}' = \vec{k} - \alpha \vec{k_o} \quad (2.31)$$

where α is a scalar such that $\vec{k}'$ has no y component (this can always be done since $\vec{k_o}$ has a non-zero y component), then ψ_r is the angle between $\vec{k}'$ and the z axis; i.e.,

$$\vec{k}' = k' \sin\psi_r \hat{x} + k' \cos\psi_r \hat{z} \quad (2.32)$$

The angle ψ_r as defined by (2.32) can range from 0 to 2π. (see fig. 6). The components of (2.31) read

$$k' \sin\psi_r = k \sin\theta_r \cos\varphi_r - \alpha k_o \sin\theta_o \cos\varphi_o \quad (2.33x)$$

$$0 = k \sin\theta_r \sin\varphi_r - \alpha k_o \sin\theta_o \sin\varphi_o \quad (2.33y)$$

$$k' \cos\psi_r = k \cos\theta_r - \alpha k_o \cos\theta_o \quad (2.33z)$$

From (2.33y) we have

$$\alpha k_o = (k \sin\theta_r \sin\varphi_r)/(\sin\theta_o \sin\varphi_o)$$

Substituting this into (2.33x), (2.33z) we solve for ψ_r:

$$k'_x = k' \sin\psi_r = k \sin\theta_r (\cos\varphi_r - \sin\varphi_r \cot\varphi_o)$$

$$k'_z = k' \cos\psi_r = k (\cos\theta_r - \sin\theta_r \sin\varphi_r \cot\theta_o \csc\varphi_o) \quad (2.34)$$

ψ_r is the polar angle in the $x_1 - x_2$ plane of the point

$$(x_1, x_2) = (\cos\theta_r - \sin\theta_r \sin\varphi_r \cot\theta_o \csc\varphi_o, \sin\theta_r(\cos\varphi_r - \sin\varphi_r \cot\varphi_o))$$

The phase-space integral of the Harvard cross section, $d\sigma/d\Omega_3 d\Omega_4 d\Psi_r$, is evaluated by Liou and Sobel $\underline{/16/}$ in terms of the Harvard coordinates $\bar{\theta}_i$, $\bar{\Psi}_i$ defined in section 2.1. The result is rather lengthy and can be found in the appendix of their paper; in terms of their factor F, the cross section is given by

$$\frac{d\sigma}{d\Omega_3 d\Omega_4 d\Psi_r} = \frac{m^3}{2(2\pi)^5 p_1} \quad F \quad \frac{1}{4}\sum_{Spins} |T|^2 \tag{2.35}$$

Elastic cross section

We shall also need the differential cross section for elastic N-N scattering. Here

$$S_{fi} = \delta_{fi} + i(2\pi)^4 \delta^{(4)}(p_3+p_4-p_1-p_2)\left(\frac{1}{(2\pi)^{3/2}}\right)^4\left[\frac{m^4}{E_1 E_2 E_3 E_4}\right]^{1/2} T_{fi} \tag{2.36}$$

The notation is the same as before; now $k = 0$.

$$d\sigma = \frac{(2\pi)^4 \delta^{(4)}(p_f - p_i)}{n_1 n_2 v} |T_{fi}|^2 \left[\frac{1}{(2\pi)^{3/2}}\right]^4 \frac{m^4}{E_1 E_2 E_3 E_4} d^3p_3 d^3p_4$$

$$= \frac{1}{(2\pi)^2}\frac{1}{|\vec{v}_1 - \vec{v}_2|}\delta(E_3+E_4-E_1-E_2)|T_{fi}|^2 \frac{m^4}{E_1 E_2 E_3 E_4} d^3p_3$$

therefore

$$d\sigma/d\Omega_3 = \frac{1}{(2\pi)^2}\frac{1}{|\vec{v}_1-\vec{v}_2|}\delta(E_3+E_4-E_1-E_2)|T_{fi}|^2\frac{m^4}{E_1 E_2 E_3 E_4} p_3^2 dp_3 \tag{2.37}$$

In the CM system

$$|\vec{v}_1 - \vec{v}_2| = 2|\vec{P}|/E \qquad \vec{P}_3 = \vec{P}' = -\vec{P}_4$$

$$E_1 = E_2 = E \qquad E_3 = E_4 = E' \qquad d\Omega_3 = d\Omega_{cm}$$

$$\frac{d\sigma}{d\Omega_{cm}} = \frac{1}{(2\pi)^2}\frac{E}{2p}\delta(2E'-2E)|T_{fi}|^2\frac{m^4}{E^2 E'^2} p'^2 dp' \tag{2.38}$$

Integrating over the delta function:

$$\int \delta(2E'-2E)\,p'^2\,dp' = \int \delta\left(2\sqrt{p'^2+m^2}-2E\right)p'^2\,dp'$$

$$= \int \frac{1}{2\,p'/E'}\,\delta(p'-p)\,p'^2\,dp'$$

$$= \tfrac{1}{2}\,p\,E \qquad \text{with } E'=E$$

Putting this result into (2.38) and summing over the spins we get the expression

$$\frac{d\sigma}{d\Omega_{cm}} = \frac{1}{(2\pi)^2}\,\frac{1}{4}\,\frac{m^4}{E^2}\left(\frac{1}{4}\sum_{spins}|T|^2\right). \tag{2.39}$$

Sometimes the invariant $\dfrac{d\sigma}{d(-t)}$ is required, where $t = (p_1 - p_3)^2$ is the invariant momentum transfer. In the CM system

$$t = -4\,p^2\sin^2\frac{\theta_{cm}}{2} = -2\,p^2(1-\cos\theta_{cm}) \tag{2.40}$$

where θ_{CM} is the angle between $\vec{p}\,'$ and $\vec{p}$. Since $d\Omega_{cm}=\sin\theta_{cm}\,d\theta_{cm}\,d\varphi_{cm}$ and because of symmetry with respect to the azimuthal angle

$$\frac{d\sigma}{d\theta_{cm}} = \int \frac{d\sigma}{d\Omega_{cm}}\sin\theta_{cm}\,d\varphi_{cm} = 2\pi\sin\theta_{cm}\,\frac{d\sigma}{d\Omega_{cm}}$$

therefore

$$\frac{d\sigma}{d(-t)} = \frac{1}{2\,p^2\sin\theta_{cm}}\,\frac{d\sigma}{d\theta_{cm}} = \frac{\pi}{p^2}\,\frac{d\sigma}{d\Omega_{cm}} \tag{2.41}$$

Substituting from (2.39) we get

$$\frac{d\sigma}{d(-t)} = \frac{1}{16\pi}\,\frac{m^4}{E^2 p^2}\left(\frac{1}{4}\sum_{spins}|T|^2\right) \tag{2.42}$$

CHAPTER 3

ONE-BOSON-EXCHANGE MODEL CALCULATION —
EXTERNAL EMISSION

3.1 Introduction

In view of the good agreement with experiments reported by Baier, Kühnelt, and Urban $\boxed{32}$ (BKU), we decided to use their method to obtain a basic calculation of ppγ. We could then add other contributions such as those due to meson currents and Δ excitation as refinements to their basic model.

Although we were able to reproduce the results of BKU we found their model to be in gross disagreement with the data of Nefkens et al $\boxed{11}$* and with other calculations at very small photon energies (for e.g. at T_{lab} = 200 MeV $\theta_3 = \theta_4 = 40^{\circ}$) it predicted cross sections that were much too large. The problem was clarified when we applied the same model to elastic N-N scattering: the S-partial wave was found to be in serious error due to the neglect of unitarization.

In our calculation we have attempted to correct for this deficiency by imposing agreement with the soft-photon theorem as a constraint on the model. For the N-N interaction part of the amplitude we use the model of Erkelenz, Holinde, Machleidt (henceforth cited as EHM) $\boxed{34}$ in the Born approximation with

---

*It is true that this experiment is outside the range of the model, because of the large 730 MeV beam energy. However the calculated cross section was about 16 times the measured cross section even at small photon energies, and this problem persisted, though not at the same magnitude, at lower incident energies.

the parameters modified to satisfy the constraint mentioned
above.

3.2 The Model

The OBE amplitude is a sum of external-emission diagrams
with one nucleon leg off mass shell (fig. 7).   The strong
interaction is represented by the lowest order exchange of
pseudoscalar, scalar, and vector mesons with form factors
included at the meson-nucleon vertices.   We have used the EHM
OBE model as a guide to meson parameters; appendix C is a
summary of this model.   For more detailed information the
reader is referred to refs. $\sqrt{34}$, 35, 37$\overline{7}$ and the review article
by Erkelenz $\sqrt{36}\overline{7}$.

In our ppγ calculation we have tried to use the mesons,
couplings, form factors and coupling constants as given by EHM
(table C.1 and eq. C.3).   However since we did not iterate
our N-N T matrix through the Lippmann-Schwinger equation, as
EHM did, modifications had to be made to restore the fit to
the N-N data.   We used the criterion that the ppγ cross section
must have the correct soft-photon behaviour.   A necessary con-
dition then, according to the Burnett-Kroll theorem (section
1.2), is that the model predict the correct elastic cross
section and its derivatives.   This condition was satisfied by
modifying the form-factor parameters (the cutoffs) and by
multiplying the ppγ cross sections by a correction factor,
R_c, equal to the ratio of the experimental elastic cross
section to the computed elastic cross section at the on-shell
point $(\bar{s}, \bar{t})$ with

$$\bar{s} = \left[(p_1 + p_2)^2 + (p_3 + p_4)^2 \right] / 2$$

$$\bar{t} = \left[(p_3 - p_1)^2 + (p_4 - p_2)^2 \right] / 2 \qquad (3.1)$$

The corresponding $\bar{T}_{lab}$ and $\bar{\Theta}_{CM}$ are

$$\bar{T}_{lab} = \frac{\bar{s} - 4m^2}{2m}$$

$$\bar{\Theta}_{cm} = 2 \sin^{-1} \left(\frac{-\bar{t}}{2m \, \bar{T}_{lab}} \right) \qquad (3.2)$$

We found that as long as $100 \text{ MeV} < T_{lab} < 730 \text{ MeV}$ and Θ_{CM} was not too close to the Coulomb peak, the computed elastic cross sections had approximately the correct dependence on Θ_{CM}. The correction factor, therefore, can only have a weak dependence on Θ_{CM} and it is sufficient to evaluate R_c at a single Θ_{CM}. We tabulated R_c at $\Theta_{CM} = 60^\circ$ at several energies from 9.69 MeV to 730.5 MeV; the correction factor at any energy was then obtained through interpolation. The result is plotted in fig. 8. The slight waves in this graph are artifacts of the cubic-spline interpolation*. The cross sections were computed with the T matrix given by eqs. (C.4) and (C.5). The parameters used are those of table C.1 with the exception of cutoffs, which are
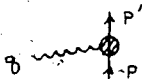
$$\left. \begin{array}{l} \Lambda_\pi = \Lambda_\eta = \Lambda_\delta = 1250 \text{ MeV} \\ \Lambda_\sigma = 1000 \text{ MeV} \\ \Lambda_P = \Lambda_\omega = \Lambda_\phi = 650 \text{ MeV} \\ \Lambda_v = 2500 \text{ MeV} \end{array} \right\} \qquad (3.3)$$

These are just the cutoffs taken from EHM (table C.1) scaled

---

*Since the points contain statistical uncertainties curve fitting would be more appropriate. Interpolation was used because it is much easier and gives adequate results.

by a factor of 0.5 (with the exception of Λ_v). The scaling

factor was treated as a parameter, determined simply by trial

and error to give the correct dependence of $d\sigma/d\Omega_{cm}$ on Θ_{CM} and

T_{lab}.

The Coulomb interaction was treated approximately and

incompletely by adding a one-photon-exchange diagram with the

"dipole" form factors. The γpp vertex is

$$\gamma^\mu F_1(q^2) + i\,\sigma^{\nu\lambda}q_\lambda\,F_2(q^2) \tag{3.4}$$

where the F_1 and F_2 are defined in terms of the electric and

magnetic form factors

$$G_E(t) = F_1(t) + \frac{t}{2m}F_2(t)$$

and $\qquad G_M(t) = F_1(t) + 2m\,F_2(t) \tag{3.5}$

with G_E and G_M accurately given by [46]

$$G_E(t) = \frac{G_M(t)}{1+\varkappa} = \left(1 - \frac{t}{0.71\ GeV^2}\right)^{-2} \tag{3.6}$$

where $1+\varkappa \simeq 2.79$ is the proton magnetic moment in units of

nuclear magneton.

Fig. 8 shows that for 100 MeV $< T_{lab} <$ 730 MeV and $\Theta_{CM} = 60^\circ$

the model gives a reasonably good dependence on the lab energy.

The distributions in Θ_{CM} at a few energies are shown in fig. 9.

For N-N bremsstrahlung the invariant T matrix was defined

by (2.15). We factor out the polarization vector, $\dot{\varepsilon}^\mu$, of the emitted

photon to obtain a four vector T^μ; i.e.,

$$T = \epsilon_\mu T^\mu \tag{3.7}$$

(For notational simplicity we shall often not distinguish between

a matrix and the matrix element). We use the meson-nucleon

couplings as given in eqs. (C.3). For the sum of the two

diagrams of fig. 10

$$T_\mu^{(\alpha)}(1,2;3,4) = -e\, g_{(\alpha)}^2\, F_{(\alpha)}^2\left((p_4-p_2)^2\right)$$

$$\times \bar{u}_3\left[\Gamma_\mu(p_3+k)\, S(p_3+k)\, M_\nu^{(\alpha,A)} + M_\nu^{(\alpha,A)}\, S(p_1-k)\,\Gamma_\mu(p_1-k)\right] u_1 \qquad (3.8)$$

$$\times \bar{u}_4\, M_s^{(\alpha,B)}\, u_2\quad \Delta_{(\alpha)}^{\nu s}(p_4-p_2)$$

where the index α specifies the meson exchanged; the index $i = 1, \ldots, 4$ in the spinors specifies both the spin and momentum, thus $u_i = u(s_i, p_i)$;

$$S(p) = (\not{p}+m)/(p^2-m^2) \qquad (3.9)$$

is the nucleon propagator; $\Gamma_\mu(p)$ is the photon-emission vertex; $M_\nu^{(\alpha,A)}$ and $M_\nu^{(\alpha,B)}$ are the meson-nucleon vertices at points A and B of fig. 10 respectively; $\Delta_{(\alpha)}^{\nu s}$ is the meson propagator; and $F_\alpha(q^2)$ are the strong interaction form factors defined in table C.1.

For reasons given in section 3.3, in writing down the photon-emission vertex Γ_μ we neglect the fact that one of the nucleon legs is off-mass shell. In this static limit

$$\Gamma_\mu = \gamma_\mu - i\,\sigma_{\mu\nu}\,k^\nu\,\frac{\varkappa}{2m} \qquad (3.10)$$

where $e\varkappa/2m$ is the anomalous part of the proton magnetic moment ($\varkappa \simeq 1.79$).

The meson propagators and meson-proton vertices are given below, in table 3.1, with $q^\mu = (p_4 - p_2)^\mu$

Meson	$M_\nu^{(\alpha,A)}$	$M_\nu^{(\alpha,B)}$	$\Delta_{(\alpha)}^{\nu s}$
scalar	1	1	$\dfrac{1}{q^2 - m^2_{(s)}}$
pseudo-scalar	$i\gamma_5$	$i\gamma_5$	$\dfrac{1}{q^2 - m^2_{(ps)}}$
vector	$\gamma_\nu + i\sigma_{\nu\lambda}q^\lambda\dfrac{f/g}{2m}$	$\gamma_\nu - i\sigma_{\nu\lambda}q^\lambda\dfrac{f/g}{2m}$	$\dfrac{-g^{\nu s}}{q^2 - m^2_{(v)}}$

Table 3.1.   Definition of the meson-proton vertices and the meson propagators used in eq. (3.8).

The gauge term $\dfrac{q^\nu q^s}{q^2 - m^2_{(v)}}$ in the vector-meson propagator does not contribute because it couples to a conserved current.   For example

$$\bar{u}_4 \, M_s^{(v,B)} \, u_2 \, q^s = \bar{u}_4 (\not{p}_4 - \not{p}_2) u_2 = 0$$

since both spinors satisfy the Dirac equation.

The last two diagrams shown in fig. 7 can be obtained from (3.8) by the transformation $s_1 p_1 \leftrightarrow s_2 p_2$, $s_3 p_3 \leftrightarrow s_4 p_4$, while the exchange terms required by the Pauli principle can be obtained from the four diagrams considered above by the transformation $s_3 p_3 \leftrightarrow s_4 p_4$ and a change of sign.   The total T matrix is then

$$T = \epsilon_\mu T^\mu = \epsilon_\mu \sum_\alpha \left[T_{(\alpha)}^\mu(1,2;3,4) \right.$$
$$\left. + T_{(\alpha)}^\mu(2,1;4,3) - T_{(\alpha)}^\mu(1,2;4,3) - T_{(\alpha)}^\mu(2,1;3,4) \right] \quad (3.11)$$

Because of the large number of terms in the amplitude (3.11), the usual trace method of summing $|T|^2$ over the proton spins is not practical. We evaluated the matrix element for each of the 16 proton spin states (and for each μ) numerically and simply summed the mod-squares of these complex numbers. The sum over the photon polarization was done by means of the relation

$$\sum_{\epsilon} (\epsilon^\mu T_\mu)(\epsilon^\nu T_\nu)^* = -T^\mu T_\mu^* \qquad (3.12)$$

To make use of this formula it is necessary that the amplitude be gauge invariant. Then $k^\mu T_\mu = 0$ and

$$(k^0 T^0)(k^0 T^0)^* = (\vec{k} \cdot \vec{T})(\vec{k} \cdot \vec{T})^* \leq \vec{k}^2 \vec{T} \cdot \vec{T}^*$$

Since k^μ is a null vector this means that

$$T^0 T^{0*} \leq \vec{T} \cdot \vec{T}^*$$

i.e., T^μ is a space-like or null vector and the right-hand side of (3.12) will always be a non-negative.

It is easy to show that each of the four terms in (3.11) is individually gauge invariant. For $i = 3,4$; $j = 1,2$

$$k^\mu \bar{u}_i \left[\Gamma_\mu(p_i+k) S(p_i+k) M^{(\omega,A)} + M^{(\omega,A)} S(p_j-k)\Gamma_\mu(p_j-k) \right] u_j$$

$$= \bar{u}_i \left[\slashed{k} \frac{(\slashed{p}_i+\slashed{k}+m)}{2 p_i \cdot k} M^{(\omega,A)} + M^{(\omega,A)} \frac{(\slashed{p}_j - \slashed{k}+m)}{-2 p_j \cdot k} \slashed{k} \right] u_j$$

$$= \bar{u}_i \left[\frac{((-\slashed{p}_i+m)\slashed{k} - 2 p_i \cdot k)}{2 p_i \cdot k} M^{(\omega,A)} + M^{(\omega,A)} \frac{\slashed{k}(-\slashed{p}_j+m) - 2 p_i \cdot k}{-2 p_j \cdot k} \right] u_j$$

$$= \bar{u}_i \left[-M^{(\omega,A)} + M^{(\omega,A)} \right] u_j = 0 \qquad \text{qed}$$

In the above we used the commutation relation for the gamma

matrices $\not{a}\not{b} + \not{b}\not{a} = -2a \cdot b$ and the fact that the spinors satisfy

the Dirac equation $(\not{p}_i - m) u_i = \bar{u}_i (\not{p}_i - m) = 0$.

Note that since $\epsilon^\mu T_\mu$ is an invariant and we do not work

in any particular gauge it makes no difference whether the

matrix element is evaluated in the lab or CM frame (in contrast

to the potential model calculations). Also the gauge condition

$k^\mu T_\mu = 0$ provides a handy numerical check - in particular at

$\theta_\gamma = 0$, since then $k^\mu = (k, 0, 0, k)$ and $T^0 = T^3$.

3.3 Discussion

We shall first discuss the problem of using the off shell

N-N amplitude in Born approximation. As mentioned before, EHM

unitarized the meson-exchange pole terms through the Lippmann-

Schwinger equation. Since we avoided this procedure, we had

to apply corrections in order to restore agreement with the

soft-photon theorem.

To study this problem in more detail in terms of partial

waves we used the simple four-pole N-N model of Arndt, Bryan,

and MacGregor (ABM) $\underline{/38/}$. The four mesons considered were

the π, ρ, ω, and a scalar, $T = 0$ meson of mass of about 400 MeV.

The $L \geq 1$ partial-wave amplitudes were then unitarized geo-

metrically; this amounts, for the uncoupled states, to pro-

jecting the Born amplitudes onto the unitary circle. Two

methods of doing this were used by the authors: 1. taking

the Born amplitude, B_L, as the real part of the unitarized

amplitude - the imaginary part being determined by elastic

unitarity, i.e. $B_L = \sin\delta_L \cos\delta_L$; 2. taking the Born

amplitude as the phase shift, i.e. $B_L = \delta_L$. We should note

that this geometric unitarization is only valid when the model

amplitude is small ($|B_L| \ll \frac{1}{2}$ for uncoupled waves).

In this (ABM) model the coupling constants were obtained

from a fit to N-N data in the energy range from 25 to 350 MeV

by means of the reduced second-derivative matrix of Arndt and

MacGregor $\underline{/39\underline{7}}$.   The $^1S_0$, $^3S_1$, $^3D_1$, and ϵ_1, phase shifts were

excluded from the fit and were treated as free parameters.

For pp scattering then, the model gives the $L \gtrless 1$ phase shifts;

the S wave can be put in from phase-shift analysis in order to

compute observables*.

The authors found the unitarity corrections to be un-

important.   This result was used by Baier, Kühnelt, and Urban

to justify the use of the Born amplitudes in their NN̄ cal-

culation.   The fallacy here is that the S wave was excluded

from consideration by Arndt, Bryan and MacGregor and must be

supplied externally, otherwise the result can be a catastrophic

disagreement with data, as we illustrate below.

Fig. 11 shows the elastic cross sections, $\frac{d\sigma}{d\Omega_{cm}}$,

evaluated at three energies.   The calculations were done by

projecting out the partial waves and summing these according to

the formulas in Stapp, Ypsilantis and Metropolis (SYM) $\underline{/40\underline{7}}$;

the series was continued until the desired accuracy was reached.

The expressions for the OBE partial-wave amplitudes are quite

lengthy, but have been written out in a number of papers (see

---

*Although to minimize the chi-squared one should use the
S wave obtained from the reduced second-derivative fit.

for e.g. refs. 41* and 42). We took the Coulomb scattering
into account by adding the non-relativistic Coulomb amplitude
(as given in SYM); i.e. we set the Coulomb phases in the nuc-
lear part of the total amplitude to zero. This amounts to
neglecting the Coulomb potential in the region of strong inter-
action and is an acceptable approximation here, because we are
mainly interested in the region $T_{lab} > 90$ MeV and Θ_{CM} large
enough that Coulomb scattering is small and we are looking at
effects that are considerably larger. The solid curve in
fig. 11 is the result with no unitarization and with the S wave
taken from the OBE model unmodified. The dashed curve is the
result with the $L \geq 1$ waves geometrically unitarized according
to $B_L = \sin\delta_L \cos\delta_L$ (see appendix E for more details). Both
of these calculations are in gross disagreement with data /71/.
The effect of the unitarization is relatively small and increases
with increasing energy and decreasing scattering angle. As the
energy increases, generally the $L \geq 1$ phase shifts increase and
unitarity corrections become increasingly important. On the
other hand the largest partial waves - the P waves - are odd
functions of cos Θ_{CM} and therefore make a vanishing contribution
as Θ_{CM} approaches $90°$.

Fig. 12 shows differential cross sections computed at the
same three energies, but this time the S wave was put in from
phase-shift analysis (according to $\alpha_o = e^{i\delta(^1S_o)} \sin\delta(^1S_o)$).

---

*Eqs. (A.7c) and (A.7d) in this paper contain a typographical
error: the expressions should not be multiplied by $2J + 1$ (as
they are), rather they should be divided by this factor.

The solid curve is the result with $\not{L} \geq 1$ unitarized as above, while the dashed curve is the result with no unitarization (except the S wave which was unitary). This time the agreement with experiments is much better and the unitarization makes a small improvement at the higher energies. The remaining, relatively small discrepancy can be attributed to the approximation in the handling of the Coulomb scattering and errors in the input of the S wave.

The above study demonstrates that the problem lies in the S wave, which the unmodified meson-pole model gives incorrectly*. This, of course, is not surprising since the S waves are known to be outside the scope of the meson-pole model. We should also point out that the problem gets worse with increasing energy, for unlike the true S wave amplitude, which goes through zero at $T_{lab} \simeq 250$ MeV, the model S wave increases with energy and continues to dominate the total amplitude. In the OBE model of EHM the S wave is corrected partly by adjusting the cutoffs in their form factors, but mainly by unitarizing through the Lippmann-Schwinger equation. Thus, unitarity corrections are small when the S wave is excluded - as in the ABM model, but are very important when applied to the total amplitude - as in the EHM model.

We shall now make a few remarks about the previous OBE $NN\gamma$ calculation of Baier, Kühnelt and Urban $\underline{/32\_7}$, since the authors appear not to have fully appreciated the problem

---

*This was confirmed by examining the partial-wave amplitudes and the phase shifts.

discussed above.   Their statement, that the S-wave phase shifts

(of the ABM model) are within two or three standard deviations

of the tabulated values, is incorrect, because the S-wave phase

shifts that ABM refer to are those from the reduced second-

derivative matrix $[76]$; i.e., it is not a model phase shift, rather

it is that S-wave phase shift which along with the model phase

shifts gives the best fit to the data.

It is not surprising, therefore, that Baier et al found

gross disagreement when using a number of N-N OBE models coupling

constants.   When used in Born approximation these models should

give the correct $L \geq 1$ partial waves but, unpredictable S waves.

Baier et al used the coupling constants from the model of ABM,

but made small corrections to these to improve the agreement of

their photon angular distributions with experiment.   However,

we found the elastic cross sections and the partial-wave

amplitudes to be quite sensitive to these variations in the

coupling constants.   Fig. 13 shows the effect of the changes

in the partial-wave amplitudes.   The dashed-dotted curves in

fig. 12 are the elastic cross sections evaluated with the

modified coupling constants* - compare these with the cross

sections from unmodified coupling constants (solid curve in

fig. 11).   We find that the cross sections are much improved

by these changes, although they are still not satisfactory.

---

*These curves were computed directly from the
relativistic Born amplitudes without partial wave decomposition.
The Coulomb scattering was included by adding photon-exchange
diagrams with form factors as given in (3.1), (3.2), (3.3).

We can thus understand the improvement in the radiative cross sections in terms of the corresponding improvement in the predicted elastic cross sections.

Any model used in NNγ calculation must have the correct soft-photon behaviour given by Low's theorem (the principle of model independence). In view of the Burnett-Kroll theorem this means that the model must first predict correct elastic cross sections and their derivatives (with respect to s and t). This requirement is clearly not satisfied by the uncorrected meson-pole model, as we have seen. The correction used in the present calculation consists of using on-shell data to modify the form factors and to normalize the radiative cross sections as outlined in section 3.2. It should be pointed out that the choice of the on-shell point (as given by (3.1) and (3.2)) at which we obtain the normalization factor is arbitrary, since there is no unique on-shell point for the expansion (1.7). Fortunately this is not usually important for two reasons: 1. as long as the choice of the on-shell point (s,t) satisfies continuity requirements (such as, that (s,t) lie within the rectangle $s \in [(p_1 + p_2)^2, (p_3 + p_4)^2]$, $t \in [(p_3 - p_1)^2, (p_4 - p_2)^2]$, it can affect $|T_{pp\gamma}|^2$ only in $O(k^0)*$ although it affects the first two terms in the expansion (1.8) individually, it makes no difference to their sum to $O(k^{-1})$) $[28]$; 2. we confine most of our calculations to the region where R_c is

---

*It is because of this property that the Low theorem can be applied unambiguously (i.e., there is on ambiguity to two orders in k).

a fairly flat function of T_{lab}. Hence, for soft photons the choice of our on-shell point will not affect results throughout the energy range, but when terms of $O(k^0)$ can be important we must ensure that the kinetic energy corresponding to $s = (p_3 + p_4)^2$ is greater than about 90 MeV.

A remark is in order with respect to the form factors, $F_\alpha(q^2)$ (table C.1 with parameters given by (3.3)). These now carry part of the burden of correcting for the use of the Born approximation in treating the strong interaction and are much more strongly damping. Thus they can no longer be regarded as the true strong-interaction form factors. In the case of the vector mesons the cutoffs are smaller than the meson masses, hence the $F_v(q^2)$ are undefined on the meson pole. Note also that the forms of $F_v(q^2)$ used by EHM are probably not realistic to begin with even with their parameters, since the values of the 'coupling constants', $g_v F_v (m_v^2)$, are unrealistically large.

Photon-Emission Vertex

With one nucleon leg off mass shell the most general form of the vertex Γ_μ, diagrammed in fig.14, contains two form factors and can be written in the form /44/

$$\bar{u}(p) \, \Gamma_\mu \, (p' = p + k) = \bar{u}(p) \left\{ \gamma_\mu - i \, \sigma_{\mu\nu} k^\nu \right.$$

$$\left. \times \left[F_2^+(p'^2) \frac{p'+m}{2m} + F_2^-(p'^2) \frac{p'-m}{2m} \right] \right\} \tag{3.13}$$

In the limit as $p' \to p = m$ the vertex, Γ_μ, becomes

$$\gamma_\mu - i \, \sigma_{\mu\nu} k^\nu \frac{\varkappa}{2m} \tag{3.14}$$

where $\dfrac{ex}{2m}$ is the anomalous proton magnetic moment. The form factors in (3.13), therefore, have the mass-shell limits

$$F_2^+ (m^2) = x$$
$$F_2^- (m^2) = \lambda^- \qquad\qquad (3.15)$$

λ^- is a constant defined by (3.15). Note that the form of the nucleon propagator given by (3.9) follows from the Ward identity

$$\bar{u}(p)\, S^{-1}(p') = (p'-p)^\mu \bar{u}(p)\, \Gamma_\mu \quad (p' = p+k) \qquad (3.16)$$

and eq. (3.13) for the form of $\bar{u}(p)\, \Gamma_\mu(p')$.

Nyman $\underline{/44\underline{/}}$ derived the form factors from their dispersion relations $\underline{/45\underline{/}}$ with the assumption of threshold dominance*, and used them in his soft-photon approximation to investigate the effect on the bremsstrahlung cross section. He found that whereas the θ_r distributions are little affected by variations in the form factors, the integrals, $\dfrac{d\sigma}{d\Omega_3\, d\Omega_4}$, are quite sensitive. This is not surprising since it is known that with the static electromagnetic vertex, the anomalous-moment terms give a fairly flat photon-angular distribution, whereas the charge terms are responsible for the quadrupole humps Furthermore, the error in $\dfrac{d\sigma}{d\Omega_3\, d\Omega_4}$ due to an incorrect form factor can be much larger than the discrepancy between a calculation with the static vertex and experiment. Thus, until the form factors are determined from measurements it is not deemed safe to use those obtained from simple assumptions (such

---

*The functions $F_2^\pm (W^2)$ develop imaginary parts above pion-production threshold; i.e. when $W \geq m + m_\pi$.

as threshold dominance) in $pp\gamma$ calculations. For this reason

we use the static vertex (3.10).

The Coulomb Effect

The proper treatment would require the inclusion of a

large number of diagrams, to order e^3 , as shown in fig. 15.

Furthermore, the Coulomb effect has been studied by Signell

and Marker $\underline{/18\underline{7}}$ and by Heller and Rich $\underline{/17\underline{7}}$ and they found the

pure Coulomb bremsstrahlung (corresponding to the first diagram

of fig. 15) to be only a small part of the total Coulomb effect.

Nevertheless we included the one-photon exchange simply because

we already had the machinery to handle vector-boson exchange.

CHAPTER 4

A CONTRIBUTION FROM ω RADIATIVE DECAY [73]

4.1 Introduction

In this chapter we consider the contribution of the ω radiative-decay process (fig. 16) to the $pp\gamma$ cross section. This is an internal-radiation process and is of $O(k)$ in the soft-photon limit. The vanishing of this contribution as $k \to 0$ can be understood in terms of the effect the characteristic length of the radiating system has on its efficiency. In the case of the external radiation the characteristic length, d, is the distance the radiating nucleon can move with energy imbalance

$$\Delta E = \left[\left(p_3{}^\mu + k^\mu \right)^2 \right]^{1/2} - m$$

$$= m \left(1 + \frac{2 p_3 \cdot k}{m^2} \right)^{1/2} - m$$

$$\simeq \frac{p_3 \cdot k}{m} \doteq k + O\left(\frac{p_3}{m} \right)$$

Thus $d = v \Delta t \sim v \frac{1}{k}$ and becomes increasingly large as $k \to 0$. In internal radiation, on the other hand, the photon is emitted from within the region of the strong interaction, thus the characteristic length is a constant: it is the range of the nuclear force (or for e.g. the pion Compton wavelength). Therefore the internal processes make increasingly less efficient radiators as $k \to 0$ and become negligible in this limit.

Ueda [47] had made a rough estimate of the ρ radiative-decay contribution, and set its upper bound at 2% of the Born terms. We anticipated the ω radiative-decay process to be

42

more important for two reasons: 1) the ωpp coupling is larger than ρpp coupling (SU(3) symmetry with the Okubo-Zweig-Iizuka (OZI) rule and the assumption of pure F-type coupling imply $g_{\omega pp} = 3g_{\rho pp}$); 2) the ω radiative width is larger than the ρ radiative width - 880 ± 50 keV against 35 ± 10 keV. By this argument* the interference from the $\omega-\pi$ process can be expected to be about 15 times that due to $\rho-\pi$ process. If Ueda's estimate of the upper limit is taken seriously then this could be an important contribution. Furthermore the inclusion of the $\omega-\pi^{\circ}-\gamma$ process has been found to be necessary in calculation of neutral pion photoproduction: it is needed to reproduce the $T = \frac{1}{2}$ magnetic dipoles $\underline{/49\underline{/}}$.

In view of the above arguments we have carried out a fully relativistic calculation of the process shown in fig. 16. This calculation, done in momentum space, is presented in section 4.2. A non-relativistic reduction is done in section 4.3.

To ascertain the importance of the relativistic corrections at $T_{lab} = 158$ MeV we have calculated the differential cross section for graph (a) of fig. 16 both relativistically and in the non-relativistic limit. As the T matrix for each graph is individually gauge invariant this is a meaningful comparison.

In section 4.3 we have also derived the space structure of the non-relativistic amplitudes, which shows that the π propagator makes this a long-range process.

---

*An important factor excluded here is the fact that the ω has almost no tensor coupling to the nucleon, while the ρ has ($f_\rho/g_\rho \approx 4$).

4.2 The Matrix Element

We neglect the tensor coupling of the ω, which is generally assumed to be small $\boxed{50}$. The interaction Lagrangian is taken to be

$$\mathcal{L}_{int} = -i\, g_\pi\, \overline{\Psi}_N \gamma_5 \vec{\tau}\cdot\vec{\pi}\, \Psi_N \; -g_\omega\, \overline{\Psi}_N \gamma_\mu \Psi_N\, \omega^\mu \qquad (4.1)$$

The $\omega\pi\gamma$ vertex is parametrized through the $\omega\to\pi^\circ\gamma$ T matrix

$$T_{\omega\pi\gamma} = g_{\omega\pi\gamma}\, \epsilon_{\mu\nu\sigma\rho}\, \epsilon^\mu_{(\omega)}\, \epsilon^\nu_{(\gamma)}\, k^\sigma p^\rho \qquad (4.2)$$

where $\epsilon^\mu_{(\omega)}\left(\epsilon^\nu_{(\gamma)}\right)$ is the ω-meson (photon) polarization vector and $k^\sigma\left(p^\rho\right)$ is the photon (pion) momentum. From (4.2) we get the decay width of the ω as

$$\Gamma(\omega\to\pi^\circ\gamma) = \frac{g^2_{\omega\pi\gamma}}{96\pi}\; \frac{\left(m^2_\omega - m^2_\pi\right)^3}{m^3_\omega} \qquad (4.3)$$

The matrix element for the process shown in fig. 16a is

$$T^{(1a)} = -i\, \epsilon^\rho_{(\gamma)}\, (\overline{u}_3 \gamma_\mu u_1)\, \epsilon_{\nu\sigma\delta\rho}\, (p_1 - p_3)^\sigma$$
$$\times\, (p_4 - p_2)^\delta\, \frac{g^{\mu\nu}}{(p_3-p_1)^2 - m^2_\omega}\; \frac{1}{(p_4-p_2)^2 - m^2_\pi}\, \overline{u}_4 \gamma_5 u_2 \qquad (4.4)$$

(for clarity of notation we do not write the product of the coupling constants $g_\pi\, g_\omega\, g_{\omega\pi\gamma}$). Since

$$k^\rho = (p_1 - p_3)^\rho - (p_4 - p_1)^\rho \qquad (4.5)$$

replacing $\epsilon^\rho_{(\gamma)}$ by k^ρ causes (4.4) to vanish; hence $T^{(1a)}$ is gauge invariant.

Introducing the following notation:

$$D_\omega(i,j) = \left[(p_i - p_j)^2 - m_\omega^2\right]^{-1}$$

$$D_\pi(i,j) = \left[(p_i - p_j)^2 - m_\pi^2\right]^{-1} \qquad \Biggr\} \quad (4.6)$$

$$f_{1\rho} = \gamma^\nu \epsilon_{\nu\sigma\delta\rho} k^\sigma (p_4 - p_2)^\delta$$

we can write

$$T^{(1a)} = (-i)\, \epsilon_{(\gamma)}^P \,(\bar{u}_3 f_{1\rho} u_1)\, D_\omega(1,3)\, D_\pi(2,4)(\bar{u}_4 \gamma_5 u_2) \quad (4.7)$$

Similarly

$$T^{(1b)} = (-i)\, \epsilon_{(\gamma)}^P \,(\bar{u}_4 f_{2\rho} u_2)\, D_\omega(2,4)\, D_\pi(1,3)(\bar{u}_3 \gamma_5 u_1) \quad (4.8)$$

where $\quad f_{2\rho} = \gamma^\nu \epsilon_{\nu\sigma\delta\rho} k^\sigma (p_3 - p_1)^\delta$.

The contributions of the exchange graphs, fig. 16c and 16d, are obtained by the interchange of labels $3 \leftrightarrow 4$ in the expressions (4.7) and (4.8). The complete matrix element is then

$$T_{int} = T^{(1a)} + T^{(1b)} - T^{(1c)} - T^{(1d)} \qquad (4.9)$$

This was evaluated numerically and added to the OBE matrix element as given in section 3.2. The rest of the calculation is the same as in the OBE case.

As a check, the calculation of $\frac{1}{4}\sum_{spins}\sum_{\epsilon} |\epsilon_\mu T_{int}^\mu|^2$, - although tedious - was also done analytically. The two methods gave identical results.

The coupling constants used in the evaluation of T_{int} were

$$\frac{g_\pi^2}{4\pi} = 14.0 \qquad \frac{g_\omega^2}{4\pi} = 5.4 \qquad \frac{g_{\omega\pi\gamma}^2}{4\pi} = 4.87 \times 10^{-2}\, GeV^{-2} \quad (4.10)$$

4.3 Non-Relativistic Reduction and the Coordinate-Space Structure of the Matrix Element

The non-relativistic reduction of the matrix elements (4.7) and (4.8) is done by means of the approximations

$$\bar{u}_i \, \gamma_\mu \, u_j \longrightarrow \bar{u}_i \, \gamma_0 \, u_j \simeq \chi_i^+ \, \chi_j$$

$$\bar{u}_i \, \gamma_5 \, u_j \longrightarrow \chi_i^+ \, \vec{\sigma} \cdot \frac{(\vec{P_j} - \vec{P_i})}{2m} \, \chi_j$$

$$\left[(p_3 - p_1)^2 - m_\omega^2 \right]^{-1} \longrightarrow -\left[\vec{q}^2 + m_\omega^2 \right]^{-1} \qquad q^\mu = (p_3 - p_1)^\mu$$

(4.11)

$$\left[(p_4 - p_2)^2 - m_\pi^2 \right]^{-1} \longrightarrow -\left[\vec{p}^2 + m_\pi^2 \right]^{-1} \qquad p^\mu = (p_4 - p_2)^\mu$$

The above replacements yield

$$T_{n.r.}^{(1a)} = i \, \frac{\vec{\varepsilon}}{2m} \cdot (\vec{k} \times \vec{p}) \frac{1}{(\vec{q}^2 + m_\omega^2)(\vec{p}^2 + m_\pi^2)} (\chi_3^+ \chi_1)(\chi_4^+ \vec{\sigma} \cdot \vec{p} \, \chi_2) \qquad (4.12)$$

$$T_{n.r.}^{(1b)} = i \, \frac{\vec{\varepsilon}}{2m} \cdot (\vec{k} \times \vec{p}) \frac{1}{(\vec{q}^2 + m_\omega^2)(\vec{p}^2 + m_\omega^2)} (\chi_4^+ \chi_2)(\chi_3^+ \vec{\sigma} \cdot \vec{q} \, \chi_1) \qquad (4.13)$$

Each of these terms represents a conserved current. In the arguments that follow we consider only the term $T^{(1a)}$. To obtain the non-relativistic cross section we use the identities

$$\sum_{\vec{\varepsilon}} (\vec{\varepsilon} \cdot \vec{A})^2 = \vec{A}^2 - \frac{(\vec{A} \cdot \vec{k})^2}{\vec{k}^2}$$

(4.14)

and $$\sum_{spins} |(\chi_i^+ \vec{\sigma} \cdot \vec{A} \, \chi_j)|^2 = 2 \vec{A}^2$$

for any 3-vector A. We get

$$\frac{1}{4}\sum_{spins}\sum_{\vec{\epsilon}}|T^{(1a)}_{n.r.}|^2 = \frac{(\vec{k}\times\vec{p})^2\,\vec{p}^{\,2}}{4\,m^2\,(\vec{q}^{\,2}+m_\omega^2)^2(\vec{p}^{\,2}+m_\pi^2)^2} \qquad (4.15)$$

The relativistic version of (4.15), derived from (4.7), is

$$\frac{1}{4}\sum_{\substack{spins\\ \epsilon^\mu}}|T^{(1a)}|^{2} = \frac{1}{2\,m^4}\Big[(k\cdot p)((p_3\cdot k)(p_1\cdot p) +$$

$$(p_1\cdot k)(p_3\cdot p)) - p^2(p_1\cdot k)(p_3\cdot k) - m^2(k\cdot p)^2\Big] \qquad (4.16)$$

$$\times \Big[(p_4\cdot p_2)-m^2\Big]\Big[D_\omega(1,3)\,D_\pi(2,4)\Big]^2$$

Eq. (4.15) can also be derived by non-relativistically reducing (4.16). The cross section is obtained by multiplying (4.15) or (4.16) by $(g_\pi\,g_\omega\,g_{\omega\pi\gamma})^2$ x (phase-space factor).

In table 4.1 we show both the relativistic and non-relativistic values of the differential cross section as obtained from $T^{(1a)}$ above. It is clear that at T_{lab} = 158 MeV the relativistic corrections are important

θ. (deg)	Relativistic	Non-relativistic
0	0.54	1.14
30	1.89	3.02
60	1.83	2.88
90	0.83	1.52
120	0.16	0.38
150	0.27	0.00
180	1.03	0.29

Table 4.1. $d\sigma/d\Omega_3\,d\Omega_4\,d\theta_r\,(\mu b/sr^2\,rad)$ at T_{lab} = 1.58 MeV

$(\theta_3=\theta_4=30°)$

Coordinate-Space Structure

Define the coordinates

$$\vec{r} = \vec{r}_1 - \vec{r}_2 \ , \qquad \vec{R} = \tfrac{1}{2}(\vec{r}_1 + \vec{r}_2)$$

$$Q = \tfrac{1}{2}(\vec{P}_1 - \vec{P}_2) , \qquad \vec{P} = \vec{P}_1 + \vec{P}_2 \tag{4.17}$$

and analogous expressions for the primed quantities which refer to the final state coordinates and momenta. The Fourier transform is then defined as [51]

$$T(\vec{r}, \vec{R}, \vec{r}', \vec{R}') = \frac{1}{(2\pi)^9} \int e^{i\vec{P}'\cdot\vec{R}' + i\vec{Q}'\cdot\vec{r}'} \ T(\vec{P}, \vec{Q}; \vec{P}', \vec{Q}')$$
$$\times \ \delta^{(3)}(\vec{P} - \vec{P}' - \vec{k}) \ e^{-i\vec{P}\cdot\vec{R} - i\vec{Q}\cdot\vec{r}} \ d^3P \ d^3Q \ d^3P' d^3Q' \tag{4.18}$$

Inserting $T^{(1a)}_{n.r.}$ for $T(\vec{P}, \vec{Q}; \vec{P}', \vec{Q}')$ from (4.12) one gets

$$T^{(1a)}(\vec{r}, \vec{R}, \vec{r}', \vec{R}') = e^{-i\vec{k}\cdot\vec{R}} \ \delta^{(3)}(\vec{R} - \vec{R}')$$
$$\times \ \delta^{(3)}(\vec{r} - \vec{r}') \ T^{(1a)}(\vec{r}) \tag{4.19}$$

where

$$T^{(1a)}(r) = -i\frac{\vec{\epsilon}}{2m}\cdot\left[\vec{k}\times\left(\vec{\nabla}_{\vec{r}} + \tfrac{1}{2}i\vec{k}\right)\right](\chi_3^+\chi_1)$$
$$\times \left[(\chi_4^+\vec{\sigma}\chi_2)\cdot\left(\vec{\nabla}_{\vec{r}} + \tfrac{1}{2}i\vec{k}\right)\right]I(\vec{r}, \vec{k}) \tag{4.20}$$

where

$$I(\vec{r}, \vec{k}) = \frac{1}{(2\pi)^3}\int \frac{d^3\ell \ e^{-i\vec{\ell}\cdot\vec{r}}}{\left[(\vec{\ell} + \tfrac{1}{2}\vec{k})^2 + m_\pi^2\right]\left[(\vec{\ell} - \tfrac{1}{2}\vec{k})^2 + m_\omega^2\right]} \tag{4.21}$$

For low-energy photons ($k\to 0$)

$$T^{(1a)}(r) = -i\frac{\vec{\epsilon}}{2m}\cdot(\vec{k}\times\vec{\nabla}_{\vec{r}})(\chi_3^+\chi_1)\left[(\chi_4^+\vec{\sigma}\chi_2)\cdot\vec{\nabla}_{\vec{r}}\right]I(r, 0) \tag{4.22}$$

where

$$I(r, 0) = \frac{1}{4\pi(m_\omega^2 - m_\pi^2)}\left(\frac{e^{-m_\pi r}}{r} - \frac{e^{-m_\omega r}}{r}\right) \tag{4.23}$$

The coordinate space expression for $T^{(1b)}$ is obtained by the simple replacement $\vec{\sigma}_1 \rightarrow \vec{\sigma}_2$. Clearly the amplitude has a short-range part and a long-range tail. At $r = 0$, $I(r,0) = 1/(4\pi)(m_\omega + m_\pi)$. Thus the large mass of ω does indeed suppress the overall contribution of this internal-radiation process.

4.4 A Discussion on the Coupling Constants

First, we point out that in the calculation of the OBE contribution we were constrained to using the parameters of the EHM model (albeit with some modifications as discussed previously) in order to not disturb the fit to the elastic data. This was not the case in the other contributions we considered: here we were free to use the known neutral-meson masses, and coupling constants consistent with physical principles and experiments. For example, we disagree with the constraint imposed by EHM on their vector meson-nucleon coupling constants that $g_\rho^2 : g_\phi^2 : g_\omega^2 = 1 : \frac{9}{2} : 9$. We do not expect the ϕ, which is a pure $\lambda\bar{\lambda}$ state in the ideal nonet-mixing scheme, to couple to protons, which have no strange quark content. This is the statement of the OZI rule $\underline{/52/}$. We shall now examine the constraints imposed on the coupling constants by vector-meson dominance (VMD) and unitary symmetry.

Consider the coupling of the nucleon to the electromagnetic field as in fig. 17a. The invariant amplitude (from the Dirac coupling alone) for this diagram can be generally written as

$$\epsilon_\mu^{(r)} \bar{N}(p') \gamma^\mu e \left[F_1^s(0) + \tau_3 F_1^v(0) \right] N(p) \qquad (4.24)$$

where $F_1^s(q^2)$ and $F_1^v(q^2)$ are the isoscalar and isovector charge

form factors $(F_1^S(0) = F_1^V(0) = \frac{1}{2})$. If we assume the isoscalar part of fig. 17a to be dominated by ω and ϕ exchange, and the isovector by ρ exchange (fig. 17b) the amplitude is

$$\epsilon_\mu^{(r)} \bar{N}(p') \gamma^\mu \left[\frac{e\,m_\omega^2}{2\gamma_\omega} \frac{g_\omega}{m_\omega^2 - g^2} + \frac{e\,m_\phi^2}{2\gamma_\phi} \frac{g_\phi}{m_\phi^2 - g^2} + \tau_3 \frac{e\,m_\rho^2}{2\gamma_\rho} \frac{g_\rho}{m_\rho^2 - g^2} \right]_{g^2 = 0} N(p) \tag{4.25}$$

where $\dfrac{e\,m_V^2}{2\gamma_V}$ $(V = \omega, \phi, \rho^0)$ is the V-γ coupling constant. Comparison of (4.24) and (4.25) gives the constraint

$$\left. \begin{aligned} \frac{g_\omega}{\gamma_\omega} + \frac{g_\phi}{\gamma_\phi} &= 1 \\[2mm] \frac{g_\rho}{\gamma_\rho} &= 1 \end{aligned} \right\} \tag{4.26}$$

thus VMD makes no statement on g_ω or g_ϕ separately. We shall now look at the SU(3) constraints.

The SU(3) structure of the electromagnetic current in fig. 17 is

$$J_{e.m.} = \sum_{i,j} \bar{B}_i \left(f_{3ij} + \frac{1}{\sqrt{3}} f_{8ij} \right) B_j \tag{4.27}$$

(f_{kij} are the SU(3) antisymmetric structure constants) since it must transform like $Q = F_3 + \frac{1}{\sqrt{3}} F_8$. Comparison of (4.27) with that due to the general SU(3) invariant F-type $\bar{B}BV$ coupling, $\sum_{i,j,k} \bar{B}_i f_{kij} B_j V_k$, shows that the photon couples only to the combination

$$\rho^0 + \frac{1}{\sqrt{3}} \omega_8 \tag{4.28}$$

where $\omega_8 (\omega_0)$ is the octet (singlet) isoscalar. If we assume ideal ω-ϕ mixing

$$\phi = \sqrt{\tfrac{2}{3}} \, \omega_8 - \sqrt{\tfrac{1}{3}} \, \omega_0$$

$$\omega = \sqrt{\tfrac{1}{3}} \, \omega_8 + \sqrt{\tfrac{2}{3}} \, \omega_0$$

OR

$$\omega_8 = \sqrt{\tfrac{2}{3}} \, \phi + \sqrt{\tfrac{1}{3}} \, \omega$$

$$\omega_0 = -\sqrt{\tfrac{1}{3}} \, \phi + \sqrt{\tfrac{2}{3}} \, \omega \cdot$$

$$\left. \right\} \qquad (4.29)$$

the combination (4.28) is

$$\rho^0 + \frac{\sqrt{2}}{3} \, \phi + \frac{1}{3} \, \omega \qquad\qquad (4.30)$$

If we ignore the mass splittings (recall the $V\gamma$ coupling constant is $e \, m_V^2 / (2 \gamma_V)$) the three independent $\gamma_\rho, \gamma_\phi, \gamma_\omega$ are reduced to one by the constraint

$$\frac{1}{\gamma_\rho^2} : \frac{1}{\gamma_\phi^2} : \frac{1}{\gamma_\omega^2} = 9 : 2 : 1 \qquad\qquad (4.31)$$

Eqs. (4.31) and (4.26) can now be combined to give

$$g_\omega + g_\phi \sqrt{2} = 3 g_\rho \qquad\qquad (4.32)$$

The OZI rule ($g_\phi = 0$) then gives

$$g_\rho^2 : g_\phi^2 : g_\omega^2 = 1 : 0 : 9 \qquad\qquad (4.33)$$

This constraint can be generalized to allow for both f- and d- type coupling of the meson octet to the baryon octet as follows. The general SU(3) invariant $\overline{B} \gamma^\mu B \, V_\mu$ coupling of the meson nonet to the baryons is

$$\mathcal{L} = \sum_{i,j=1}^{8} g_\rho \left[\alpha \, d_{mij} \, \overline{B}_i (i \gamma_\mu) B_j V_m^\mu + (1-\alpha)(-i \, f_{mij}) \right.$$

$$\left. \times \overline{B}_i (i \gamma_\mu) B_j V_m^\mu \right] + \sum_{i=1}^{8} g_0 \, \overline{B}_i (i \gamma_\mu) B_i V_\mu^0 \qquad\qquad (4.34)$$

$$= g_\rho \left(\frac{3 - 4\alpha}{\sqrt{3}} \right) \overline{P} P \, \omega_8 + g_0 \, \overline{P} P \, \omega_0 + \text{ other terms}$$

With the $\omega-\phi$ mixing as given by (4.32) this is

$$\mathcal{L} = \left[g_\rho \sqrt{2} \frac{(3-4\alpha)}{3} - g_0 \sqrt{\frac{1}{3}} \right] \bar{P} P \phi$$

$$+ \left[g_\rho \frac{(3-4\alpha)}{3} + g_0 \sqrt{\frac{2}{3}} \right] \bar{P} P \omega \qquad (4.35)$$

We can read off g_ϕ and g_ω from (4.35); setting $g_\phi = 0$ gives

$$g_0 = g_\rho \sqrt{\frac{2}{3}} (3 - 4\alpha)$$

$$g_\omega = (3 - 4\alpha) g_\rho \qquad (4.36)$$

which reduces to (4.33) when $\alpha = 0$. Note that in this argument we did not use VMD.

Our choice of g^2_ω (4.10) is dictated by the reasoning presented above; $g^2_{\omega\pi\gamma}$ was determined from (4.3) with $\Gamma(\omega \to \pi\gamma)$ = 0.89 MeV $\underline{/53/}$.

CHAPTER 5

RESULTS AND DISCUSSION

The coplanar, symmetric cross sections, $\frac{d\sigma}{d\Omega_3 \, d\Omega_4 \, d\theta_\gamma}$,
at various lab energies and angles θ_3, θ_4 are shown plotted in
figs. 18-34. The curves marked "OBE" are the results of the
OBE-external-emission calculation outlined in chapter 3. We
were not able to fix the sign of the $\omega-\pi^\circ$ amplitude (eq. 4.9)
relative to the OBE, we therefore show the results for both
signs. These are marked "OBE $\pm$ internal" in the figures. The
cross sections were calculated at 10° intervals in θ_γ; the
curves were then drawn by interpolation*.

Fig. 19 shows a comparison with the preliminary results of
the Triumf experiment of Beveridge et al $\underline{/\,10\,\underline{/}}$ and two other
calculations: a Hamada-Johnston potential calculation of
Bohannon (marked "HJ") and a soft-photon approximation calculation
of Fearing (marked "SPA"). The experimental and the two sets of
calculated points were adapted from fig. 6 of ref. 31**. The
differences among the calculations are still too small relative
to the experimental errors. The SPA is almost consistently
low, while the HJ calculation is high; however part of this
difference is probably due to relativistic corrections not model

---

*Since all observables are generally differentiable functions in θ_γ they must have a zero slope at $\theta_\gamma = 0$ and 180° in the symmetric geometry. As can be seen in the figures this requirement was sometimes not met by the interpolation procedure.

**The OBE calculation shown in this figure did not include the correction described in chapter 3.

dependence.   Relativistic corrections, as discussed by Liou and

Sobel $\underline{/16\_7}$, lower the cross section and are largest at forward

and backward angles.   A comparison of the OBE and the SPA cal-

culation provides a better indicator of model dependence since

both are fully relativistic.   It appears unlikely a definite

conclusion regarding potentials will be made on the basis of

this experiment.   Fig. 37 is a plot of the off-shell parameters

$[(p_1-k)^2-m^2]/m^2$, $[(p_2-k)^2-m^2]/m^2$, $[(p_3+k)^2-m^2]/m^2$, $[(p_4+k)^2-m^2]/m^2$

and the photon energy, k, as a function of Θ_γ .   It shows that

the virtual nucleon is farther off-mass shell at the forward and

backward angles - the region where the largest model dependence

is observed.   On the other hand the photon-energy distribution,

$k(\Theta_\gamma)$, does not appear to be a useful indicator of where (in

Θ_γ) model dependence should be observed.   The problem here is

that we do not know how the higher order terms in the k expansion

depend on Θ_γ to be able to predict their importance - even when

we know the photon energy.

The ω radiative-decay contribution (labelled "internal" in

fig. 19) is not negligible for this experiment: it is largest

in the forward and backward photon directions (about 10% at the

forward direction).   We are thus faced with having to include

meson-current correction as well as rescattering, Coulomb effect

and relativistic corrections before meaningful comparisons can be

made between potential-model calculations and the experiment.

Should experiments be performed at larger energies and

smaller proton angles the meson-current corrections will be even

larger. At $T_{lab} = 400$ MeV, $\theta_3 \doteq \theta_4 = 12°$ (fig. 15) the $\omega-\pi°$

contribution is about 27% in the forward photon direction and 23%

in the backward photon direction; the effect on the integrated

cross section $d\sigma/d\Omega_3 d\Omega_4$ is 18%, as can be seen in table 5.1.

Fig. 29 shows that at 158 MeV $\theta_3 = \theta_4 = 30°$ the $\omega-\pi°$ con-

tribution is a fraction of the size of the error bars; for

$\theta \geq 35°$ ($T_{lab} = 158$ MeV) it is negligible. This behaviour is

expected since the photon energy, k, decreases with increasing

proton angle θ and the $\omega-\pi°$ amplitude is of $O(k)$ in the soft-

photon limit.

The 99 MeV calculations (figs. 31 and 33 and table 5.1)

are actually beyond the range of this model and should not be

taken seriously. The maximum values of $\bar{T}_{lab}$, as computed from

$\bar{s} = \frac{1}{2}\left[(p_1 + p_2)^2 + (p_3 + p_4)^2\right]$, are 71.3, 63.6 and 58.4 MeV for

$\theta = 35°$, $30°$ and $25°$ respectively. Recall that the present OBE

model is not valid when $\bar{T}_{lab} < 100$ MeV. What the calculations

of figs. 14 and 16 show is that the one-photon-exchange con-

tribution is indeed negligible as observed previously by Heller

and Rich $\underline{/17/}$ and Signell and Marker $\underline{/18/}$.

In figs. 21 to 28 we present a study of the various con-

tributions to the 200 MeV $\theta = 16.3°$ calculation. Figs. 21 and

22 show how each contribution affects the coherent sum, while

fig. 23-28 show the distributions due to each contribution

individually. We observe that the scalar-meson exchange

enhances the cross section, particularly at the peaks of the

quadrupole humps, while the vector mesons reduce the cross

section. The general enhancement at the backward photon

direction is due to the phase-space factor, which has a minimum at $\theta_\gamma \simeq 70^\circ$.

We get a better understanding of the shape of these distributions from fig. 34, which shows the contributions from the Dirac ("$\varkappa_p = 0$" curve) and anomalous-magnetic moment (" $\varkappa_p$ term" curve) coupling of the photon to the radiating proton. The Dirac term contains a charge and magnetic-moment part while the anomalous term contains only a magnetic-moment part. We find that the main contribution is due to the magnetic-moment amplitude, which is roughly isotropic. The charge amplitude still gives rise to the quadrupole distribution, but this is not large enough to be seen in the total distribution.

Finally, we come to the comparison of our calculation with the results from Orsay [54]. This is one of the two experiments where cross-section data were obtained at small and unequal proton exit angles θ_3 and θ_4. The discrepancy with previous calculations has been discussed by a number of authors [8, 17, 55, 56]. It has been suggested (by Jovanovich [17]) that this experiment possibly indicates a failure of the Hamada-Johnston potential off-energy shell. However our calculation (figs. 35 and 36) was done in a completely different way and yet we find essentially the same discrepancy. Furthermore, we find that this cannot be accounted for by the ω-π° current correction or relativistic corrections*. Jovanovich [17] has suggested that the 42 MeV

---

*Relativistic corrections in the context of this experiment have also been discussed by Celenza et al [55].

Manitoba experiment shows the same type of discrepancy at small

and unequal proton angles.   The Orsay results thus remain as an

enigma.

T_{lab} (MeV)	θ_3, θ_4 (deg)	Present work			SPA [27]	Hamada-Johnston Potential [19]	Experiment
		OBE	OBE +internal	OBE -internal			
99	25	4.19					3.77 ± 0.23** [48b]
	30	5.94				≈5.0*	5.14 ± 0.22** [48b]
	35	8.96				≈7.3*	9.0 ± 0.3** [48b]
	40	19.8				≈17*	18.8 ± 1.2** [48b]
156	15, 18	4.05	3.96	4.17			
	15, 21	4.28	4.21	4.40			
	15, 24	4.40	4.33	4.50			
	15, 27	4.41	4.35	4.50			
158	30	8.71	8.65	8.84	7.9	9.15	10.2 ± 1.7 [4c]
							7.9 ± 1.6 [4b]
	35	12.7			11.8	13.2	14.7 ± 2.5 [4c]
							12.4 ± 2.5 [4b]
	40	32.5				33.0	23.8 ± 4.8 [4b]
200	12	3.42	3.25	3.66			
	16.3	4.85	4.66	5.13			
	25	8.38	8.21	8.69			
	30	11.6			10.0	12.1	13.0 ± 2.4 [6]
	35	17.1			15.3	17.5	14.0 ± 2.7 [6]
	40	46.4	46.3	46.5		49.1	29.0 ± 6.0 [6]
400	12	10.7	9.09	13.1			

Table 5.1 Integrated cross sections $d\sigma/d\Omega_3 \, d\Omega_4$ $(\mu b/sr^2)$.

"OBE" is the present one-boson-exchange external-emission calculation.

"OBE ± internal" includes the ω radiative-decay contribution

(chapter 4), coherently added with either relative sign. "SPA" is the soft-photon-approximation calculation of Nyman [27].

* Estimated from figs. 13 and 14 of ref. 19.
** Additional normalization factor of 1 ± 0.02 to be applied.

CHAPTER 6

A CONTRIBUTION FROM Δ EXCITATION

6.1 Introduction

In this chapter we consider the simplest radiative processes involving Δ excitation with π and ρ exchange (fig. 38). This contribution is of particular interest at the larger incident energy of 730 MeV of the UCLA experiment [11], where in certain kinematic situations it can dominate the cross section. Recently, Tiator, Weber, and Drechsel [63] published the results of a calculation in which the above mentioned Δ graphs were added incoherently to the first term of the Low expansion. In the present work these Δ graphs are added coherently to the OBE model of chapter 3 and the results are compared with the UCLA data. We find the interference terms to be very important, and when they are included some of the conclusions made in [63] need to be modified.

To estimate, a priori, the importance of this process we evaluated the four-momenta-squared of the virtual baryon: $(p_1 - k)^2$, $(p_2 - k)^2$, $(p_3 + k)^2$, $(p_4 + k)^2$. At $T_{lab} = 200$ MeV, $\theta_3 = \theta_4 = 12^o$, the smallest and largest value of these invariants is 0.64 GeV^2 and 1.06 GeV^2. The on-shell value is $m^2 = 0.88$ GeV^2. Compared with $m_\Delta^2 = 1.52$ GeV^2 the off-shell excursions are not large, therefore we expect the nucleon-pole terms to dominate. On the other hand at $T_{lab} = 730$ MeV, $\theta_3 = 67^o$, $\varphi_3 = -1.09^o$, $\theta_\gamma = 50.5^o$, $\varphi_\gamma = 180^o$ (G7 geometry of the UCLA experiment [11]) the smallest and largest value of the

invariants is .52 GeV^2 and 1.27 GeV^2. The largest value is now somewhat closer to m_Δ^2. We therefore expected that the Δ contribution may be significant at the energy of the UCLA experiment.

6.2 The Matrix Element

$\Delta N\pi$ Vertex and Δ Propagator

The most general charge independent $\Delta N\pi$ interaction can be written [57]

$$\mathcal{L}_{\Delta N\pi} = g^* \, \overline{\Psi}_\Delta^\mu \, \vec{T} \, \theta_{\mu\nu} \, \Psi_N \, \partial^\nu \vec{\phi}_\pi \;\; + h.c. \tag{6.1}$$

where $\quad \theta_{\mu\nu} = g_{\mu\nu} + \left[\tfrac{1}{2}(1+4Z)A + Z\right]\gamma_\mu \gamma_\nu$,

A, Z are complex constants,

$\vec{T}$ are 4 x 2 matrices in isospin space analogous to the τ matrices in $NN\pi$ coupling,

$$\Psi_\Delta^\mu = \begin{bmatrix} \Delta^{++} \\ \Delta^+ \\ \Delta^0 \\ \Delta^- \end{bmatrix}^\mu \quad \text{and} \quad \Psi_N = \begin{bmatrix} p \\ n \end{bmatrix}.$$

The explicit isospin structure can be obtained by forming the invariant

$$\sum_{t^* t} \overline{\Psi}_\Delta(t^*) \left\langle 1 \tfrac{1}{2} \, m \, t \,\big|\, \tfrac{3}{2} \, t^* \right\rangle \Psi_N(t) \, \phi(m) \tag{6.2}$$

The $\phi(m)$, m = +1, 0, -1, are annihilation operators of the π^m; in terms of the cartesian fields ϕ_i, they are

$$\phi(m) = \vec{\epsilon}(m) \cdot \vec{\phi}$$

where

$$\vec{\epsilon}(+1) = \tfrac{1}{\sqrt{2}}(-1, i, 0) \tag{6.3}$$
$$\vec{\epsilon}(-1) = \tfrac{1}{\sqrt{2}}(i, i, 0)$$
$$\vec{\epsilon}(0) = (0, 0, 1)$$

The $\vec{T}$ matrices can now be read off from (6.2) (up to an overall real constant*):

$$\vec{T}_{t^* t} = -\left\langle 1\, \tfrac{1}{2}\, m\, t \,\Big|\, \tfrac{3}{2}\, t^* \right\rangle \vec{\epsilon}(m)$$

$$-\vec{T}_{t^* t} =$$

$t^* \backslash t$	$\tfrac{1}{2}$	$-\tfrac{1}{2}$
$\tfrac{3}{2}$	$\vec{\epsilon}(+1)$	0
$\tfrac{1}{2}$	$\vec{\epsilon}(0)\sqrt{\tfrac{2}{3}}$	$\vec{\epsilon}(+1)\tfrac{1}{\sqrt{3}}$
$-\tfrac{1}{2}$	$\vec{\epsilon}(-1)\tfrac{1}{\sqrt{3}}$	$\vec{\epsilon}(0)\sqrt{\tfrac{2}{3}}$
$-\tfrac{3}{2}$	0	$\vec{\epsilon}(-1)$

(6.4)

The coupling (6.1) is commonly and conveniently written in terms of doublets $\bar{N}^*_i = \bar{\psi}_\Delta T_i$ (or $N^*_i = T_i^+ \psi_\Delta$). According to (6.4) they are

$$N^*_1 = \frac{1}{\sqrt{2}} \begin{pmatrix} \Delta^{++} - \Delta^\circ/\sqrt{3} \\ \Delta^+/\sqrt{3} - \Delta^- \end{pmatrix}$$

$$N^*_2 = \frac{i}{\sqrt{2}} \begin{pmatrix} \Delta^{++} + \Delta^\circ/\sqrt{3} \\ \Delta^+/\sqrt{3} + \Delta^- \end{pmatrix} \qquad (6.5)$$

$$N^*_3 = -\sqrt{\frac{2}{3}} \begin{pmatrix} \Delta^+ \\ \Delta^\circ \end{pmatrix}$$

The general spin 3/2 propagator is a sum of the Rarita-Schwinger propagator $\underline{/72\_7}$ and a non-pole term that depends on the parameter A, defined above $\underline{/57\_7}$; this term vanishes when A = -1. The total Lagrangian (free-field part plus interaction) is found to be invariant under the point transformation

---

*The minus sign in (6.4) with the Condon and Shortly sign convention used here results in the doublets, N^*_i (6.5), as given in the literature.

$$\psi'^{\mu}_{\Delta} = \psi^{\mu}_{\Delta} + a\,\gamma^{\mu}\gamma_{\lambda}\,\psi^{\lambda}_{\Delta}$$

$$A' = (A - 2a^{*})/(1 + 4a^{*})$$

$$\psi'_{N} = \psi_{N}$$ (6.6)

$$\phi'_{\pi} = \phi_{\pi}$$

The S matrix is therefore independent of A; without loss of generality we took A = -1 to get the simplest $\triangle$ propagator:

$$S_{\rho\nu}(p^{*}) = \frac{1}{3}\,\frac{\not{p}^{*} + m_{\Delta}}{p^{*2} - m^{2}_{\Delta}}\left[-g_{\rho\nu} - \gamma_{\nu}\gamma_{\rho} + \frac{1}{m_{\Delta}}\left(\gamma_{\rho}\,p^{*}_{\nu} - \gamma_{\nu}\,p^{*}_{\rho}\right) + \frac{2}{m^{2}_{\Delta}}\,p^{*}_{\rho}\,p^{*}_{\nu}\right]$$ (6.7)

To take the width of the $\triangle$ into account and to remove the $p^{*2} = m^{2}_{\Delta}$ singularity we made the replacement in the above propagator:

$$\frac{1}{p^{*2} - m^{2}_{\Delta}} \longrightarrow \frac{1}{p^{*2} - m^{2}_{\Delta} + i\,m_{\Delta}\,\Gamma\,f(p^{*2})}$$ (6.8)

where $$f(p^{*}) = \left(\frac{p^{*2} - \Lambda}{m^{2}_{\Delta} - \Lambda}\right)^{\frac{1}{2}}$$

$$\Lambda = (\text{threshold value of } p^{*2} \text{ for the decay}$$
$$\triangle \rightarrow N\pi) = (m + m_{\pi})^{2}$$

Γ is the $\triangle$ width = 115 MeV

Olsson, Turner and Osypowski $\underline{/57/}$ found from their analysis of πN scattering that Z must lie in the range $-0.8 \le Z \le 0$. Olsson and Osypowski $\underline{/58/}$ further restricted Z by comparing with a multipole analysis of pion photoproduction in the $\triangle$-resonance region: they concluded that $Z = 0 \pm \frac{1}{4}$. We have nevertheless used $Z = -\frac{1}{2}$ since, along with A = -1, it

considerably simplifies the $\triangle N\pi$ interaction; i.e. we have used

$$\mathcal{L}_{\triangle N\pi} = g^* \left(\bar{N}_i^{*\mu} N \, \partial_\mu \pi_i + \bar{N} N_i^{*\mu} \, \partial_\mu \pi_i \right)$$

(6.9)

For the case of $\triangle^+ p\,\pi^\circ$ coupling this reads

$$\mathcal{L}_{\triangle^+ p\pi^\circ} = -g^* \sqrt{\tfrac{2}{3}} \left(\bar{\psi}^\mu \psi \, \partial_\mu \phi_\pi + \bar{\psi} \psi^\mu \, \partial_\mu \phi_\pi \right)$$

(6.10)

where ψ^μ, ψ, ϕ_π are the $\triangle^+$, proton, and π° fields respectively.

We can now write the matrix elements corresponding to diagrams I and II of fig. 39:

$$\phi_\pi(x) = \frac{1}{\sqrt{V}} \int \frac{d^3q}{\sqrt{2\omega_q}} \left(a_q \, e^{-iqx} + a_q^+ \, e^{iqx} \right)$$

thus $\partial_\mu \phi_\pi(x) \longrightarrow -i q_\mu$ in both diagrams and

$$T_I = -g^* \sqrt{\tfrac{2}{3}} \, \bar{u}^\mu(p^*) \, (-i q_\mu) \, u(p)$$

$$T_{II} = -g^* \sqrt{\tfrac{2}{3}} \, \bar{u}(p) \, (-i q_\mu) \, u^\mu(p^*)$$

(6.11)

$\triangle N\gamma$ Vertex

The general, gauge-invariant $\triangle N\gamma$ couplings were investigated by Gourdin and Salin [58]. They showed that for free fields, there are two such couplings:

$$\bar{\psi}_{\triangle\mu} \gamma_\nu \gamma_5 \psi_N F^{\mu\nu} + h.c.$$

and

$$\partial_\nu \bar{\psi}_{\triangle\mu} \gamma_5 \psi_N F^{\mu\nu} + h.c.$$

the first of these producing mainly magnetic transitions, the other primarily electric transitions. From analysis of pion photoproduction experiments it is known that the process

$\gamma p \to \Delta \to N\pi$ is dominated by the magnetic transition*.
We consider only the dominant $\gamma_\nu \gamma_5$ coupling. Olsson and
Osypowski $\underline{/60\underline{7}}$ add an off-shell term to this coupling so that
the total Lagrangian is invariant under the point transformation
defined in (6.6). (This extra term vanishes when the Δ field
is on mass shell). The resultant interaction is

$$\mathscr{L}_{\Delta\gamma N} = -e\, C\, \bar{N}^{*3\mu}\, \Phi_{\mu\nu\lambda}\, N\, F^{\nu\lambda} + h.c. \qquad (6.12)$$

where $\quad F_{\nu\lambda} = \partial_\nu A_\lambda - \partial_\lambda A_\nu \quad ,$

$$\Phi_{\mu\nu\lambda} = \left\{ g_{\mu\nu} + \left[Y + \tfrac{1}{2}(1+4Y)A \right] \gamma_\mu \gamma_\nu \right\} \gamma_\lambda \, i\gamma_5 \; ,$$

Y is an arbitrary constant,
and $\quad$ A is the constant defined before, which we set as $A = -1$.
The authors determined, from a comparison with pion-photoproduction
multipole analysis, that $Y = \tfrac{1}{4} \pm \tfrac{1}{4}$. For simplicity we took
$Y = -\tfrac{1}{2}$, the value that along with $A = -1$ removes the off-shell
term in (6.12). For the $\Delta^+ \gamma p$ (6.12) reads

$$\mathscr{L}_{\Delta^+ \gamma p} = e\sqrt{\tfrac{2}{3}}\, C\left[\bar{\Psi}^\mu \gamma^\nu i\gamma_5 \Psi F_{\mu\nu} - \bar{\Psi}\gamma^\nu i\gamma_5 \Psi^\mu F_{\mu\nu} \right] \qquad (6.13)$$

(In the notation of Peccei $\underline{/61\underline{7}}$ $C = \dfrac{\chi^*}{2m}$, where m = nucleon mass).
We can now obtain the matrix elements for diagrams I and II of

---

*For example, the analysis of Berends and Donnachie $\underline{/59\underline{7}}$
suggests that the isospin 3/2, electric-quadrupole amplitude
vanishes near the resonance region. Note that because of parity
and angular-momentum conservation only two multipoles can con-
tribute to $\quad \gamma + N \to \Delta \to \pi + N \quad$: the magnetic dipole M_{1+}^3, and
electric quadrupole E_{1+}^3 (the superscript is twice the total
isospin).

fig. 40: $\qquad A_\mu(x) \sim \epsilon_\mu (a\, e^{-ikx} + a^+ e^{ikx})$

$$\partial_\nu A_\mu \sim i k_\nu \epsilon_\mu (-a\, e^{-ikx} + a^+ e^{ikx})$$

for both diagrams $\quad \partial_\nu A_\mu \longrightarrow i k_\nu \epsilon_\mu$

and $\quad T_I = -e\, C \sqrt{\tfrac{2}{3}}\, \bar{u}(p)\, \gamma^\nu i \gamma_5\, u_\mu(p^*)\, i (k_\mu \epsilon_\nu - k_\nu \epsilon_\mu)$

$$= e\, C \sqrt{\tfrac{2}{3}}\, \bar{u}(p)\, (\not{\epsilon}\, k_\mu - \not{k}\, \epsilon_\mu)\, \gamma_5\, u^\mu(p^*)$$

$$\tag{6.14}$$

$$T_{II} = -e\, C \sqrt{\tfrac{2}{3}}\, \bar{u}^\mu(p^*)\, (\not{\epsilon}\, k_\mu - \not{k}\, \epsilon_\mu)\, \gamma_5\, u(p)$$

$\triangle N\rho$ Vertex

In analogy to the $\triangle N\gamma$ coupling (eq. (6.12) without the off-shell term) we took the $\triangle N\rho$ coupling to be

$$\mathcal{L}_{\triangle N\rho} = -C'\, \bar{\Psi}_{\triangle\mu}\, \vec{T}\, \gamma_\nu i \gamma_5\, \Psi_N\, (\partial^\mu \vec{\rho}^\nu - \partial^\nu \vec{\rho}^\mu) + h.c. \tag{6.15}$$

In particular

$$\mathcal{L}_{\triangle^+ p\rho^0} = \sqrt{\tfrac{2}{3}}\, C' \left[\bar{\Psi}^\mu \gamma^\nu i \gamma_5 \Psi - \bar{\Psi} \gamma^\nu i \gamma_5 \Psi^\mu \right]$$
$$\times (\partial_\mu \rho_\nu - \partial_\nu \rho_\mu) \tag{6.16}$$

We can relate the coupling constant C' to C by assuming vector-meson dominance (VMD).

Consider the coupling of a photon to the $\triangle^+ p$ under the assumption of VMD (fig. 41); note that isospin conservation forbids the ω and ϕ, so that only the ρ^0 is involved. The matrix element for this process, according to (6.16), is

$$T = \sum_{\epsilon_{(P)}} \frac{e\, m_P^2}{2\, \gamma_P}\, \epsilon_{(\gamma)}^{\lambda}\, \epsilon_{(P)\lambda}\, \left(-C'\sqrt{\tfrac{2}{3}}\right)$$

$$\times\, \bar{u}^{\mu}(p^*)\left(\not{\epsilon}_{(P)}\, k_{\mu} - \not{k}\, \epsilon_{(P)\mu}\right)\gamma_5\, u(p) \qquad (6.17)$$

making the replacement

$$\sum_{\epsilon_{(P)}} \epsilon_{(P)\lambda}\, \epsilon_{(P)\nu} = -g_{\lambda\nu} + \frac{k^{\lambda} k^{\nu}}{m_P^2} \qquad (6.18)$$

with $k^2 = 0$ we have

$$T = -\frac{e\, C'}{2\, \gamma_P}\sqrt{\tfrac{2}{3}}\; \bar{u}^{\mu}(p^*)\left(\not{\epsilon}_{(\gamma)}\, k_{\mu} - \not{k}\, \epsilon_{\mu}\right)\gamma_5\, u(p) \qquad (6.19)$$

Comparing (6.19) with T_{II} of (6.14), and using $\gamma_P = g_P$ (eq. 4.26) we get

$$C' = 2\, g_P\, C \qquad (6.20)$$

The Bremsstrahlung Matrix Element

Putting the various pieces together we get the following matrix element for the π-exchange processes shown in fig. 42.

$$T^{\mu}_{(1a)+(1b)} = -\frac{2}{9}\, \frac{e\, C\, g^*\, g_{\pi}\, F^*(q^2)^2}{q^2 - m_{\pi}^2}\, \bar{u}_3\left[\frac{(\gamma^{\mu} k^{\rho} - \not{k}\, g^{\mu\rho})\gamma_5\, S_{\rho\nu}(p_3+k)\, q^{\nu}}{(p_3+k)^2 - m_{\Delta}^2 + i\, m_{\Delta}\, \Gamma\, \not{f}((p_3+k)^2)}\right.$$

$$\left. - \frac{q^{\rho}\, S_{\rho\nu}(p_1-k)(\gamma^{\mu} k^{\nu} - \not{k}\, g^{\nu\mu})\gamma_5}{(p_1-k)^2 - m_{\Delta}^2 + i\, m_{\Delta}\, \Gamma\, \not{f}((p_1-k)^2)}\right]u_1\, (\bar{u}_4\, \gamma_5\, u_2) \qquad (6.21)$$

where

$$S_{\rho\nu}(p^*) = (\not{p}^* + m_{\Delta})\left[-3g_{\rho\nu} + \gamma_{\rho}\gamma_{\nu} + \frac{1}{m_{\Delta}}(\gamma_{\rho}\, p^*_{\nu} - \gamma_{\nu}\, p^*_{\rho}) + \frac{2}{m_{\Delta}^2}\, p^*_{\rho}\, p^*_{\nu}\right]$$

$f(p^{*2})$ is defined in (6.8.)

$F(q^2)$ is a form factor appearing at each vertex involving an exchanged meson. Following [64] and [63] we take the monopole form (the same for each vertex)

$$F(q^2)^2 = \Lambda^2/(\Lambda^2 - q^2) \qquad (6.22)$$

with $\Lambda = 1.5$ GeV^2.

For the ρ-exchange processes the corresponding matrix element is

$$T_{(1a)+(1b)}^{\mu} = \frac{2}{9} e\, C C' g_\rho\, F(q^2)^2\, \bar{u}_3 \Big\{ (\gamma^\mu k^\rho - \slashed{k} g^{\mu\rho})\gamma_5$$

$$\times\ \frac{S_{\rho\nu}(p_3+k)(q^\nu\gamma^\beta - \slashed{q}\, g^{\nu\beta})\gamma_5}{(p_3+k)^2 - m_\Delta^2 + i\, m_\Delta\, \Gamma\, f((p_3+k)^2)}$$

$$+\ \frac{(q^\rho\gamma^\beta - \slashed{q}\, g^{\rho\beta})\gamma_5\, S_{\rho\nu}(p_1-k)(\gamma^\mu k^\nu - \slashed{k} g^{\mu\nu})}{(p_1-k)^2 - m_\Delta^2 + i\, m_\Delta\, \Gamma\, f((p_1-k)^2)} \qquad (6.23)$$

$$\times\ \gamma_5 \Big\}\, u_1\ \bar{u}_4 \Big(\gamma_\beta - i\, \sigma_{\beta\alpha}\, q^\alpha\, \frac{f_\rho/g_\rho}{2m}\Big)\, u_2 \Big(\frac{1}{q^2 - m_\pi^2}\Big)$$

Values of the coupling constants:

$$\frac{g_\pi^2}{4\pi} = 14 \qquad \frac{g_\rho}{4\pi} = 0.6 \qquad f_\rho/g_\rho = 3.7$$

$$\frac{g^{*2}}{4\pi}\,(\Delta N\pi) = 1.875 \times 10^{-5}\ \text{MeV} \qquad \text{from the } \Delta \text{ decay width (appendix F).}$$

$$= 0.352\ m_\pi^{-2} \qquad (\text{with } m_\pi = 137\ \text{MeV.})$$

$$|C|\ (N\Delta\gamma) = 4.33/(2m) \qquad \text{from the multipole analysis of pion photoproduction of Olsson [65].}$$

$$C'\ (N\Delta\rho) = 2\, C\, g_\rho \qquad \text{from the VMD argument given above (6.20).}$$

An important aspect was the determination of the relative signs of these constants, as the interference terms critically

depend on these.   The relative signs are as follows: $g^*g_\pi < 0$ - determined from the quark-model constraint (E.19); $C < 0$ - from the quark-model constraint (G.5); $g_\rho > 0$ ($\mathcal{L}_{NN\rho} = -g_\rho \bar{\Psi} \gamma_\mu \Psi \rho_\mu$ + derivative coupling) - from analogy with $\mathcal{L}_{NN\gamma}$; $C' < 0$ - from the VMD constraint (eq. 6.20). These sign relationships are summarized in fig. 43.

6.3 Results and Discussion

The differential cross sections $d\sigma/d\Omega_3 d\Omega_\gamma dk$ vs k are plotted in figs. 44-49; the results are compared with data from the five photon detectors, G7, G8, G10, G11, and G12 of the 730 MeV UCLA experiment [11].   As expected, for small photon energies, k, the predicted results show a 1/k dependence and are in approximate agreement with the EED calculation of Nefkens et al [11]*.   At larger photon energies our cross sections increase with the photon energy thus showing a minimum at some intermediate k.   This behaviour is qualitatively in agreement with that of the complete soft-photon calculation of Fearing [31]. It should be pointed out that the presence of higher order terms in the expansion in k of the cross section is not necessarily due to off-shell effects.   These may be due to the expansion of the phase-space factor or the momentum variables in the amplitudes. Indeed, the phase-space factor is singular at the maximum kinematically allowed k.

The above applies to the OBE calculation with and without

---

*The 'external-emission dominance' or 'EED' is a calculation from the leading term of Low's expansion.

the Δ term added. We turn our attention to the region of larger photon energy $(k \gtrsim 80 \text{ MeV})$, where the Δ terms become significant. We can write the total cross section as

$$| T_{OBE} + T_{(\Delta,\pi)} + T_{(\Delta,\rho)} |^2 = | T_{OBE} |^2 + (2 \, Re \, T_{OBE} \, T^*_{(\Delta,\pi)} + | T_{(\Delta,\pi)} |^2) + (2 \, Re \, T_{OBE} \, T^*_{(\Delta,\rho)} + 2 \, Re \, T_{(\Delta,\pi)} \, T^*_{(\Delta,\rho)} + | T_{(\Delta,\rho)} |^2) \quad (6.23)$$

The last three terms in brackets in (6.23) are the result of adding the (Δ,ρ) amplitude. In general $T_{(\Delta,\rho)}$ and $T_{(\Delta,\pi)}$ differ in phase by $180°$, and the term $2 \, Re \, T_{(\Delta,\pi)} \, T^*_{(\Delta,\rho)}$ is negative. This is illustrated in fig. 46 for the spectrum of G8, and is in agreement with the finding of Tiator, Weber and Drechsel [63]. However when the other interference terms of (6.23) are included the addition of (Δ,ρ) process can actually enhance the total isobar effect, as is the case in the G7 spectrum (fig. 44) and part of the G8 spectrum (fig. 45). In this case ($2 \, Re \, T_{OBE} \, T^*_{(\Delta,\pi)} + | T_{(\Delta,\pi)} |^2$) is negative, and $2 \, Re \, T_{OBE} \, T^*_{(\Delta,\rho)}$ is positive but smaller in absolute value than the negative $2 \, Re \, T_{(\Delta,\pi)} \, T^*_{(\Delta,\rho)} + | T_{(\Delta,\rho)} |^2$ part. Because of this cancellation the (Δ,ρ) process causes only a slight decrease in cross section. In the G10, G11, G12 spectra (fig. 47, 48, 49) $T_{(\Delta,\pi)}$ interferes constructively with T_{OBE} and $T_{(\Delta,\rho)}$ interferes destructively with T_{OBE}. The effect is that (Δ,π) causes a large increase in cross section while (Δ,ρ) causes a substantial decrease. Thus the isobar terms can increase or decrease the cross section, depending on the kinematic situation. When the (Δ,π) decreases the cross section the (Δ,ρ) can enhance the total isobar effect, even though $T_{(\Delta,\pi)}$ and $T_{(\Delta,\rho)}$ interfere destructively.

We find good agreement with the experiment except in the cases of the G11 and G12 spectra where the calculation falls below the data, particularly at small k. A similar discrepancy between the G11, G12 spectra at low k and the EED prediction was noted by the experimentalists $\underline{/}11\underline{/}$. It is suspected that this discrepancy is due to the rapid variation of the cross section over the solid angle acceptance of the photon counters. (The calculations are not corrected for this).

The measured G10 spectrum suggests an increase at $k \gtrsim 80$ MeV which requires the inclusion of the Δ terms. However due to the crudeness of the OBE calculation and the size of the error bars a definite conclusion cannot be made. Furthermore, for the measured G7 and G8 spectra the OBE calculation alone provides a satisfactory fit.

CONCLUDING REMARKS

We have used a simple relativistic model based on the one-boson-exchange model of N-N scattering of Erkelenz, Holinde, and Machleidt $\underline{/34\underline{7}}$ and constrained by the soft-photon theorem. The model yields ppγ cross sections, for lab energies in the range of 158 MeV to 730 MeV, that are in reasonable agreement with most experiments. The exceptions are the Orsay measurements $\underline{/54\underline{7}}$ and the G11 and G12 spectra of the UCLA experiment $\underline{/11\underline{7}}$ - they are data points where other calculations show a similar discrepancy.

We have considered the contribution of the ω-π current diagram (fig. 16) to the ppγ cross section. For the 200 MeV $\theta = 16.3^{\circ}$ Triumf geometry this can be as large as 10%; for other experiments it is negligible. It is thus another correction which must be considered in potential-model calculations when comparing with the Triumf data.

The $\triangle$-excitation diagrams, on the other hand, are significant only at the upper end of the photon spectra of the 730 MeV UCLA experiment. The interference between the $\triangle$ terms and the background was found to be important. In some cases the $\triangle$ excitation lowered the cross section and the $\triangle$ terms with ρ exchange enhanced the total isobar effect.

We conclude by making a suggestion regarding future experiments. It appears that in all the experiments performed so far we have not been able to measure significant model differences. Going to higher energies (above 200 MeV) may

71

prove to be self defeating as it will increase the corrections

and uncertainties in the potential-model calculations. An

investigation of Fearing [66] suggests that asymmetries in ppγ *

may be more sensitive to the off-shell effects. Of special

interest are those asymmetries that are forbidden (by parity

conservation) in elastic scattering, since, in this case, the

soft-photon theorem determines only the leading term in the k

expansion [74]. It may well turn out that experiments with

polarized proton beams are more suitable for seeing off-shell

effects. The answer will have to await further calculations.

Finally, in view of the fact that a number of calculations

show a similar discrepancy with the Orsay data it would be useful

to have the measurements repeated. This could be done perhaps by

running the experiment at Triumf at the asymmetric angles of the

Orsay measurements.

---

*The asymmetry along the direction $\hat{i}$ is defined as
$A_i = (d\sigma_+ - d\sigma_-)/(d\sigma_+ + d\sigma_-)$, where $d\sigma_\pm$ is the ppγ cross section
with the incident proton spin parallel or antiparallel to $\hat{i}$.

$$V^{(em)}_{fn} \; G^{(+)}_n \; t_{ni}$$

$$t_{fn} \; G^{(+)}_n \; V^{(em)}_{ni}$$

$$\sum_m t_{fn} \; G^{(+)}_n \; V^{(em)}_{nm} \; G^{(+)}_m \; t_{mi}$$
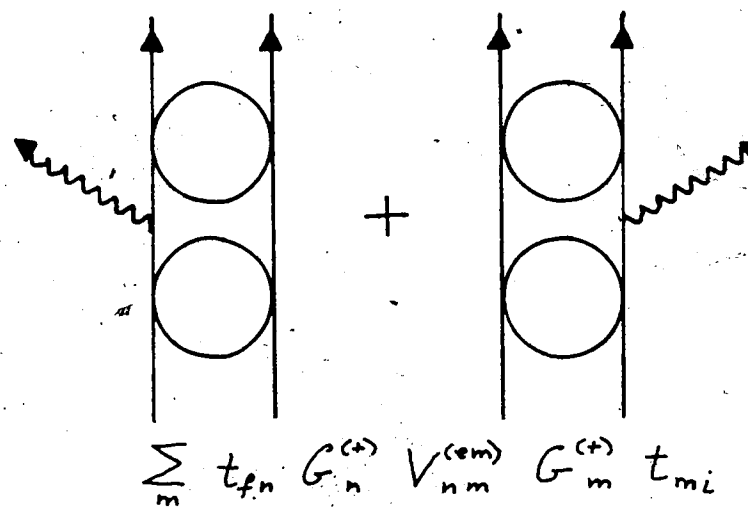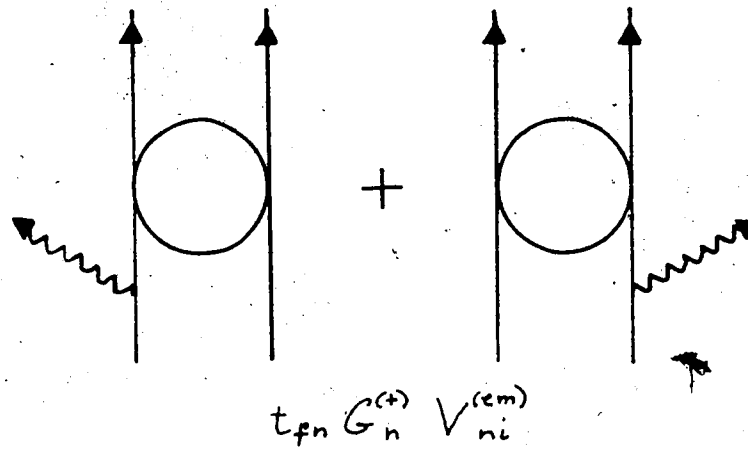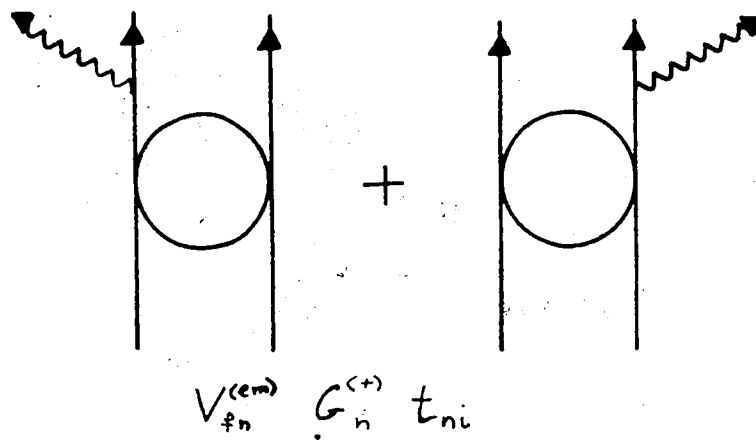
Figure 1. Diagrammatic representation of eq. (1.3).
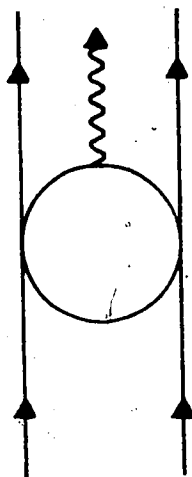
Figure 2. The general internal-radiation process.
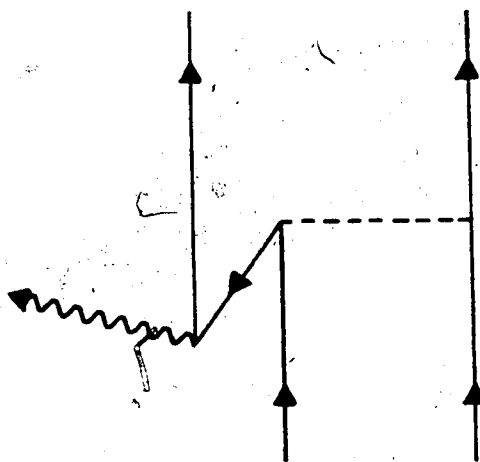
Figure 3. Pair-creation current: a diagram not included
in a potential-model calculation.
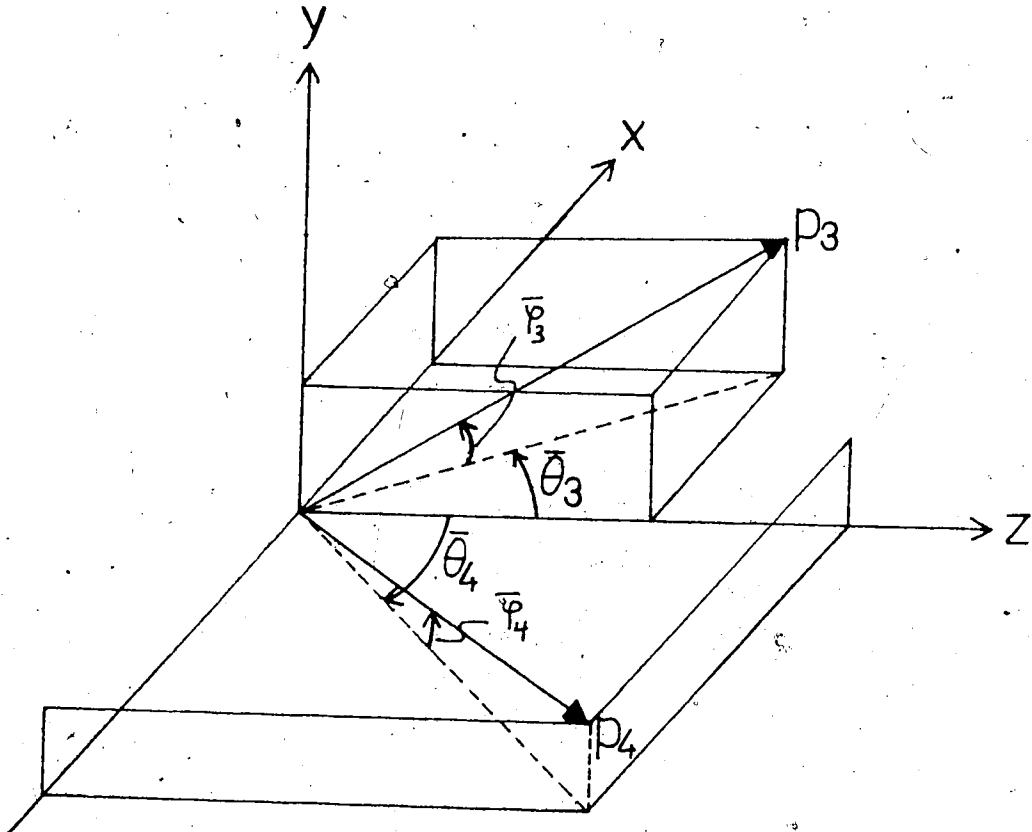
Figure 4. Proton momenta in terms of the Harvard angles.
The photon momentum, k, (not shown) has a
negative y component and may have a positive
($0 \leq \bar{\theta}_\gamma \leq \pi$) or negative ($\pi < \theta_\gamma < 2\pi$) x com-
ponent, according to energy-momentum conservation.
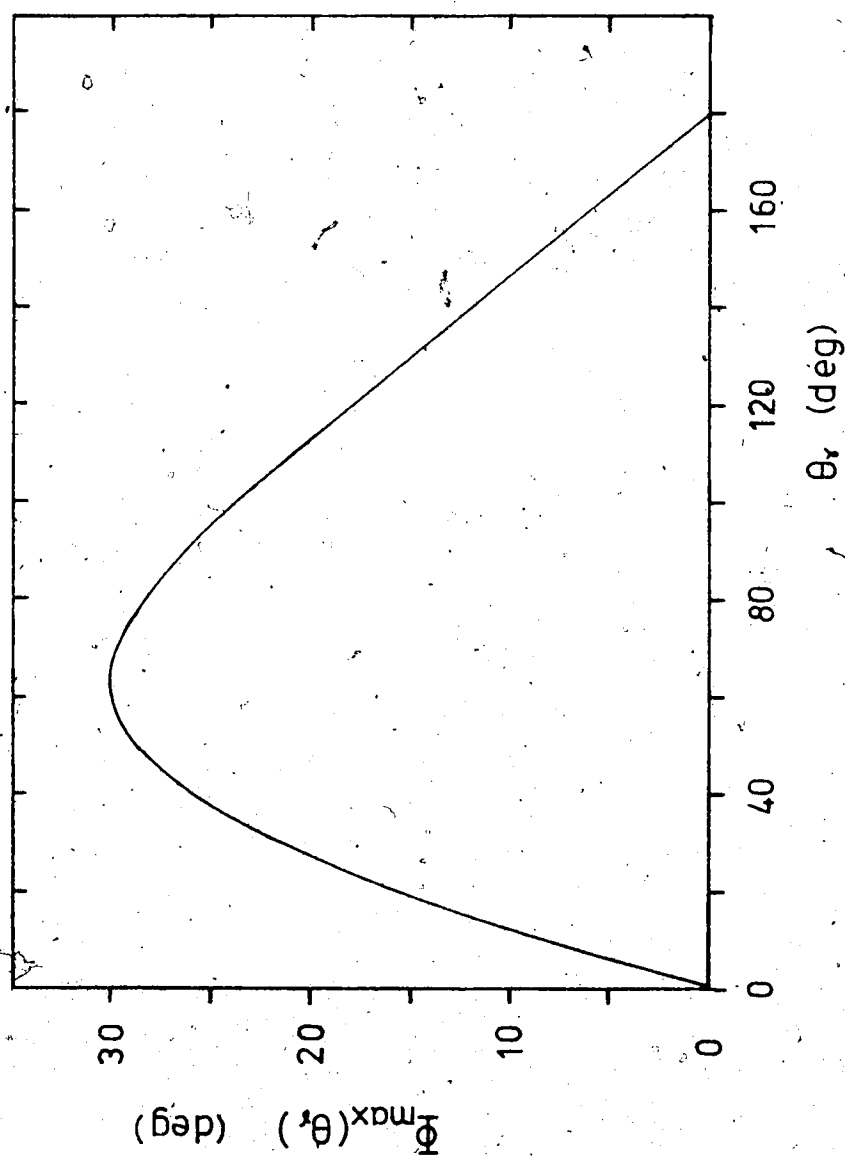
Figure 5. Maximum noncoplanarity as a function of the photon polar angle for the TRIUMF geometry: $T_{lab} = 200$ MeV, $\theta_3 = \theta_4 = 16.3°$.
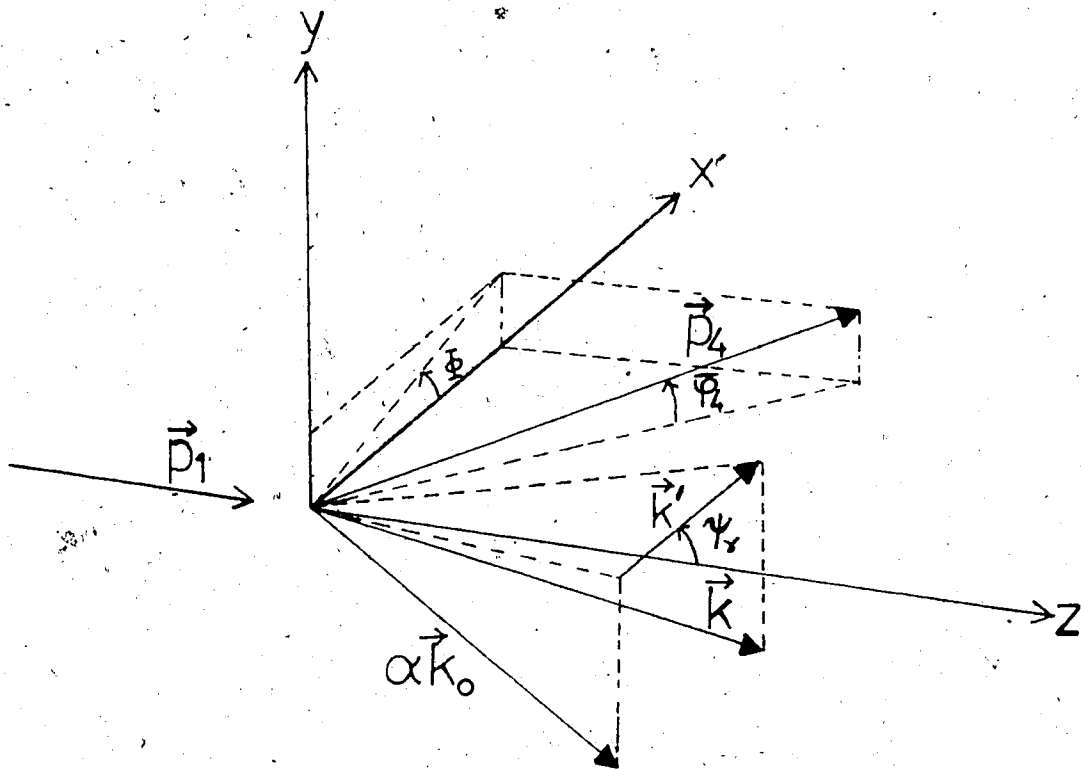
Figure 6.   Definition of γ_r . $\vec{k}_o$ is the momentum of the
limiting gamma ray; α is chosen such that $\alpha k_{oy} = k_y$;
thus $k' = k - \alpha k_o$ has no y component. γ_r is the
angle between k' and the z-axis.
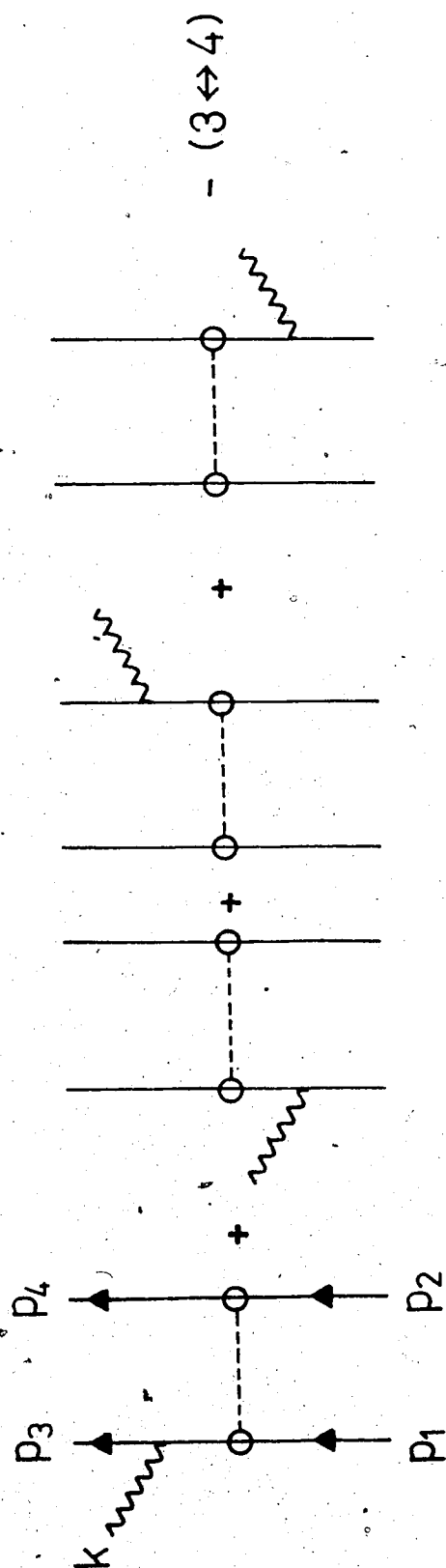
Figure 7. OBE external-emission diagrams for each of the seven exchanged mesons considered. The circles at the strong interaction vertices represent the form factors.
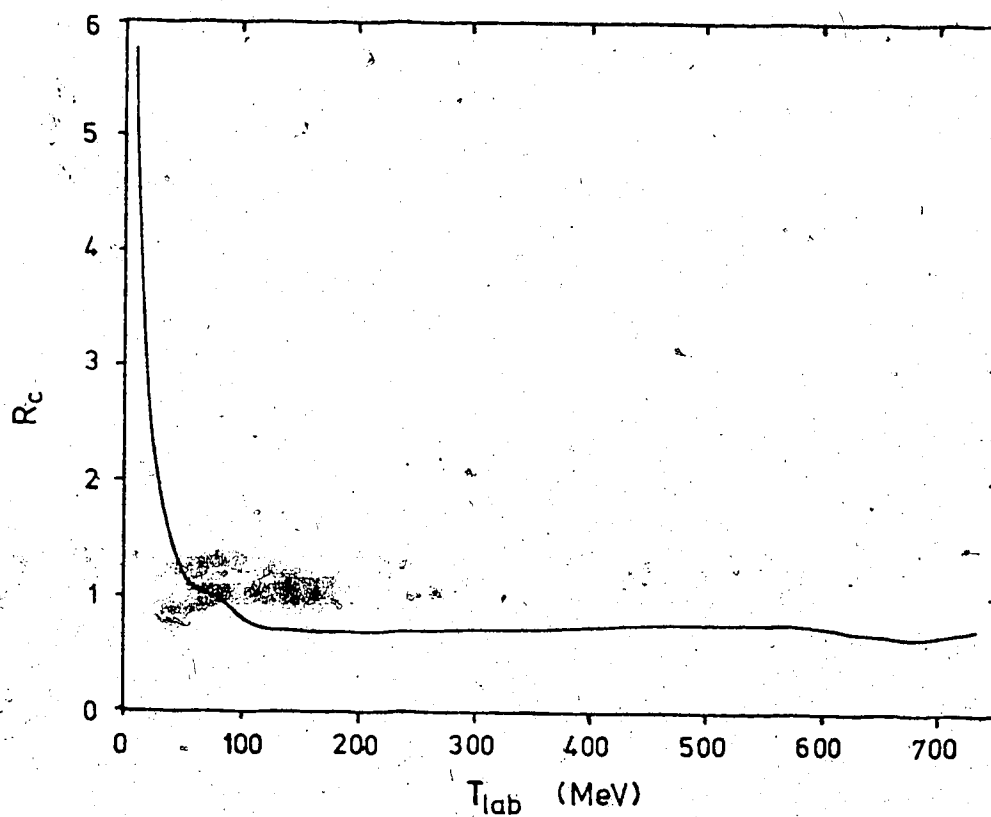
Figure 8. The ratio of experimental to calculated
elastic p-p scattering differential cross
section. $R_C = d\sigma/d\Omega_{cm}(exp.)/d\sigma/d\Omega_{cm}(calc.)$
at $\theta_{cm} = 60^o$, where $d\sigma/d\Omega_{cm}(calc.)$
is the differential cross section computed with
the model of Erkelenz, Holinde, and Machleidt [34]
in Born approximation with the form factors
modified as given in eq. (3.3).
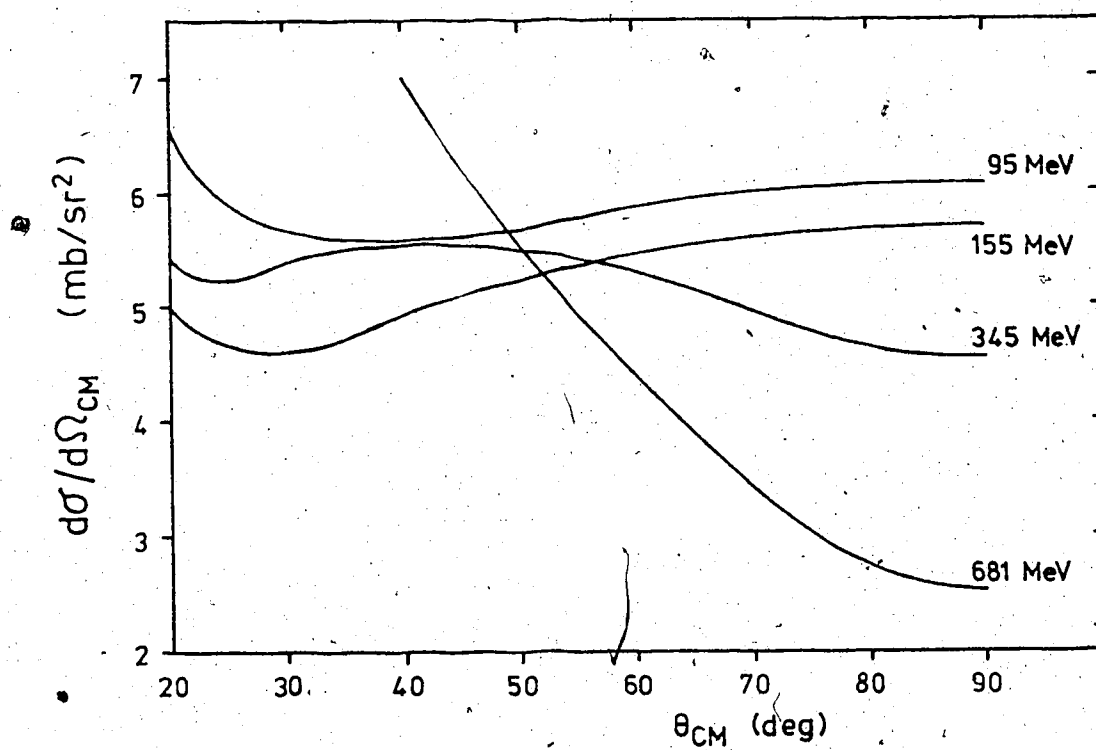
Figure 9. Elastic differential cross section computed from the EHM model in Born approximation with the modified form factors (as given in eq. (3.3)).

81
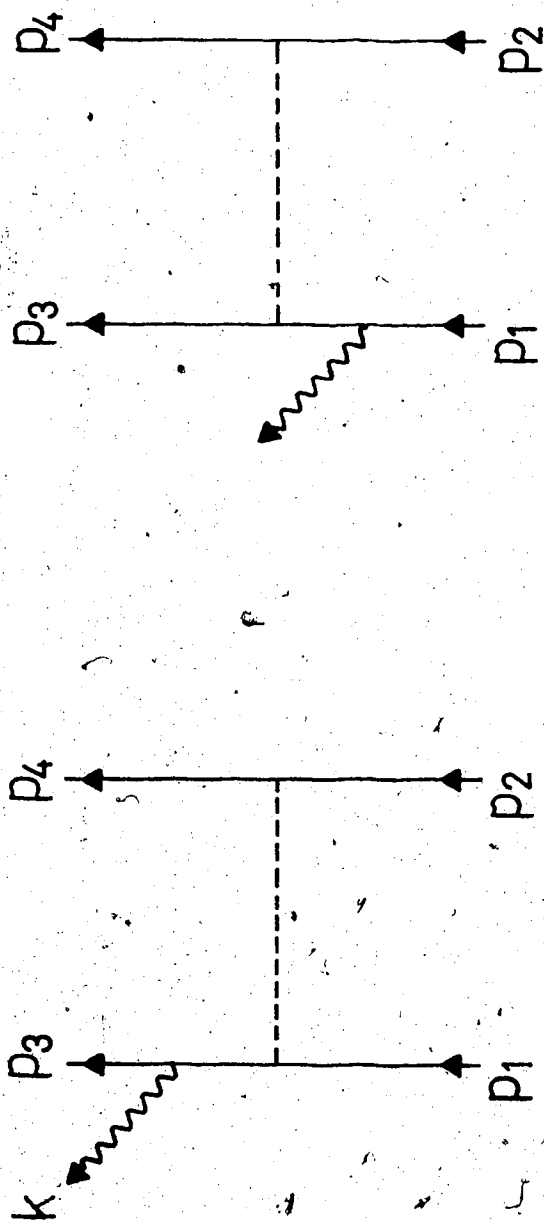
Figure 10. Diagrams corresponding to the matrix element of eq. (3.8).
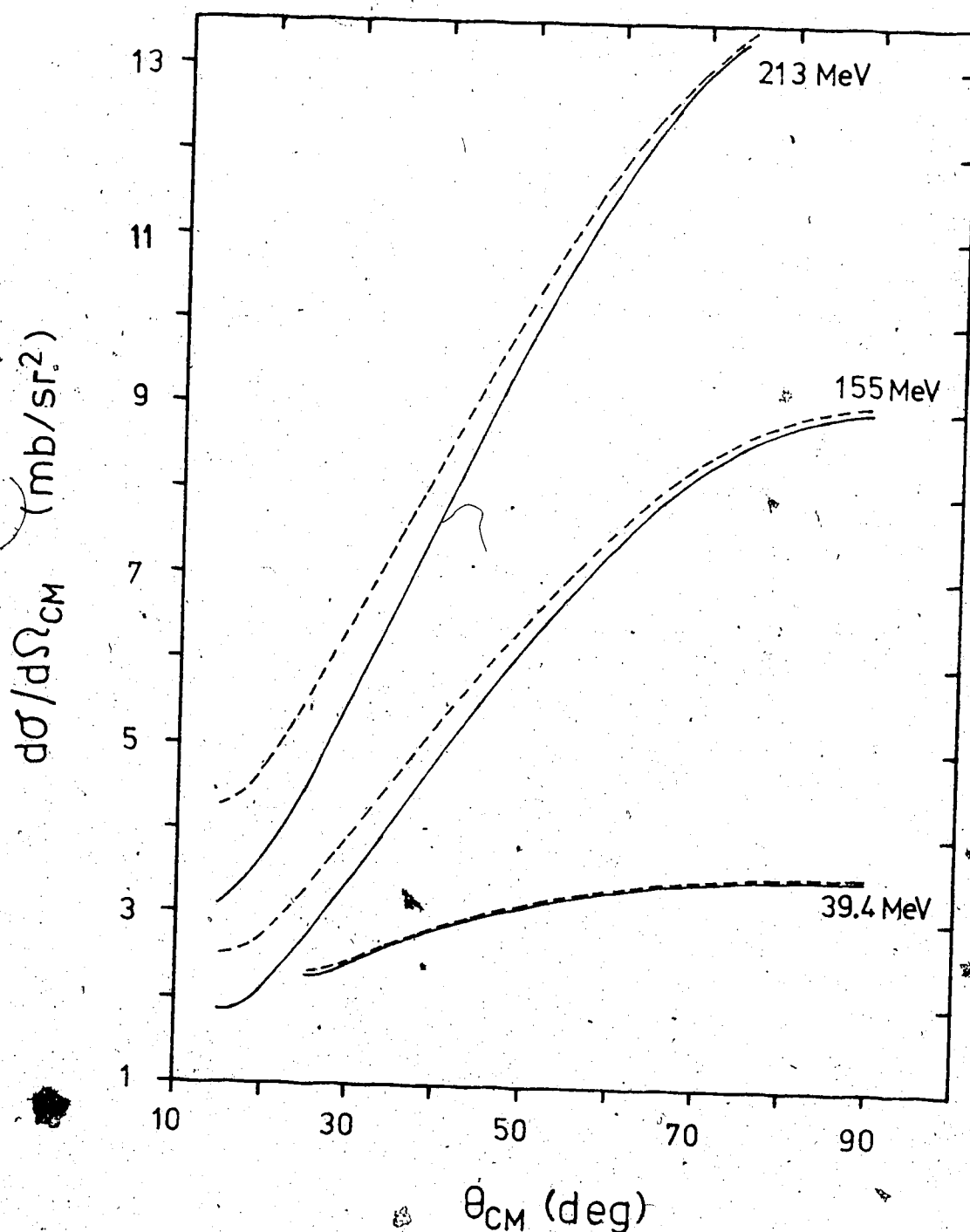
Figure 11. Elastic (p-p) differential cross sections from the four-pole model of Arndt, Bryan and Macgregor [38] with no unitarization (solid curves) and with L≥1 waves unitarized (dashed curves). In both cases the S wave was obtained from the unmodified Born terms.
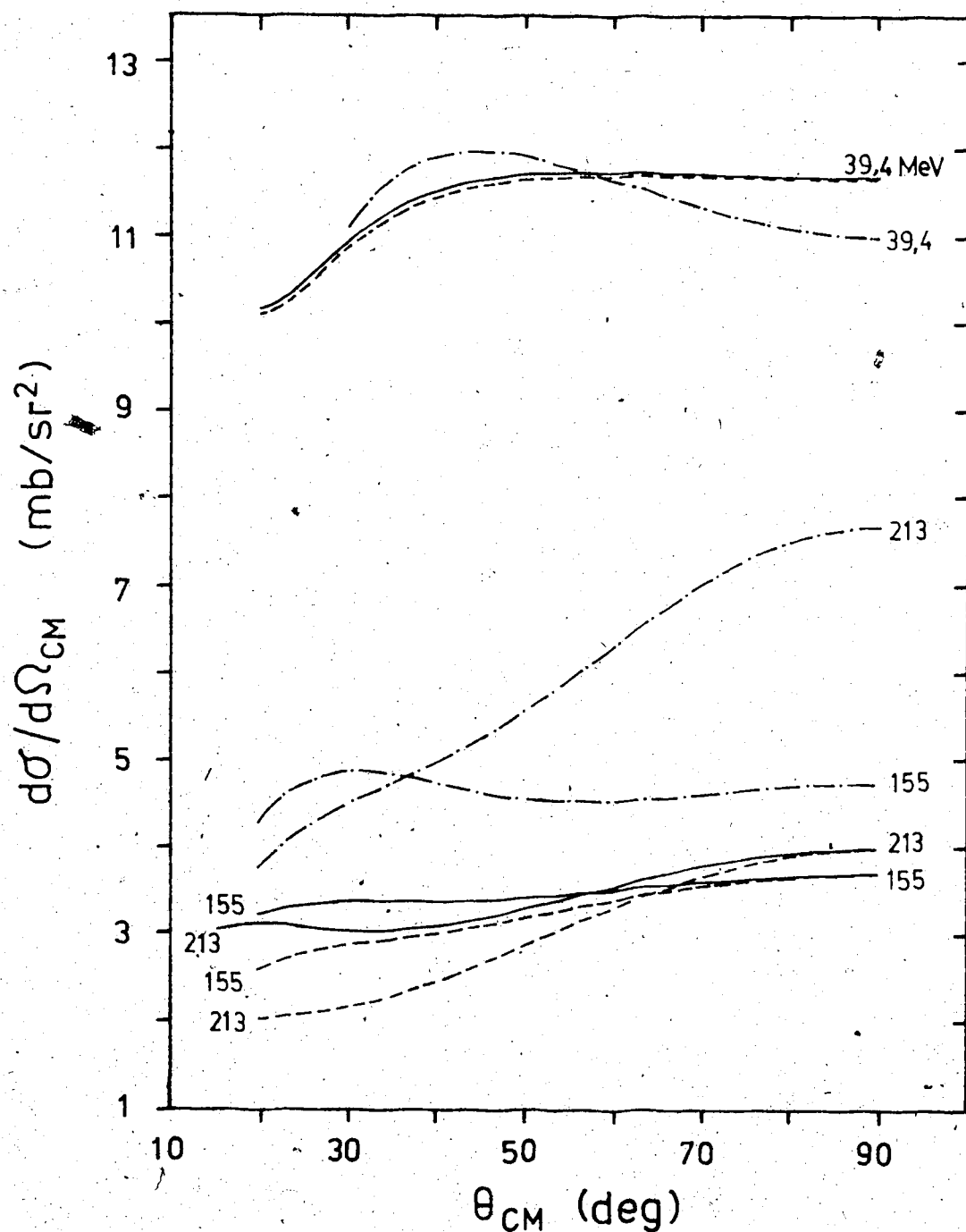
Figure 12. Elastic (p-p) differential cross sections from the
four-pole model of Arndt, Bryan and Macgregor [38]
with the $L \geq 1$ waves unitarized and the S wave
obtained from experiment (solid curve), with
$L \geq 1$ waves not unitarized and the S wave obtained
from experiment (dashed curves), and with model
parameters as modified by Baier, Kühnelt and
Urban [32] and no unitarization (dash-dotted curves).
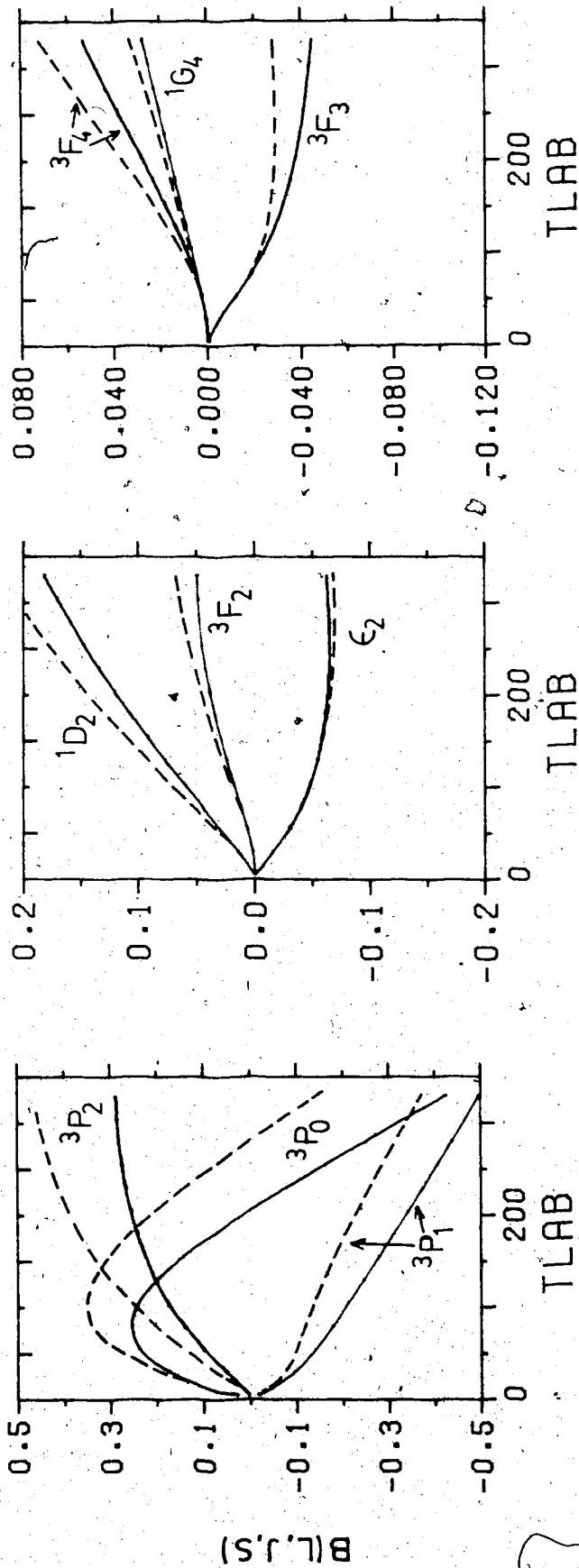
Figure 13. Born partial-wave amplitudes, B(L,J,S), computed from the four-pole boson-exchange model (with no unitarization): with the parameters of Bryan, Arndt and Macgregor [38] (solid curve), and with the parameters as modified by Baier et al (ref. 32, set A) (dashed curve).
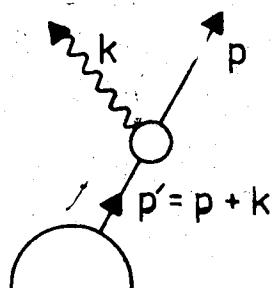
Figure 14. Photon-emission vertex.
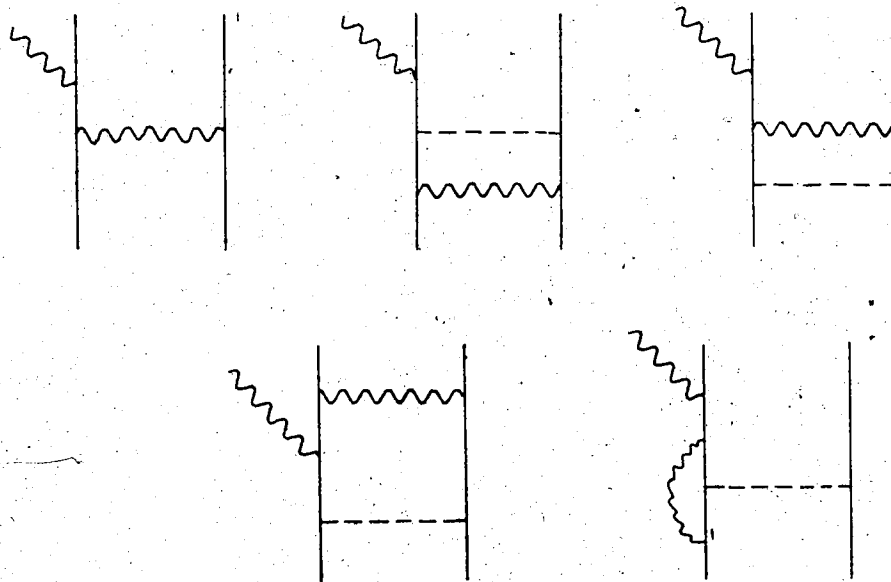
Figure 15.   Some OBE diagrams to third order
in the electromagnetic interaction.
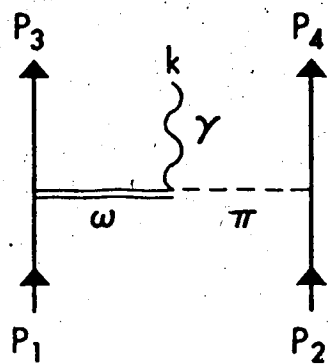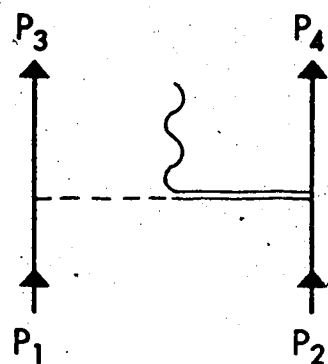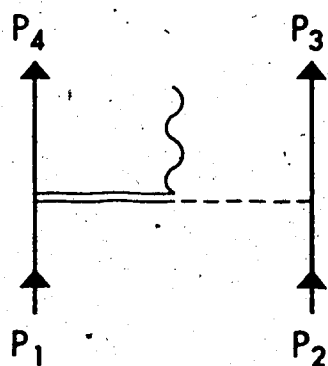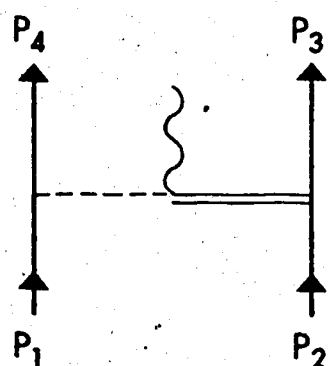
Figure 16. The ω radiative-decay diagrams.

$q^\mu q_\mu = 0$

(a)

$q^\mu q_\mu = 0$

(b)
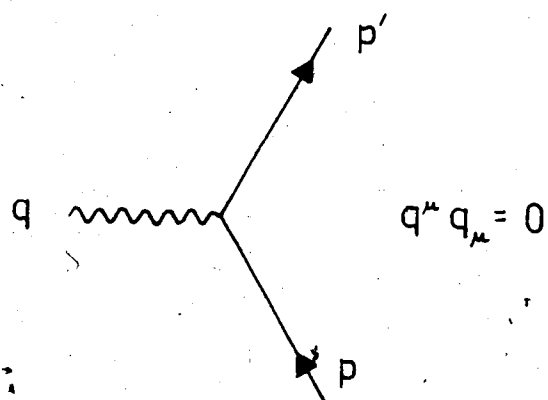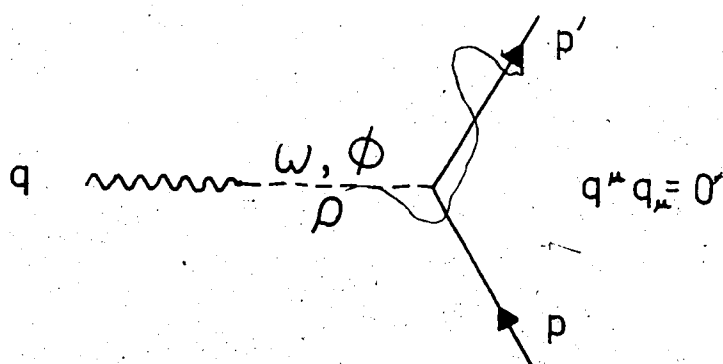
Figure 17.   The γNN vertex in the vector-
meson-dominance model.
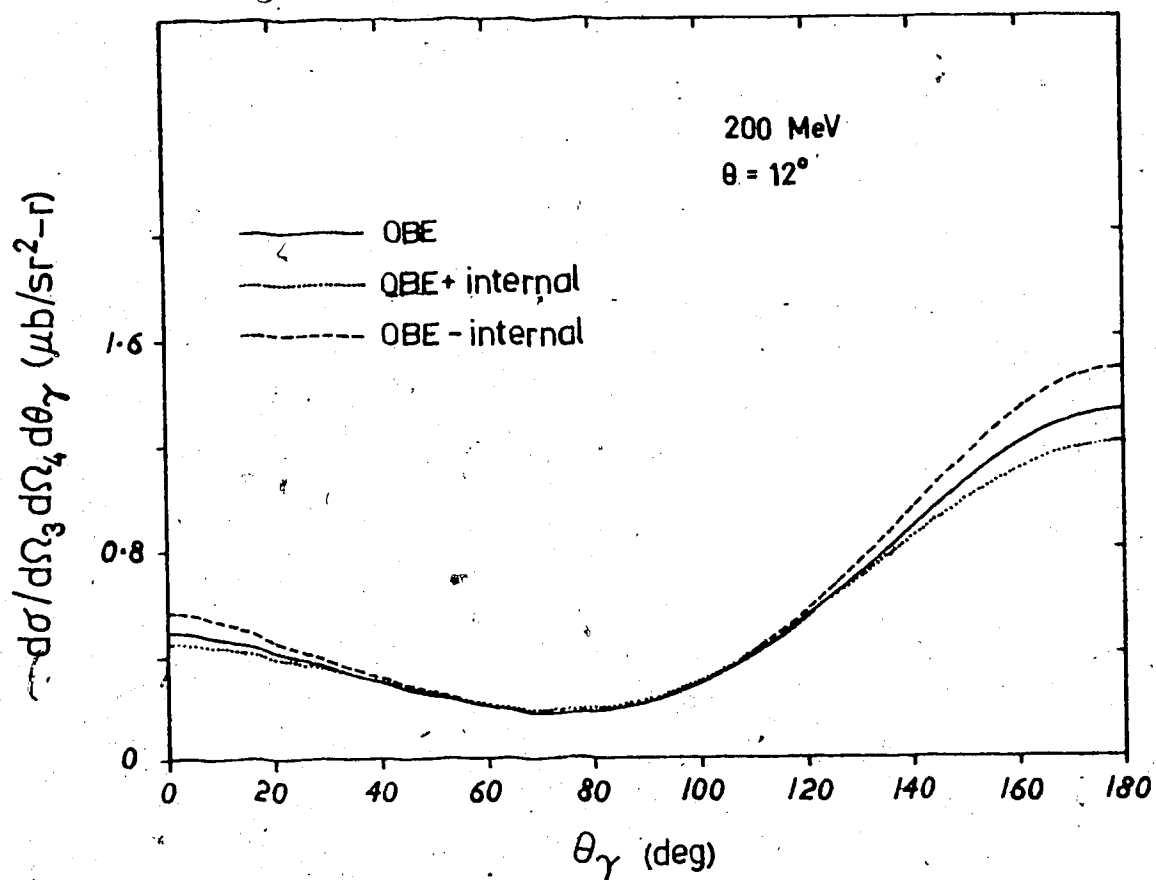
Figure 18. Proton-proton bremsstrahlung differential
cross section **in** the coplanar, symmetric
geometry. "OBE" is the result from the
OBE external-emission model (chapter 3).
"OBE±internal" includes the ω radiative-
decay contribution (chapter 4), coherently
added with either relative sign.
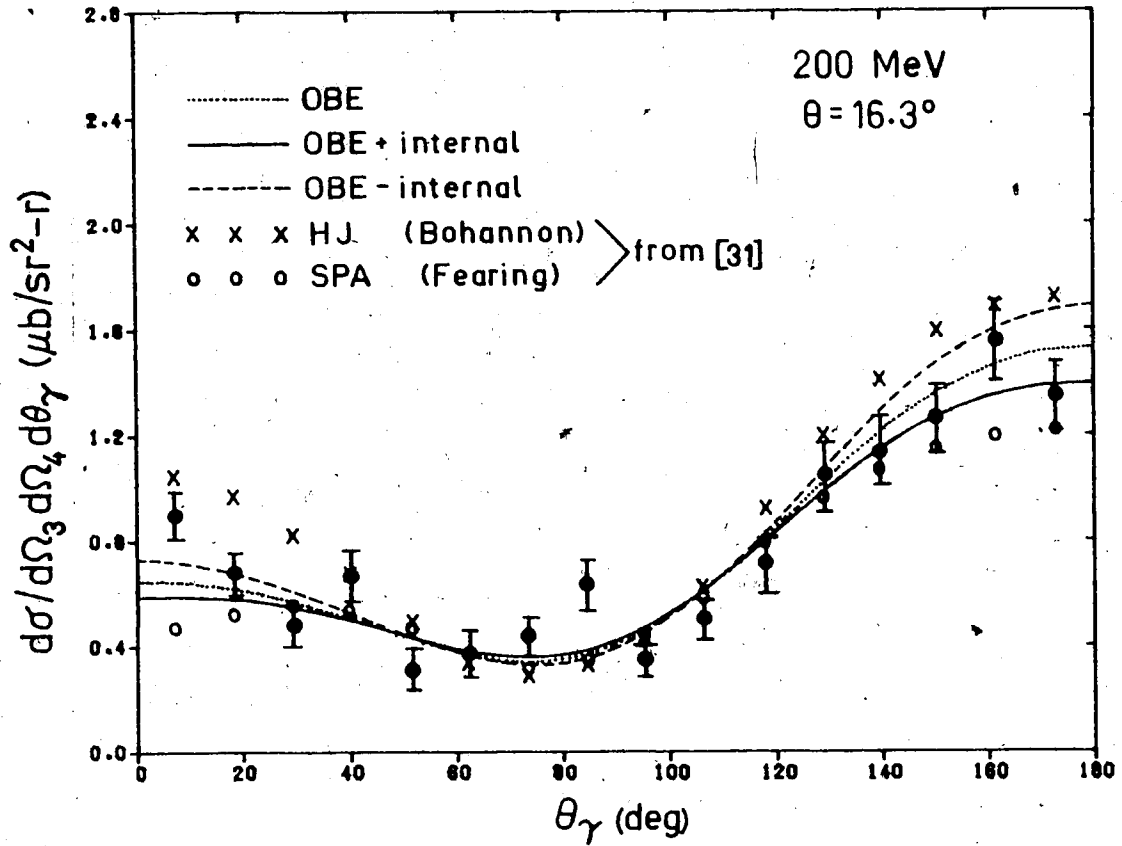
Figure 19. See caption to fig. 18. "HJ" is a Hamada-
Johnston potential-model calculation. "SPA"
is a soft-photon-approximation calculation.
The data points (solid circles) are pre-
liminary results from Trimuf $\lceil 10 \rfloor$. The
HJ, SPA, and data points were taken from
fig. 6 of ref. 31.
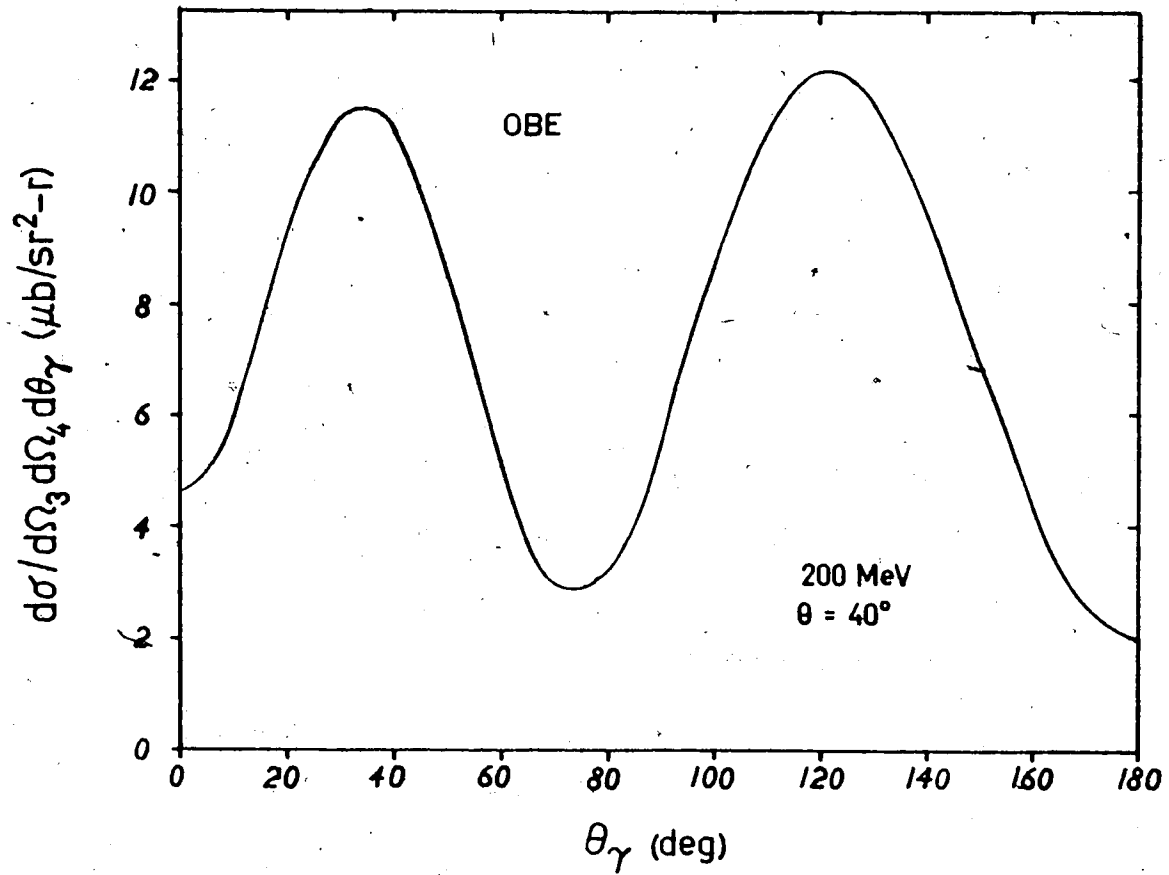
Figure 20. See caption to fig. 18. The ω radiative-decay contribution is negligible here.
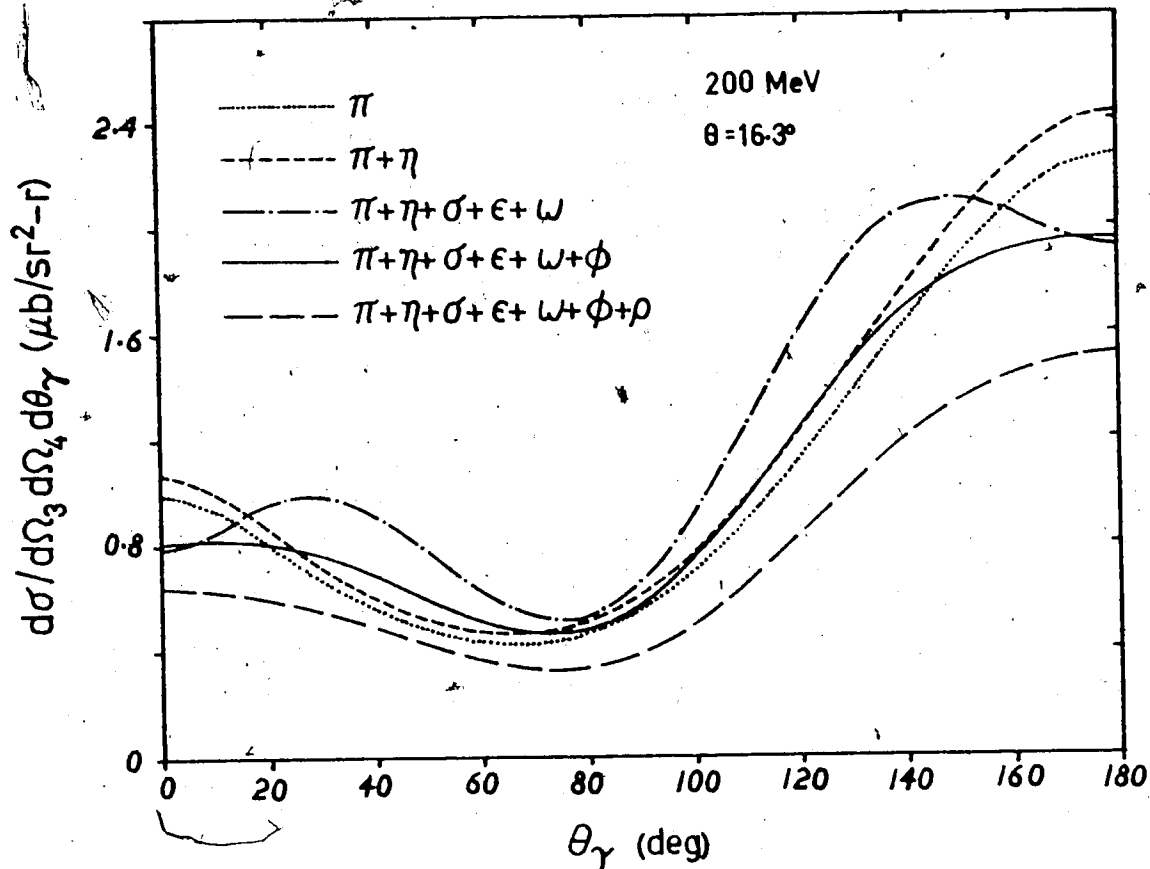
Figure 21. Contributions to the OBE external-emission model for T_{lab} = 200 MeV, $\theta_3 = \theta_4$ = 16.3 (Triumf geometry). The curves show the coherent addition of the indicated meson-exchange contributions.
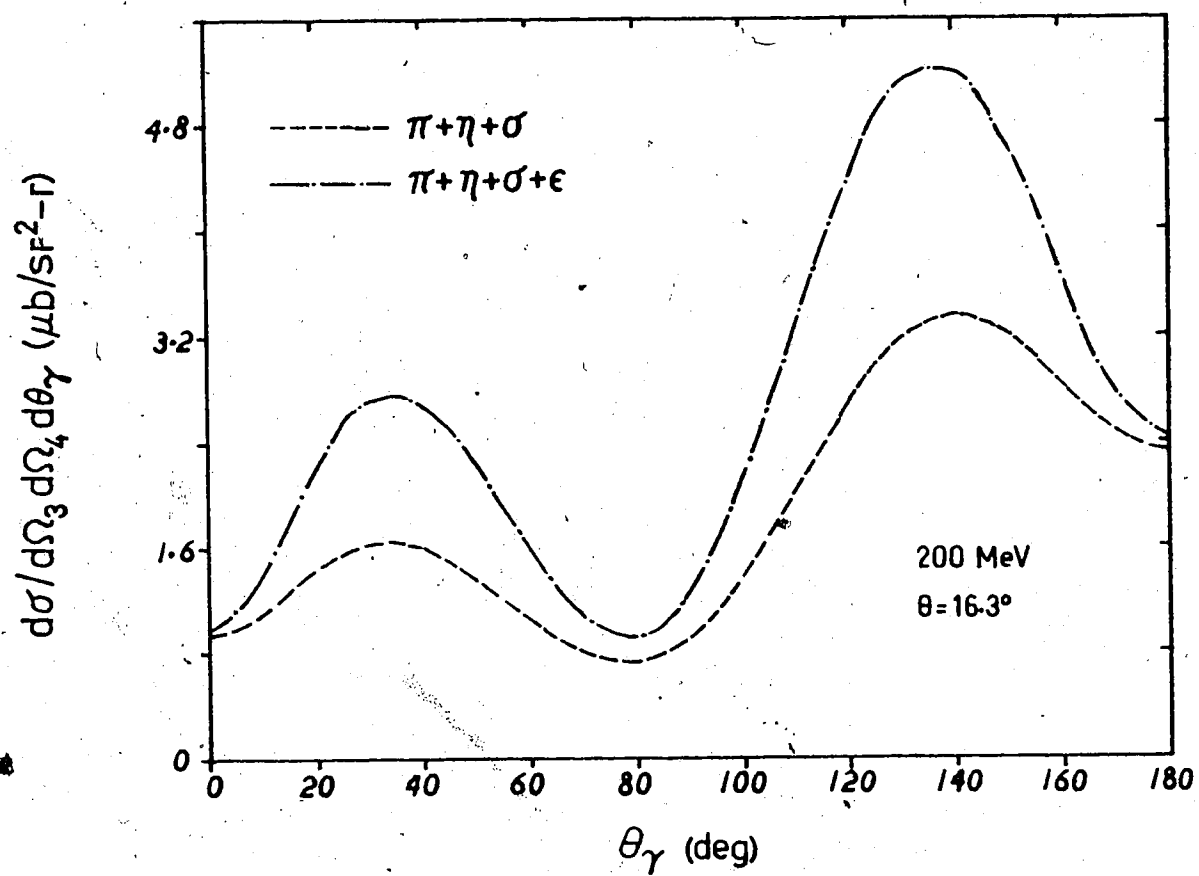
Figure 22. See caption to fig. 21.
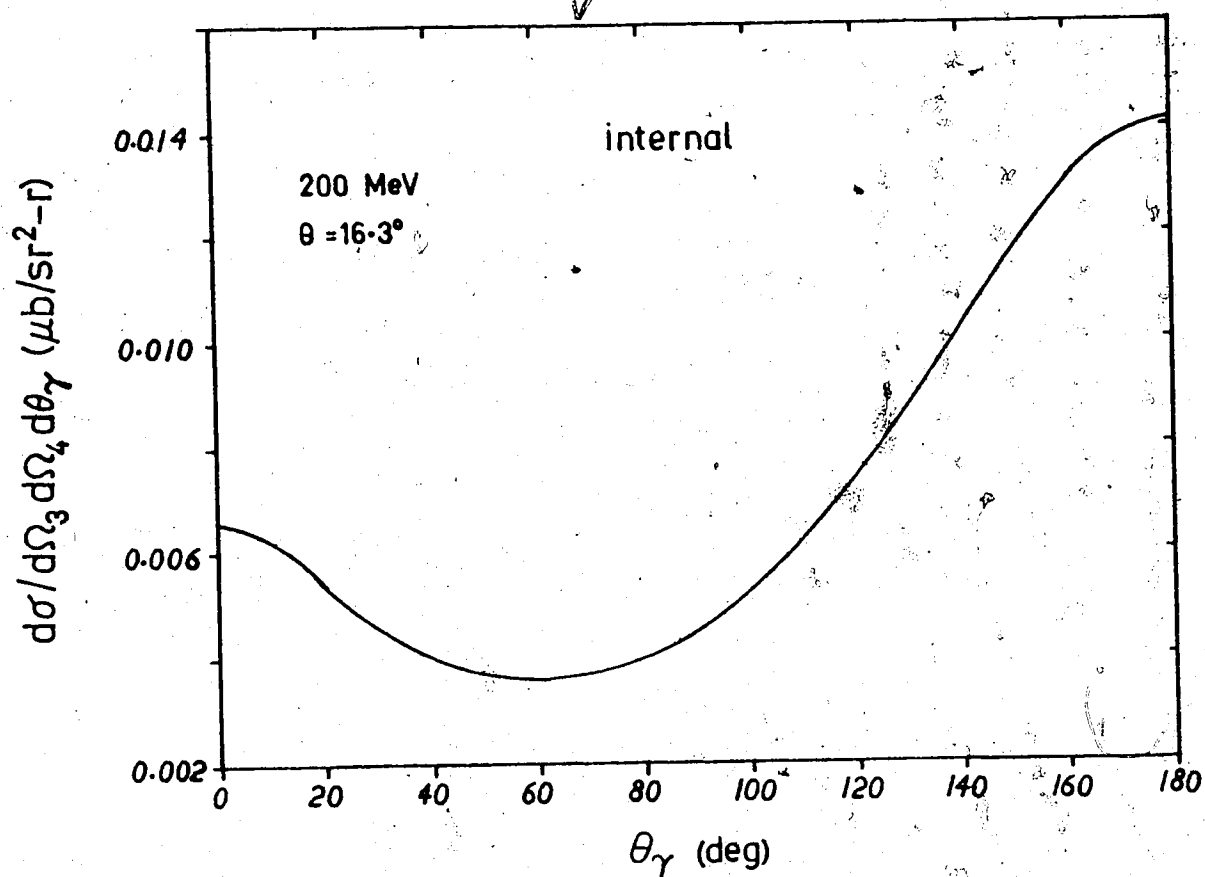
Figure 23.   See caption to fig. 21. "Internal" is the
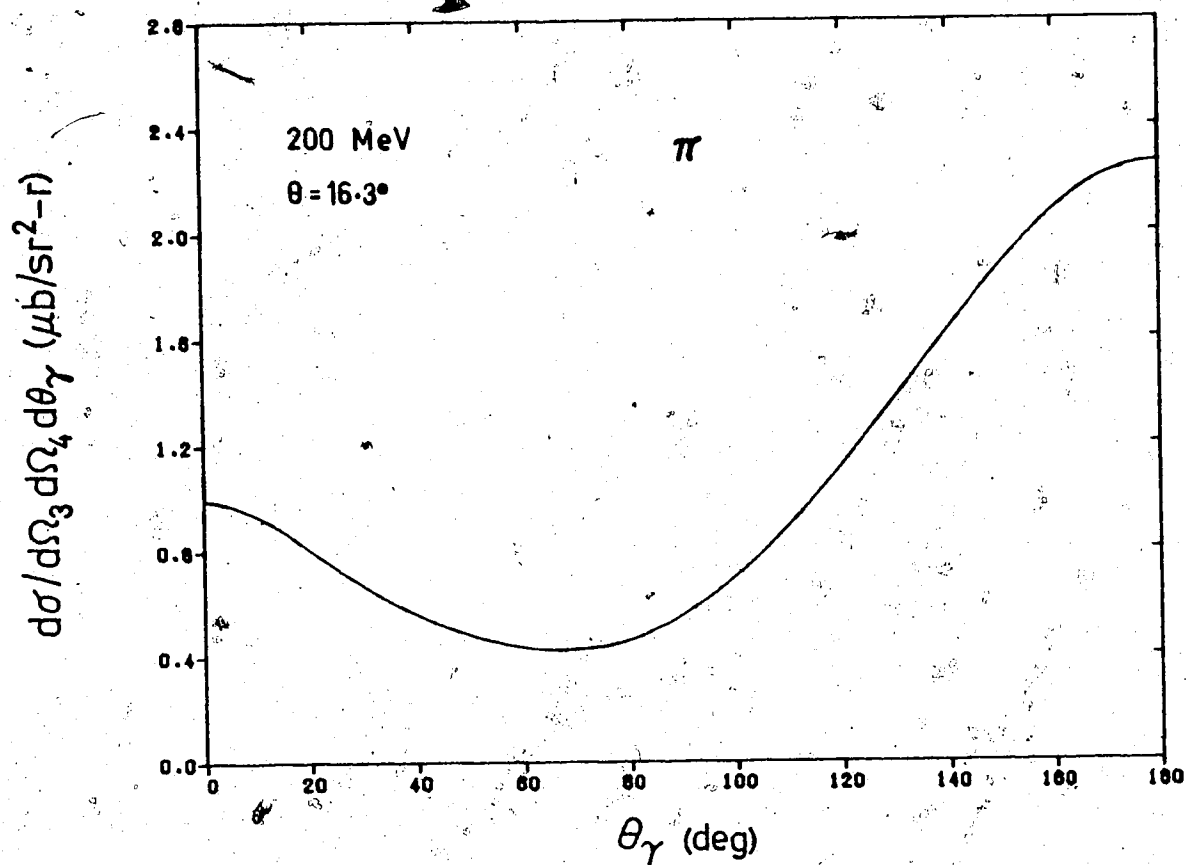   contribution from the ω radiative-decay
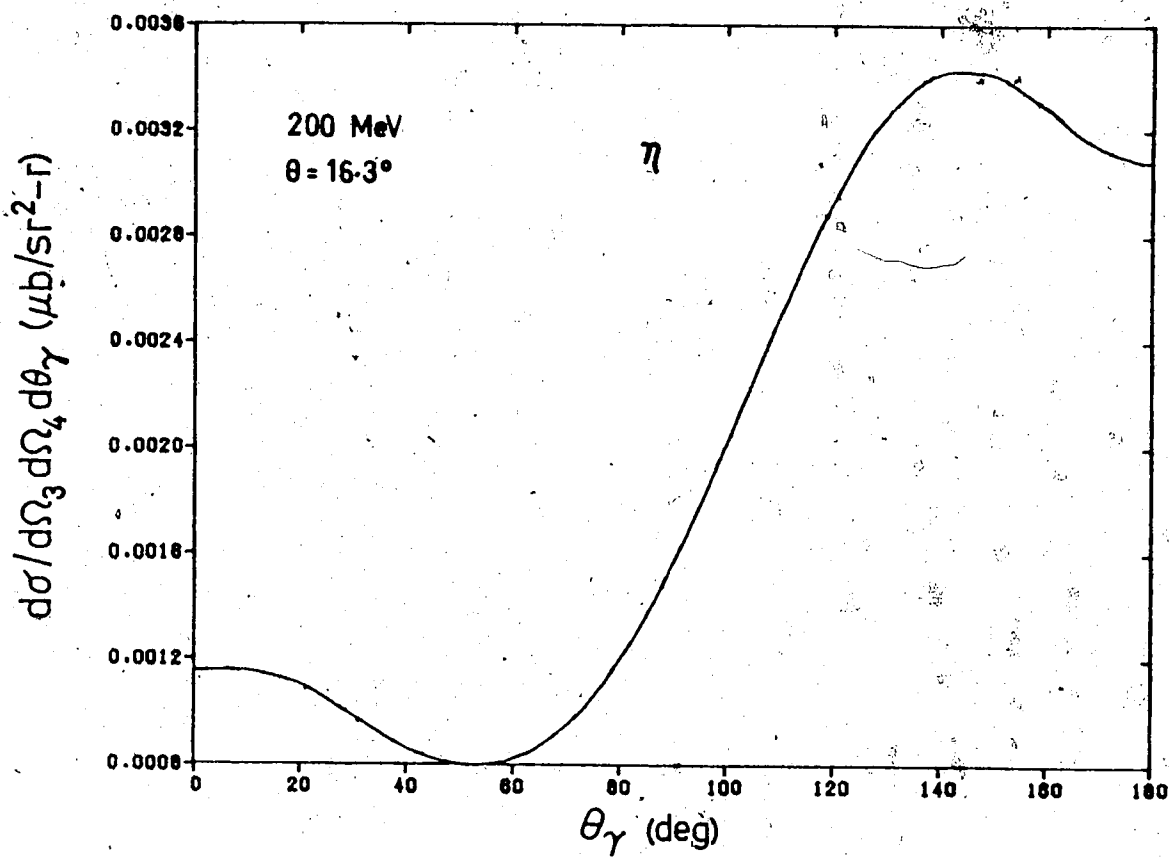   process.

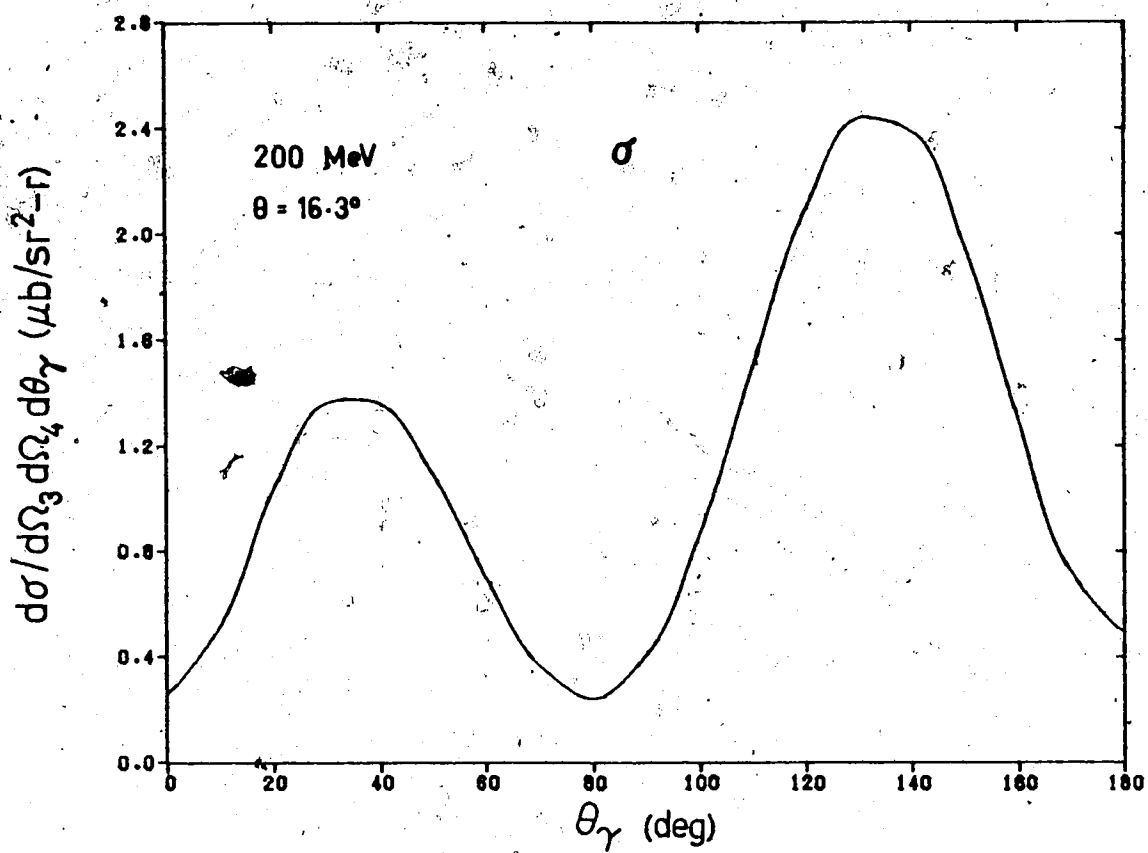Figure 24. See caption to fig. 21.

Figure 25.   See caption to fig. 21.
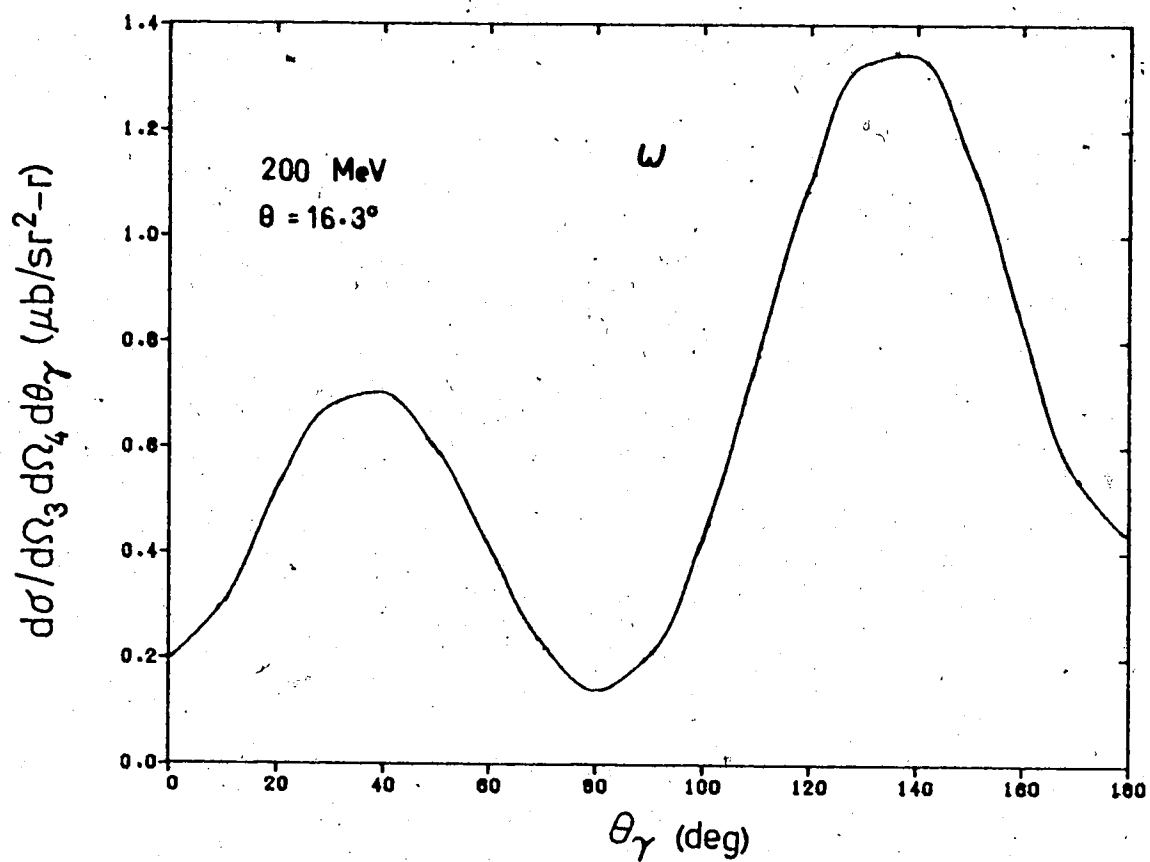
Figure 26. See caption to fig. 21.
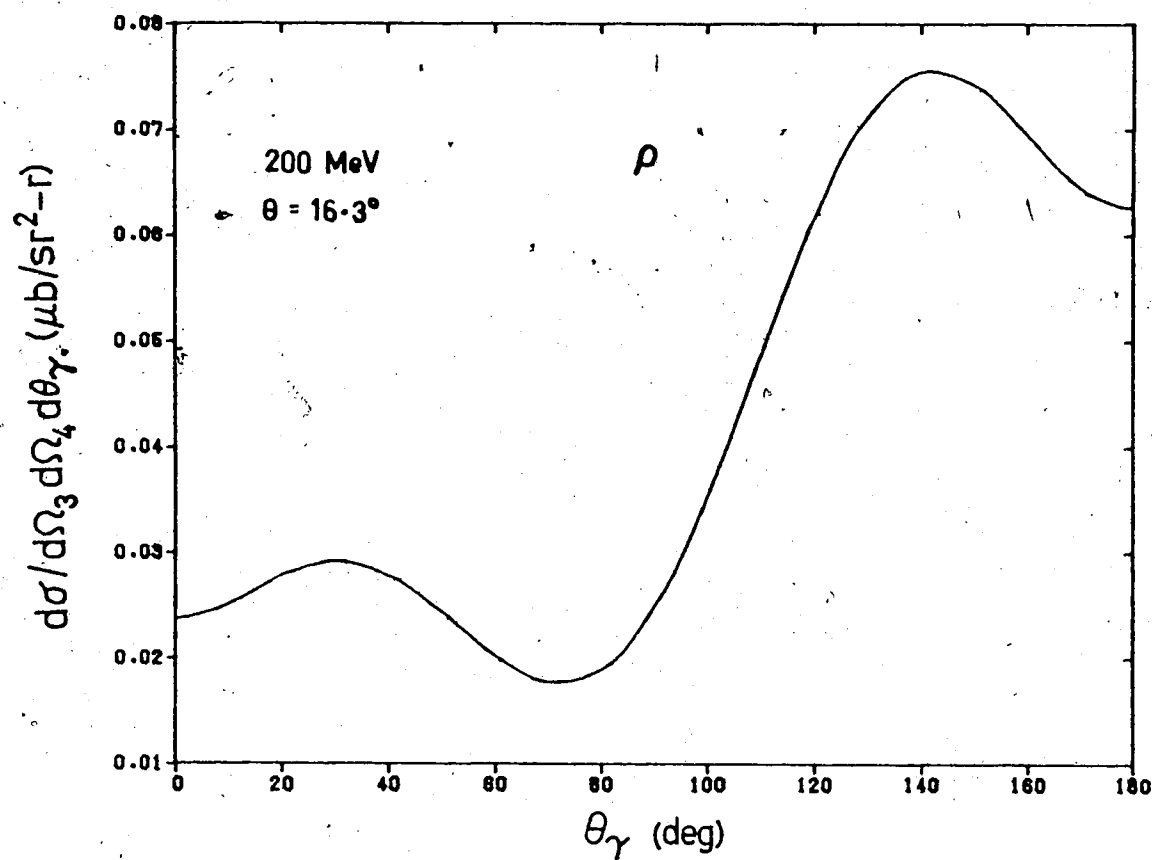
Figure 27. See caption to fig. 21.

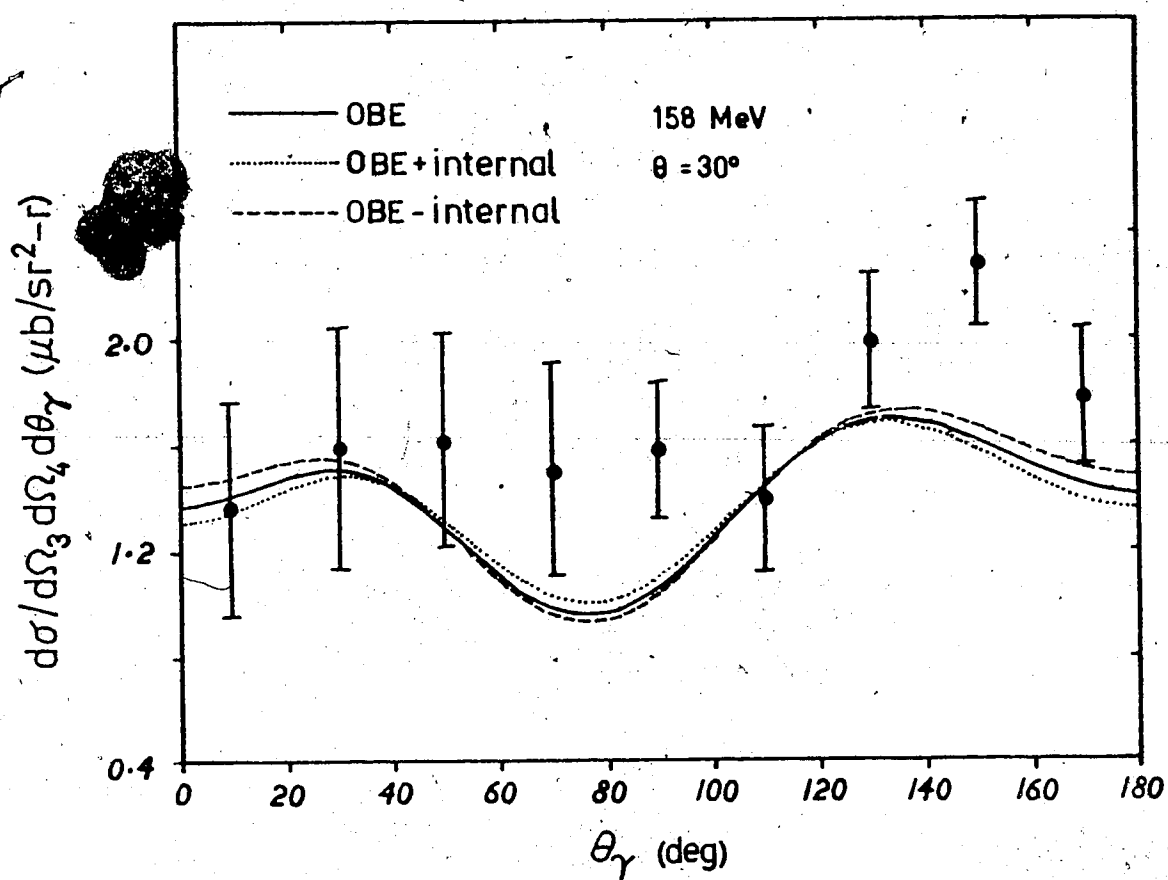Figure 28. See caption to fig. 21.

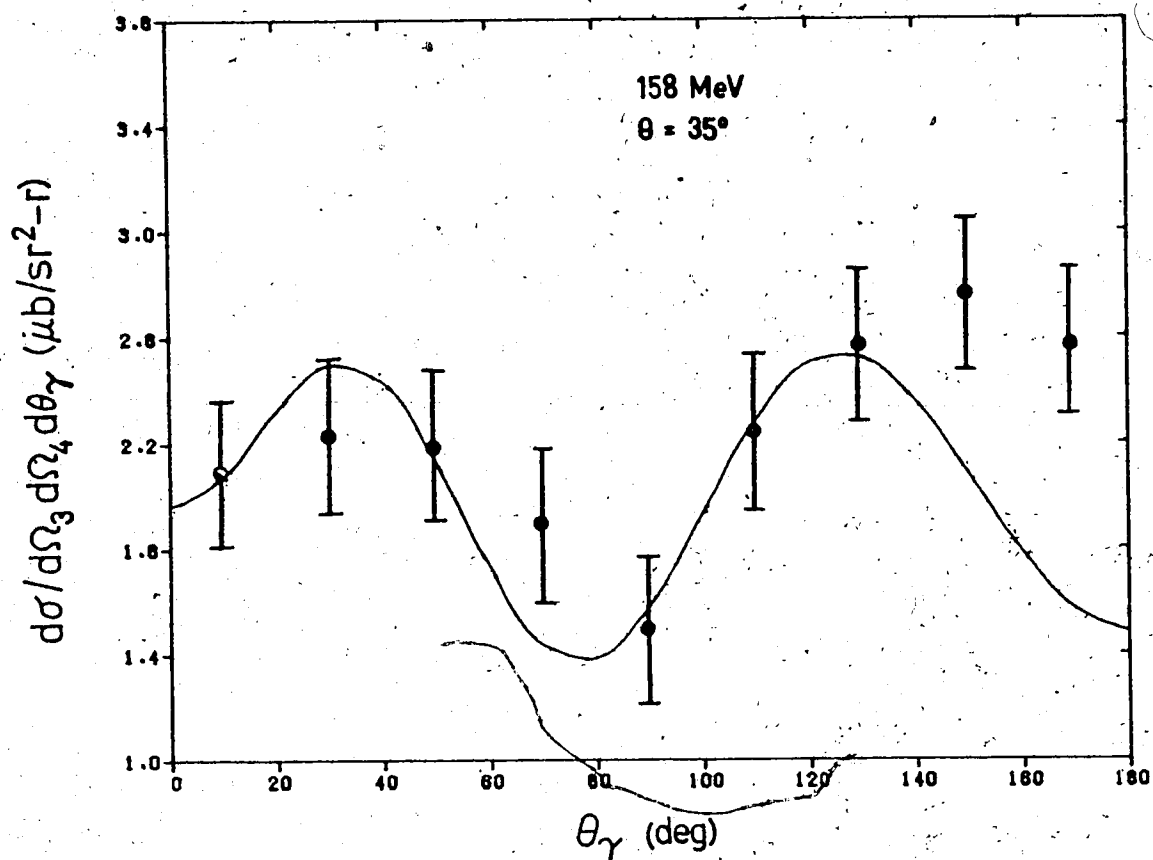Figure 29. See caption to fig. 18. The data
points are from ref. 4.

Figure 30. See caption to fig. 18. Only the OBE calculation is shown here. The data points are from ref. 4.

Figure 31.   See caption to fig. 18. The curve
             marked "OBE + γ exchange" includes
             the one-photon-exchange contribution.
             The data are from ref. 48.

Figure 32. See caption to fig. 18.
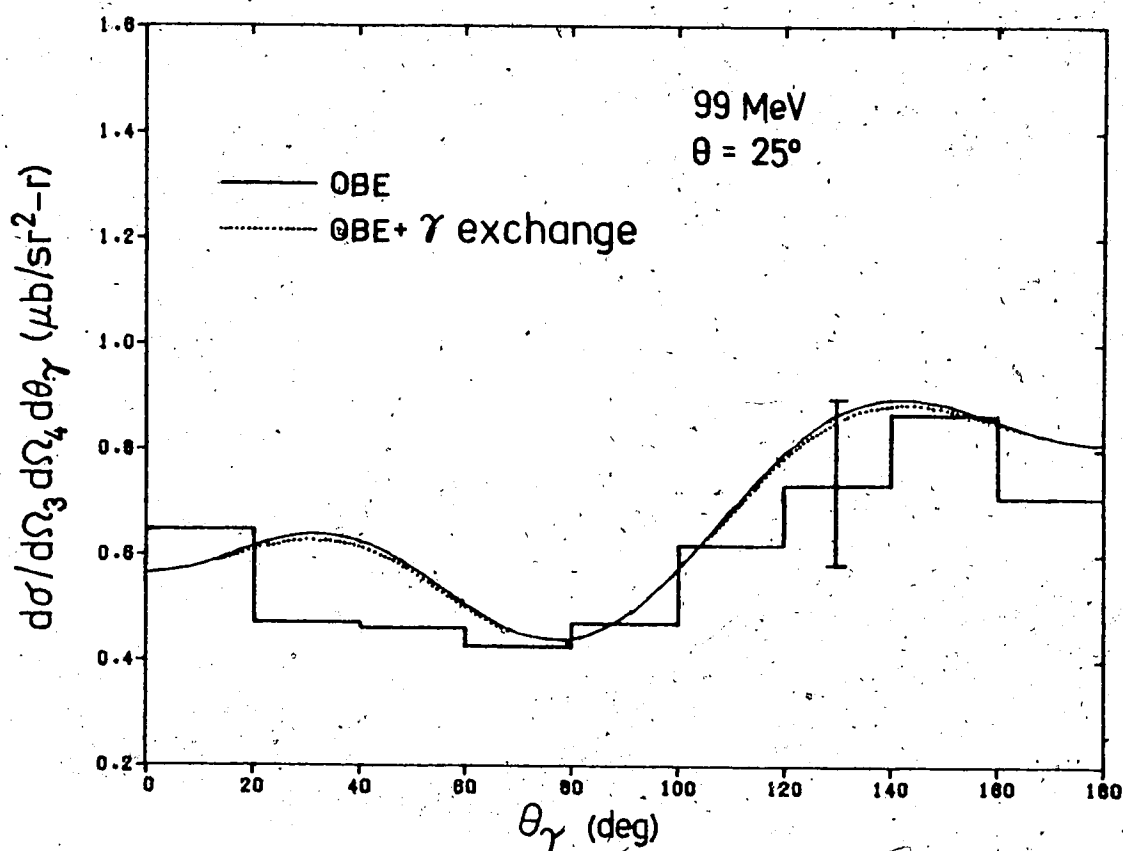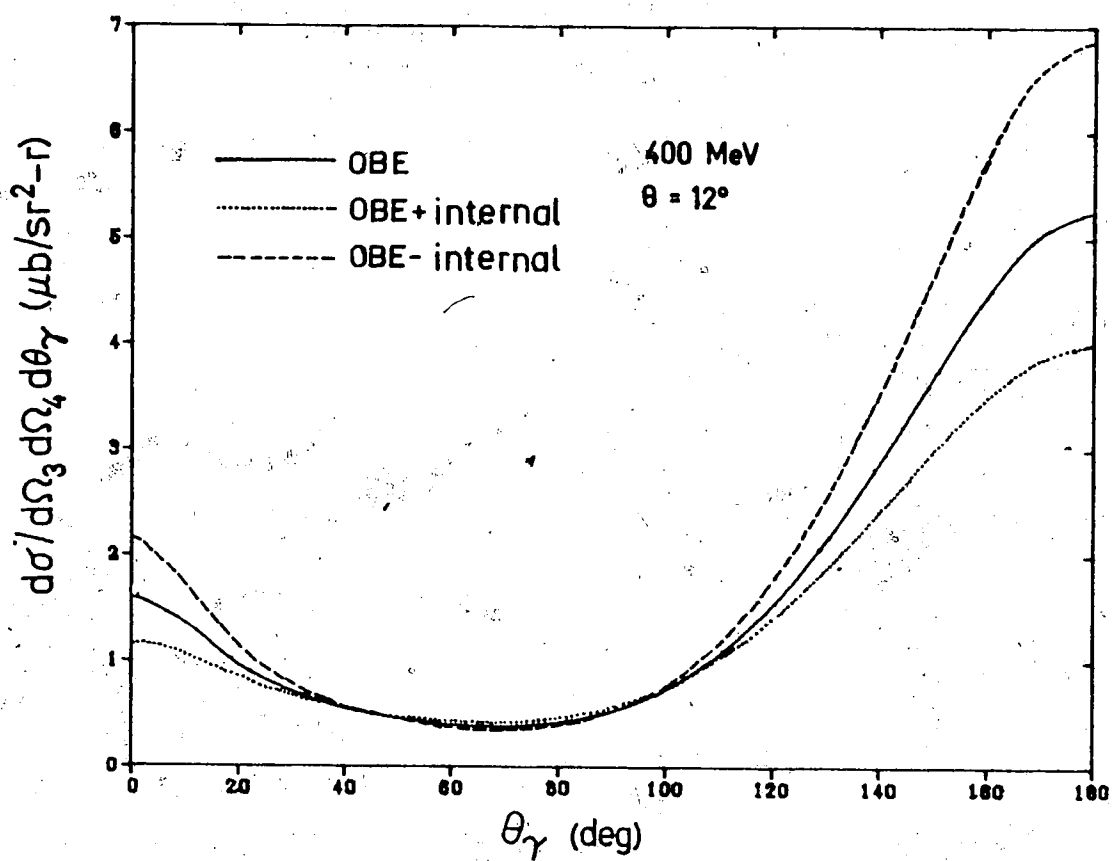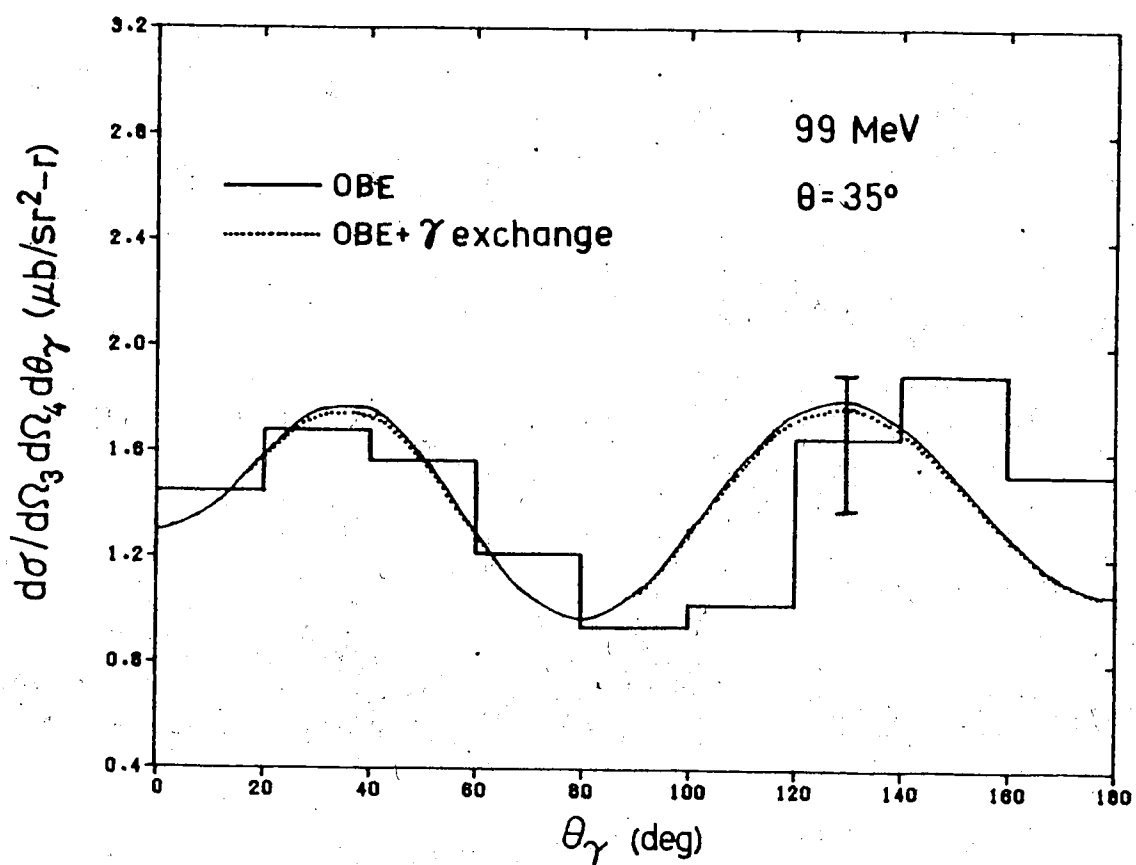
Figure 33. See caption to fig. 18. The curve
marked "OBE + γ exchange" includes
the one-photon-exchange contribution.
The data are from ref. 48.
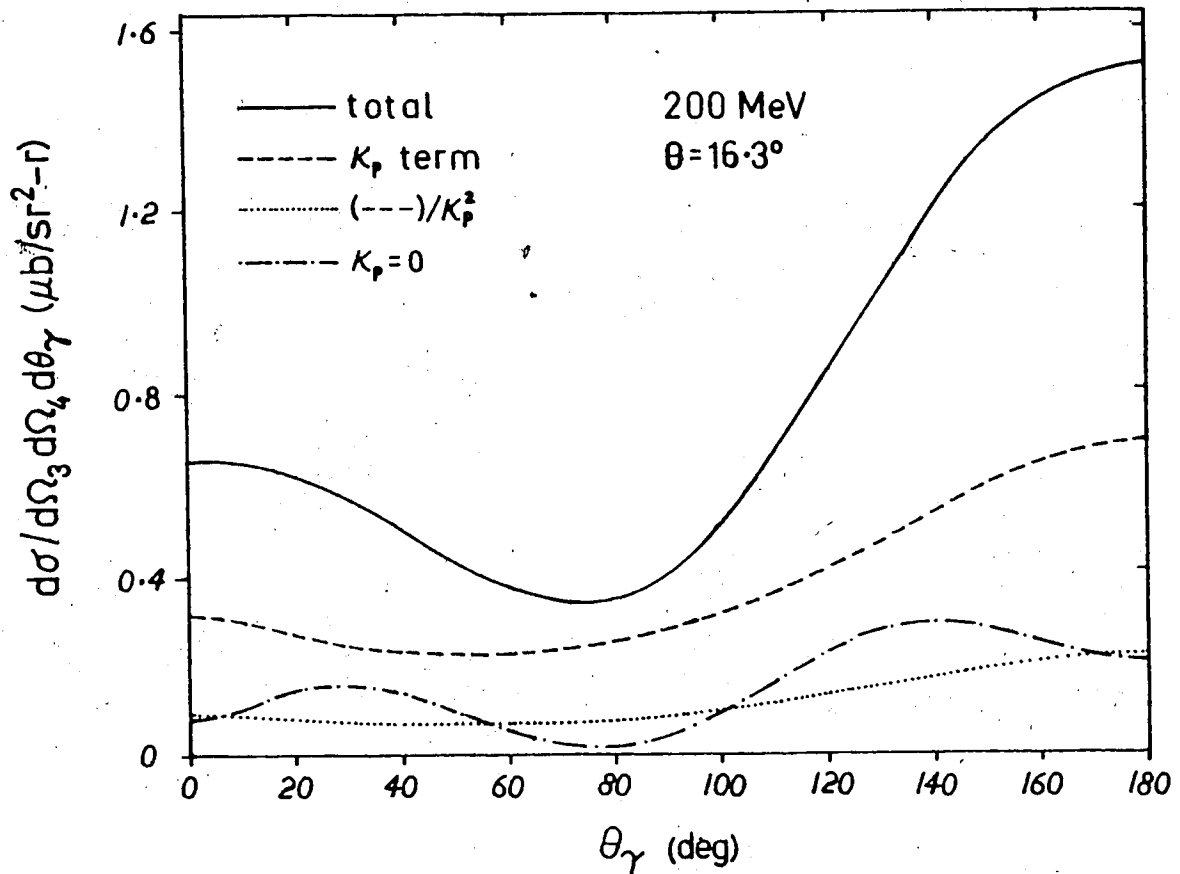
Figure 34. Differential cross section for the Triumf
geometry (T_{lab} = 200 MeV, $\theta_3 = \theta_4$ = 16.3°)
computed from the OBE external-emission model
The plot shows the contribution from the Dirac
coupling (dash-dotted curve), anomalous
magnetic-moment coupling (dashed curve), and
the complete calculation (solid curve). χ_P
is the anomalous moment of the proton. The
dotted curve is the anomalous magnetic
moment cross section divided by χ_P^2 .
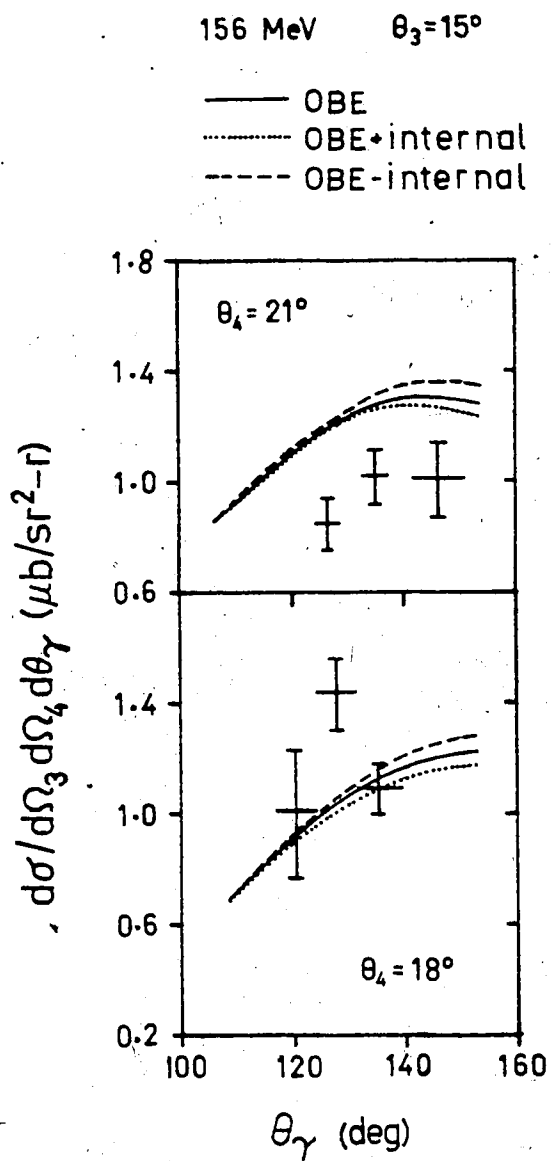
Figure 35. See caption to fig. 18. The
            data points are from ref. 54.

156 MeV $\theta_3 = 15°$

——— OBE
——·— OBE+internal
----- OBE-internal
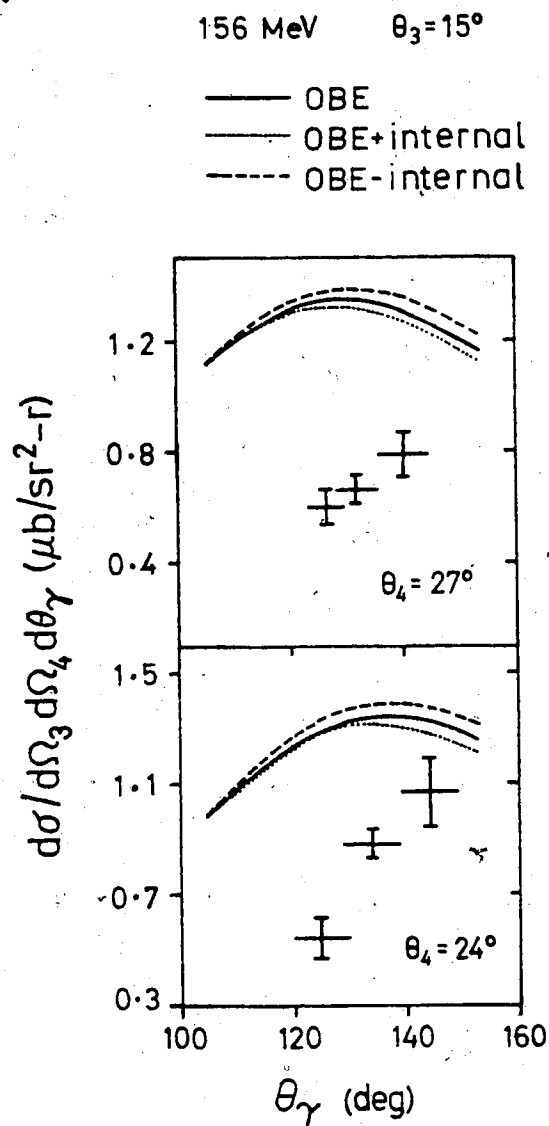
Figure 36. See caption to fig. 18. The
            data points are from ref. 54.
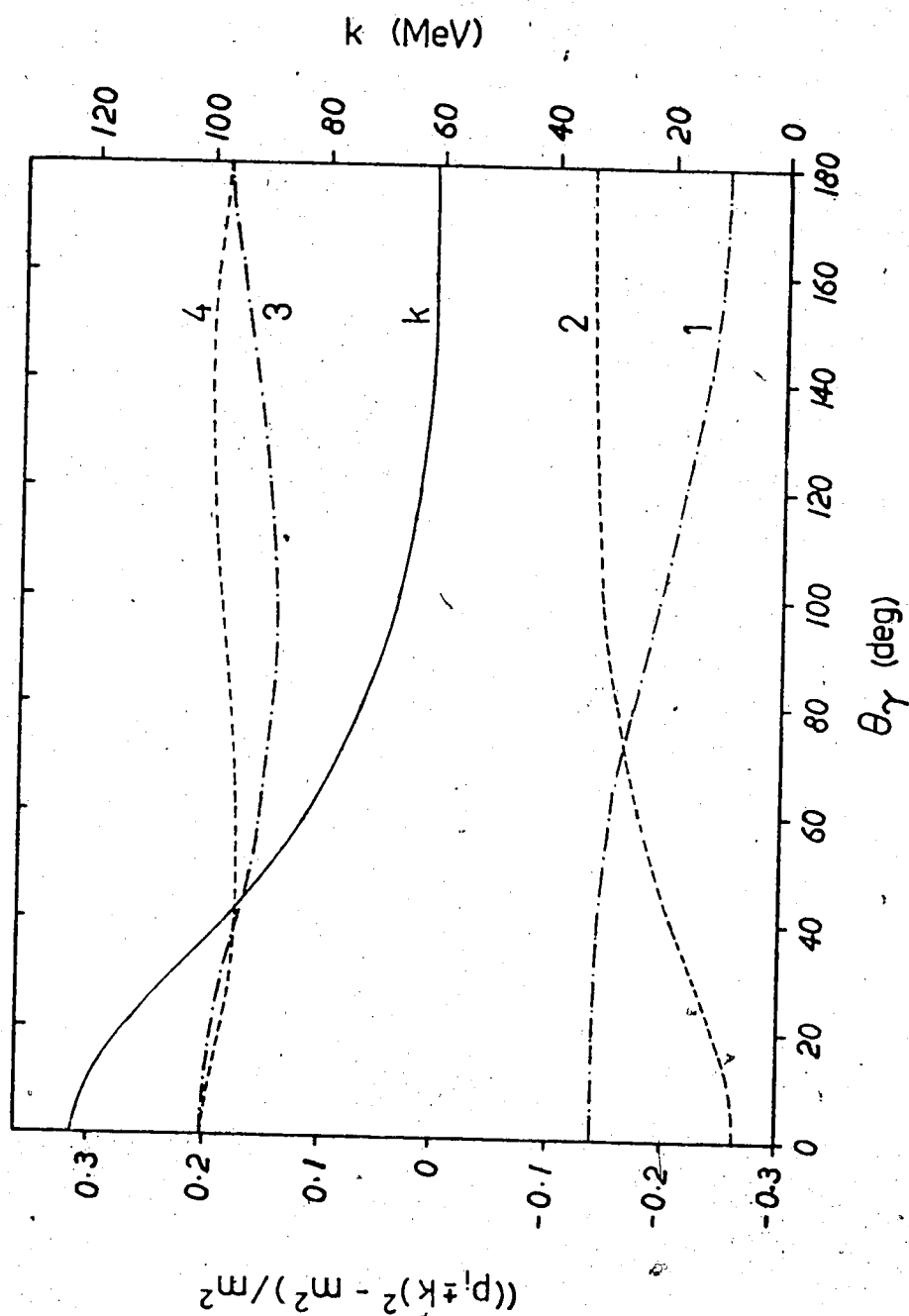
Figure 37. The four off mass-shell parameters, $\left[(p_i - k)^2 - m^2\right]/m^2$, and $\left[(p_i + k)^2 - m^2\right]/m^2$, $i = 1, 2$ and $\left[(p_i + k)^2 - m^2\right]/m^2$, $i = 3, 4$, for the Triumf geometry ($T_{lab} = 200$ MeV, $\theta_3 = \theta_4 = 16.3°$); and the photon momentum, k.

Figure 38. Δ excitation diagram.

(I)

(II)
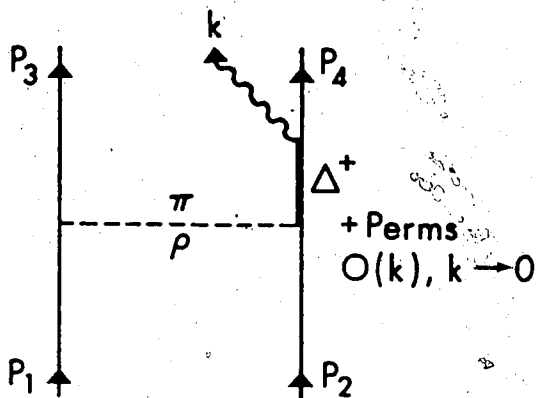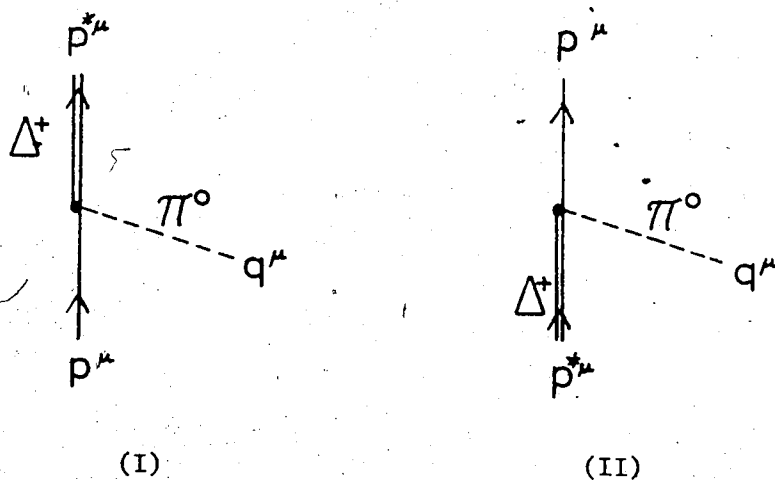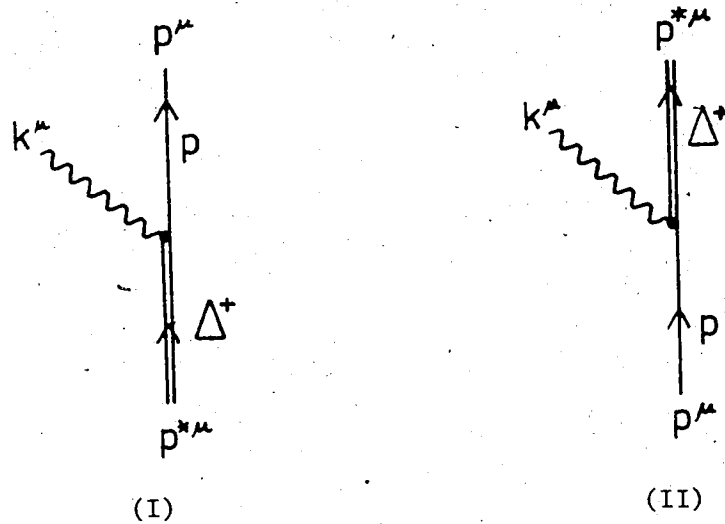
Figure 39. $\Delta p \pi$ vertices.

Figure 40. Δ|pγ vertices.

Figure 41. Δ pγ vertex in the vector-
meson-dominance model.

110
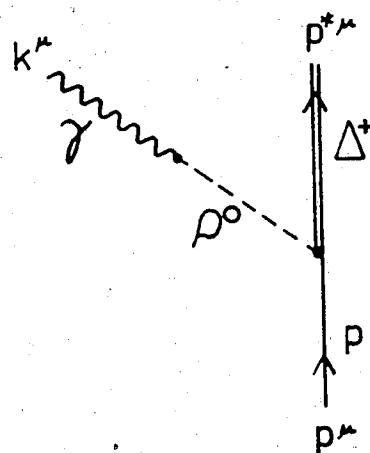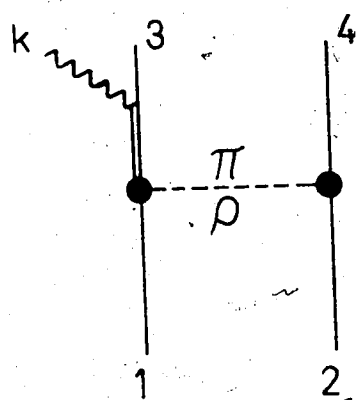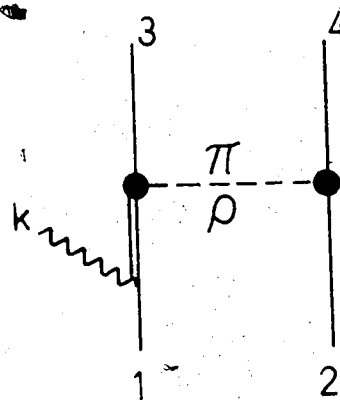
Figure 42. Diagrams corresponding to the
terms in eqs. (6.21) and (6.23).
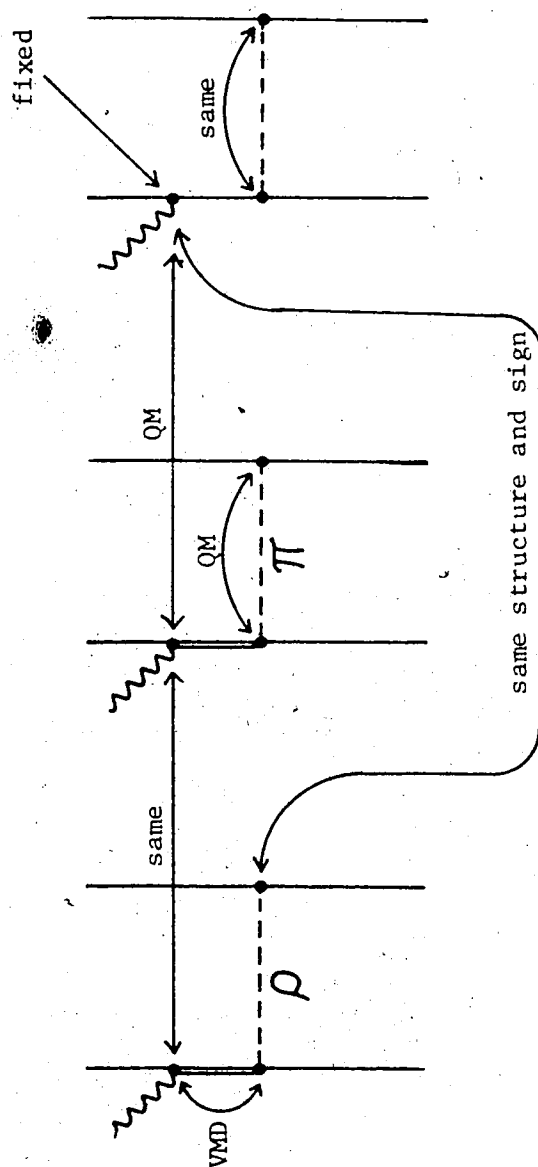
Figure 43. Relationships among the signs of the coupling constants: the arrows join vertices, the product of which has been determined in sign. Abbreviations used: QM - quark model, VMD - vector-meson dominance.
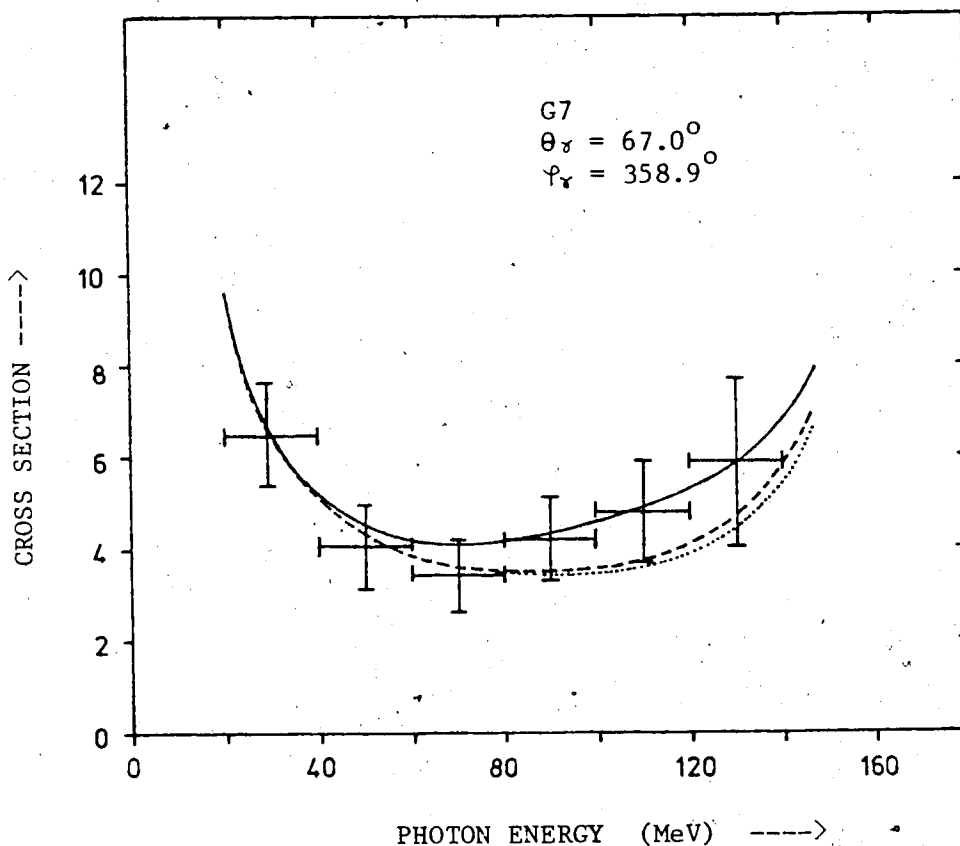
Figure 44. The ppγ differential cross section, $d\sigma/d\Omega_3 d\Omega_\gamma dk$ (nb/sr^2 - MeV), as a function of the photon energy, k, for the geometry of the UCLA experiment $[\,11\,]$ (T_{lab} = 730 MeV, θ_3 = 50.5°, φ_3 = 180°). The The solid curve is the OBE external-emission (nucleon pole) result; the dashed curve includes the Δ-excitation-with-π-exchange diagrams (added coherently); the dotted curve includes the total Δ-excitation effect, as described in chapter 6. The data points are from ref. 11. (The angles α and β of this reference are related to $\bar{\theta}_\gamma$ and $\bar{\varphi}_\gamma$, defined in section 2.1, by $\bar{\theta}_\gamma$ = 360° - α, $\bar{\varphi}_\gamma$ = - β).
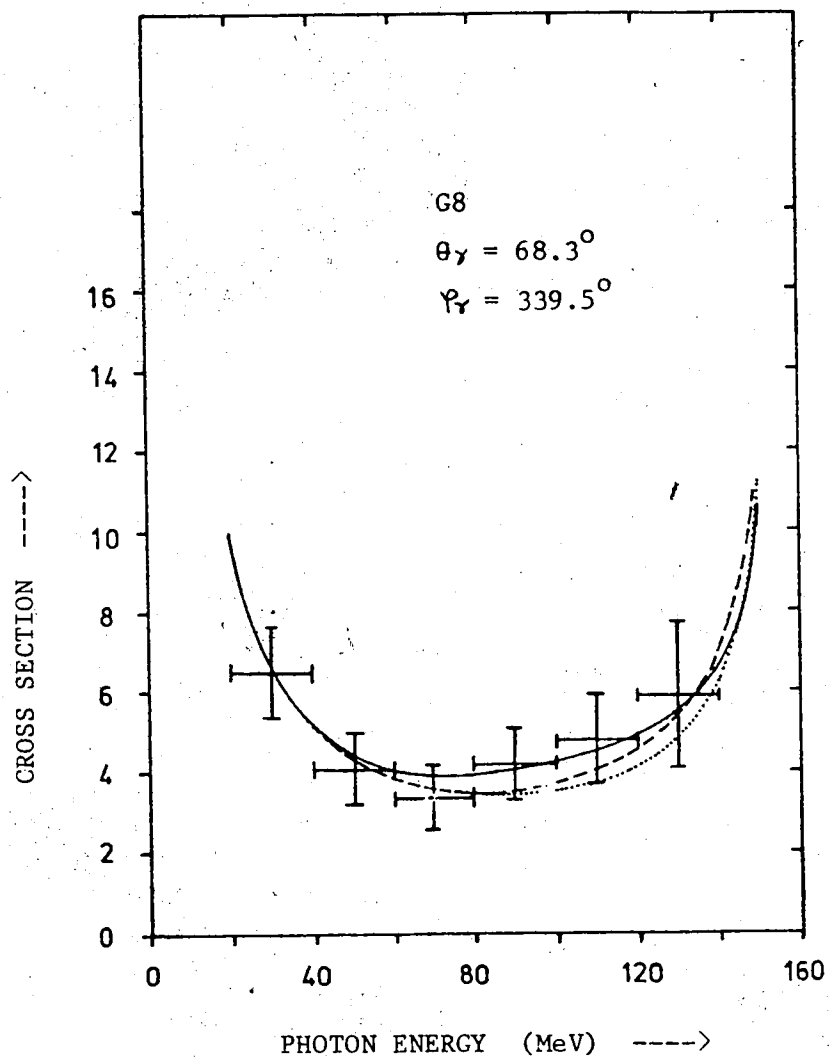
Figure 45.   See caption to fig. 44.
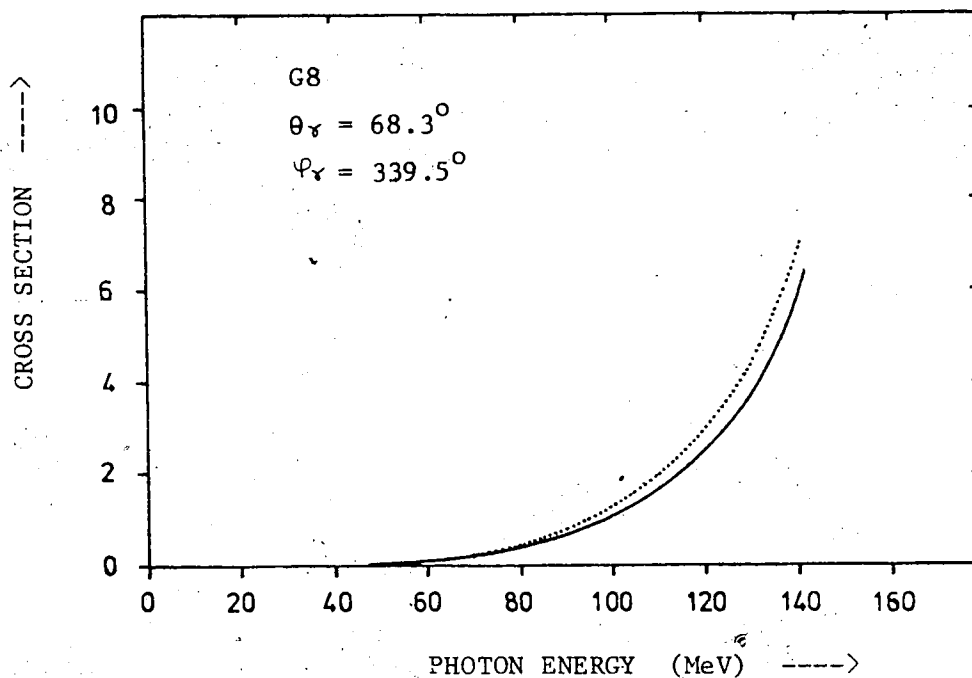
Figure 46. The differential cross section,
$d\sigma/d\Omega_3 d\Omega_\gamma$ dk (nb/sr^2 - MeV)

for the G8 geometry of the UCLA
experiment (see also the caption
to fig. 44) from the Δ excitation
alone. The dotted curve includes
only the π-exchange diagrams while
the solid curve includes the π-
and the ρ-exchange diagrams.
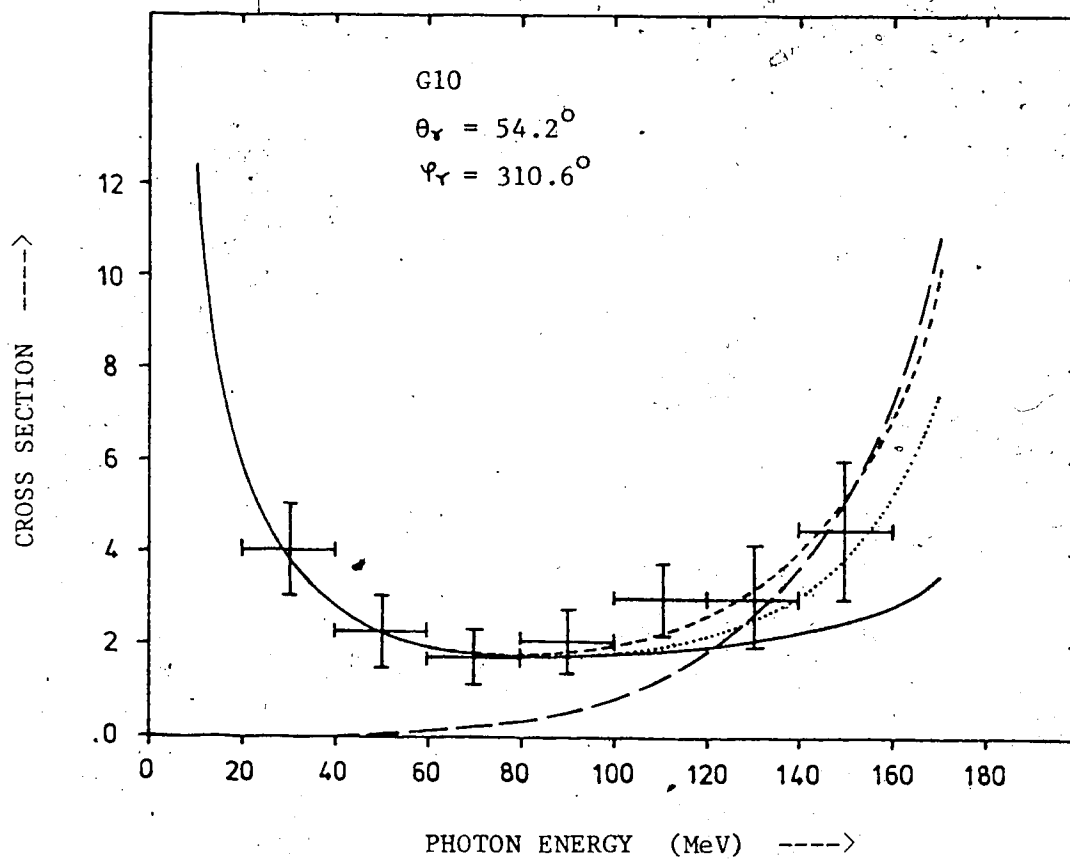
Figure 47. See caption to fig. 44.
The long-dashed curve is the
contribution from the Δ
excitation with π exchange.

G11

$\theta_\gamma = 44.4^\circ$

$\varphi_\gamma = 298.4^\circ$
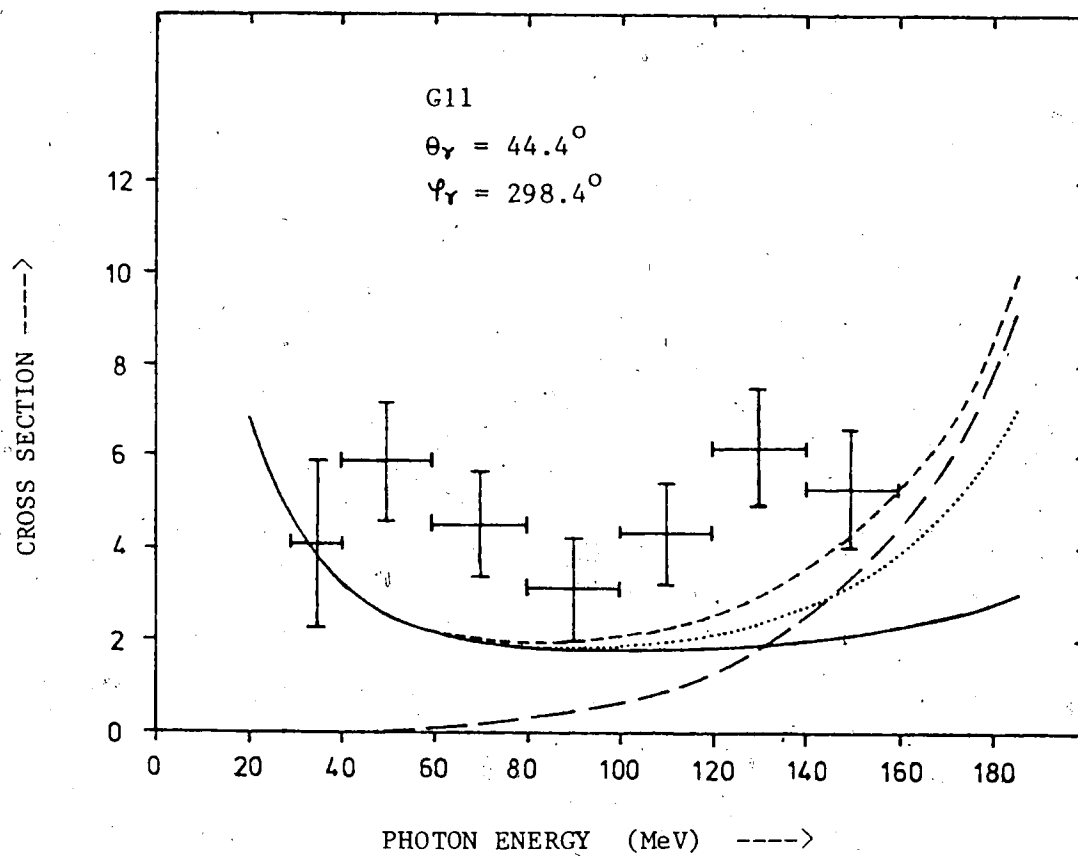
Figure 48. See caption to fig. 44.
The long-dashed curve is the
contribution from the Δ
excitation with π exchange.
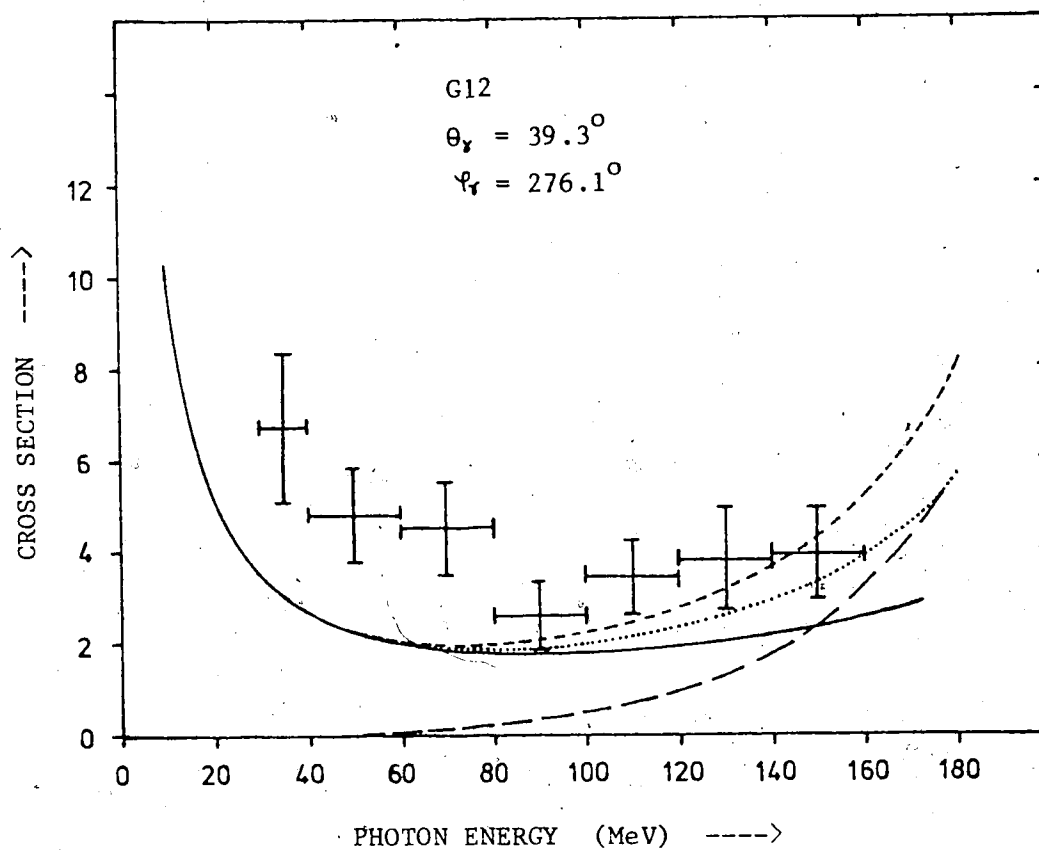
Figure 49. See caption to fig. 44.
The long-dashed curve is the
contribution from the Δ
excitation with π exchange.

$$p^{\mu} = (E, \vec{p}\,)$$

$$q^{\mu} = (\omega, \vec{q}\,)$$

$$p^{*\mu} = (W, \vec{p}^{*})$$
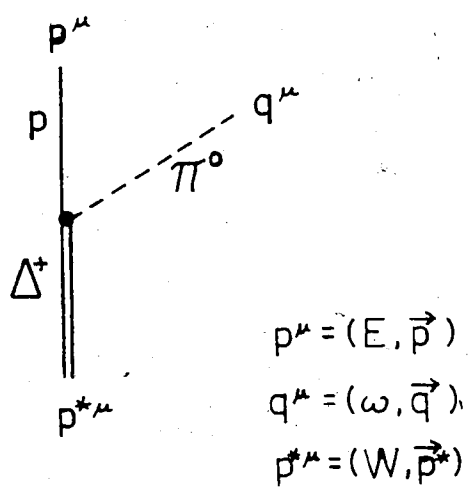
Figure 50. Definition of the kinematic variables
used in appendix F.

REFERENCES

1. J. Ashkin and R.E. Marshak, Phys. Rev. 76(1949)58.

2. M.I. Sobel and A.H. Cromer, Phys. Rev. 132(1963)2698.

3. R. Wilson, Phys. Rev. 85(1952)563.

4a. B. Gottschalk, W.J. Shlaer, and K.H. Wang, Phys. Lett.
        16(1965)294.

4b. B. Gottschalk, W.J. Shlaer, and K.H. Wang, Nucl. Phys.
        75(1966)549.

4c. B. Gottschalk, W.J. Shlaer, and K.H. Wang, Nucl. Phys.
        A94(1967)491.

5. R.E. Warner, Can. J. of Phys. 44(1966)1225.

6. K.W. Rothe, P.F.M. Koehler, and E.H. Thorndike, Phys. Rev.
        Lett. 16(1966)1118.

   K.W. Rothe, P.F.M. Koehler, and E.H. Thorndike, Phys. Rev.
        157(1967)1247.

7. M.K. Liou, Proceedings of the Second International Conference
        on the Nucleon-Nucleon Interaction, Vancouver,
        Canada, June 27-30, 1977, edited by H.W. Fearing
        (American Institute of Physics, 1978), p.516.

8. J.V. Jovanovich, Proceedings of the Second International
        Conference on the Nucleon-Nucleon Interaction,
        Vancouver, Canada, June 27-30, 1977, edited by
        H.W. Fearing (American Institute of Physics, 1978),
        p.451.

9. J.V. Jovanovich, L.G. Greeniaus, J. McKeown, T.W. Millar,
   D.G. Peterson, W.F. Prickett, K.F. Suen, and J.C. Thompson,
        Phys. Rev. Lett. 26(1971)277.

10. J.L. Beveridge, D.P. Gurd, J.G. Rogers, H.W. Fearing,
    A.N. Anderson, J.M. Cameron, L.G. Greeniaus, C.A. Goulding,
    J.V. Jovanovich, C.A. Smith, A.W. Stetz, J.R. Richardson,
    and R. Frascaria, Proceedings of the Second International
        Conference on the Nucleon-Nucleon Interaction,
        Vancouver, Canada, June 27-30, 1977, edited by
        H.W. Fearing (American Institute of Physics,
        1978), p.446.

11. B.M. Nefkens, O.R. Sander, and D.I. Sober, Phys. Rev. Lett. $\underline{38}$(1977)876.

    B.M. Nefkens, Proceedings of the Second International Conference on the Nucleon-Nucleon Interaction, Vancouver, Canada, June 27-30, 1977, edited by H.W. Fearing (American Institute of Physics, 1978), p.477.

12. M.L. Halbert, Proceedings of the Gull Lake Symposium on the Two-Body Force in Nuclei, Sept. 7-10, 1971, edited by S.M. Austin and G.M. Crawley (Plenum, New York, 1973).

13. D. Marker and P. Signell, Phys. Rev. $\underline{185}$(1969)1286.

14. G. Schiffer and D. Drechsel, Nucl. Phys. $\underline{A148}$(1970)286.

15. M.K. Liou and K.S. Cho, Nucl. Phys. $\underline{A160}$(1971)417.

16. M.K. Liou and M.I. Sobel, Ann. Phys. $\underline{72}$(1972)323.

17. L. Heller and M. Rich, Phys. Rev. $\underline{C10}$(1974)479.

18. P. Signell and D. Marker, Phys. Lett. $\underline{28B}$(1968)79.

19. V.R. Brown, Phys. Lett. $\underline{25B}$(1967)506.

    V.R. Brown, Phys. Rev. $\underline{177}$(1969)1498.

    V.R. Brown, Phys. Rev. $\underline{C6}$(1972)1110.

20. D. Drechsel and L.C. Maximon, Ann. Phys. $\underline{49}$(1968)403.

21. I. Duck and W.A. Pearce, Phys. Lett. $\underline{21}$(1966)669.

22. P. Signell, Proceedings of the International Conference on Few Particle Problems and the Nuclear Interaction, Los Angeles, California, 1972, edited by I. Slaus et al (North Holland, Amsterdam, 1973).

23. I. Slaus, J.W. Verba, J.R. Richardson, R.F. Carlson, W.T.H. van Oers, and L.S. August, Phys. Rev. Lett. $\underline{17}$(1966)536.

24. M.I. Sobel, Phys. Rev. $\underline{138}$(1965)B1517.

25. D. Marker and P. Signell, Phys. Rev. $\underline{185}$(1969)1286.

    P. Signell and D. Marker, Phys. Lett. $\underline{26B}$(1968)559.

26. F.E. Low, Phys. Rev. $\underline{110}$(1958)974.

27a. E.M. Nyman, Phys. Lett. $\underline{25B}$(1967)135.

27b. E.M. Nyman, Phys. Rev. 170(1968)1628.

28. H.W. Fearing, Phys. Rev. D7(1973)243.

29. T.H. Burnett and N.M. Kroll, Phys. Rev. Lett. 20(1968)86.

30. H.W. Fearing, Phys. Rev. C6(1972)1136.

31. H.W. Fearing, Proceedings of the Second International Conference on the Nucleon-Nucleon Interaction, Vancouver, Canada, June 27-30, 1977, edited by H.W. Fearing (American Institute of Physics, 1978).

32. R. Baier, H. Kühnelt, and P. Urban, Nucl. Phys. B11(1969)675.

33. J.D. Bjorken and S.D. Drell, Relativistic Quantum Mechanics (McGraw-Hill, 1964).

34. K. Erkelenz, K. Holinde, and R. Machleidt, Phys. Lett. 49B(1974)209.

35. K. Holinde, K. Erkelenz, and R. Alzetta, Nucl. Phys. A194(1972)161.

36. K. Erkelenz, Physics Reports 13(1974)191.

37. K. Holinde and R. Machleidt, Nucl. Phys. A247(1975)495.

38. R.A. Arndt, R.A. Bryan, and M.H. Macgregor, Phys. Lett. 21(1966)314.

39. R.A. Arndt and M.H. Macgregor, Phys. Rev. 141(1966)873.

40. H.P. Stapp, T.J. Ypsilantis, and N. Metropolis, Phys. Rev. 105(1957)302.

41. S. Sawada, T. Ueda, W. Watari, and M. Yonezawa, Prog. Theor. Phys. 28(1962)991.

42. J. Binstock and R.A. Bryan, Phys. Rev.D4(1971)1341.

43. J.A. McClure and S.D. Drell, Nuovo Cimento 37(1965)1638.

44. E.M. Nyman, Nucl. Phys. A154(1970)77.
    E.M. Nyman, Nucl. Phys. A160(1971)517.
    E.M. Nyman, Physics Reports 9(1974)179.

45. A.M. Bincer, Phys. Rev. 118(1960)855.

46.   J.R. Dunning Jr., K.W. Chen, A.A. Cone, G. Hartwig,
      N.F. Ramsey, J.K. Walker, and R. Wilson,   Phys. Rev.
      141(1966)1286.

47.   Y. Ueda,   Phys. Rev. 145(1965)1214.

48a. F. Sannes, J. Trischuk, D.G. Stairs,   Phys. Rev. Lett.
      21(1968)1474.

48b. F. Sannes, J. Trischuk, D.G. Stairs,   Nucl. Phys. A146(1970)
      438.

49.   I. Blomqvist and J.M. Laget,   Nucl. Phys. A280(1977)405.

50.   H. Pilkuhn, W. Schmidt, A.D. Martin, C. Michael, F. Steiner,
      B.R. Martin, M.M. Nagels, and J.J. de Swart,   Nucl. Phys.
      B65(1973)460.

51.   P. Herczeg and P. Singer,   Phys. Rev. D11(1975)611.

52.   S. Okubo,   Phys. Lett. 5(1963)165.
      G. Zweig, CERN report 8419/TH412, 1964.

53.   Particle Data Group,   Phys. Lett. 75B(1978)No.1.

54.   A. Willis, V. Comparat, R. Frascaria, N. Marty, M. Morlet,
      N. Willis,   Phys. Rev. Lett. 28(1972)1063.

      M. Morlet et al.,   Proceedings of the International Con-
            ference on Few Particle Problems and the
            Nuclear Interaction, Los Angeles, California,
            1972, edited by I. Slaus et al (North Holland,
            Amsterdam, 1973).

55.   L.S. Celenza, M.K. Liou, M.I. Sobel,   Phys. Rev. C8(1973)
            838.

56.   V.R. Brown,   Phys. Rev. C6(1972)1110.

57.   M.G. Olsson, L. Turner, and E.T. Osypowski,   Phys. Rev.
            D7(1973)3444.

58.   M. Gourdin and Ph. Salin,   Nuovo Cimento 27(1963)309 and
            ibid. p.193.

59.   F.A. Berends and A. Donnachie,   Nucl. Phys. B84(1975)342.

60.   M.G. Olsson and E.T. Osypowski,   Nucl. Phys. B87(1975)399.

61.   R.D. Peccei,   Phys. Rev. 181(1969)1902.

62.   Particle Data Group,   Rev. Mod. Phys. 48(1976)No.2, part II.

63. L. Tiator, H.J. Weber, and D. Drechsel, Nucl. Phys.
        A306(1978)468.

64. A.M. Green, J.A. Niskanen, Nucl. Phys. A249(1975)493.

65. M.G. Olsson, Nucl. Phys. B78(1974)55.

66. H.W. Fearing, Proceedings of the Eighth International
        Conference on Few Body Systems and Nuclear
        Forces, Graz, Austria, August 24-30, 1978,
        edited by H. Zingl et al (Springer-Verlag,
        Berlin, Heidelberg, New York, 1978), vol. 1,
        p.94.

67. T. Hamada and I.D. Johnston, Nucl. Phys. 34(1962)382.

68. R.V. Reid, Ann. Phys. 50(1968)411.

69. R. Bryan and B.L. Scott, Phys. Rev. 177(1969)1435.

70. F. Tabakin, Ann. Phys. 30(1964)51.

71. R.A. Arndt, R.H. Hackman, and L.D. Roper, Phys. Rev.
        C9(1974)555.

72. W. Rarita and J. Schwinger, Phys. Rev. 60(1941)61; or
        see for e.g. H. Pilkuhn, The Interactions of
        Hadrons (North-Holland, Amsterdam, 1967).

73. A.N. Kamal and A. Szyjewicz, Nucl. Phys. A285(1977)397.

74. A. Szyjewicz and A.N. Kamal, Proceedings of the Second
        International Conference on the Nucleon-
        Nucleon Interaction, Vancouver, Canada,
        June 27-30, 1977, edited by H.W. Fearing
        (American Institute of Physics, 1978),
        p.502.

     A. Szyjewicz and A.N. Kamal, Proceedings of the Eighth
        International Conference on Few Body Systems
        and Nuclear Forces, Graz, Austria, August
        24-30, 1978, edited by H. Zingl et al
        (Springer-Verlag, Berlin, Heidelberg, New
        York, 1978), vol. 1, p.88.

75. L. Heller, Proceedings of the Eighth International
        Conference on Few Body Systems and Nuclear
        Forces, Graz, Austria, August 24-30, 1978,
        edited by H. Zingl et al (Springer-Verlag,
        Berlin, Heidelberg, New York, 1978), vol. 2,
        p.68.

75. (contd.)
M. Moravcsik, Proceedings of the Second International Con-
ference on the Nucleon-Nucleon Interaction,
Vancouver, Canada, June 27-30, 1977, edited by
H.W. Fearing (American Institute of Physics,
1978), p.515.

M. Moravcsik, Phys. Lett. 65B (1976)409.

76. R.A. Arndt and M.H. MacGregor, Phys. Rev. 141(1966)873.

The equation of momentum conservation along the beam axis (from eqs. (2.9) and (2.12)):

$$p_3 \cos\theta_3 + p_4 \cos\theta_4 + (E_{tot} - E_3 - E_4)\cos\theta_\gamma = p_1 \qquad (A.1)$$

is solved here for $p_4 = p_4(p_3, \theta_\gamma)$.

Eq. (A.1) can be rewritten as

$$p_4 \cos\theta_4 + A = (p_4^2 + m^2)^{\frac{1}{2}} \cos\theta_\gamma \qquad (A.2)$$

where $A = (E_{tot} - E_3)\cos\theta_\gamma - (p_1 - p_3\cos\theta_3)$

Squaring (A.2) gives the quadratic equation

$$p_4^2(\cos^2\theta_4 - \cos^2\theta_\gamma) + 2p_4 A \cos\theta_4 + (A^2 - m^2\cos^2\theta_\gamma) = 0 \qquad (A.3)$$

When $\cos^2\theta_4 = \cos^2\theta_\gamma$ the solution is

$$p_4 = -\frac{(A^2 - m^2\cos^2\theta_\gamma)}{2A\cos\theta_4} \qquad (A.4)$$

when $\cos^2\theta_4 \neq \cos^2\theta_\gamma$ (A.3) has the two roots

$$p_4 = \frac{-A\cos\theta_4 \pm \sqrt{\Delta}}{\cos^2\theta_4 - \cos^2\theta_\gamma} \qquad (A.5)$$

where the discriminant

$$\Delta = A^2\cos^2\theta_4 - (\cos^2\theta_4 - \cos^2\theta_\gamma)(A^2 - m^2\cos^2\theta_\gamma)$$

$$= \cos^2\theta_\gamma\left[A^2 + m^2(\cos^2\theta_4 - \cos^2\theta_\gamma)\right]$$

The root with the lower sign is in fact an extraneous root formed when (A.2) was squared. To demonstrate this reexpress the solutions (A.5) in terms of p_4 using eq. (A.1); this must

lead to an identity (this procedure is similar to substituting the solutions back into eq. (A.1)). We find

$$A = E_4 \cos\theta_r - p_4 \cos\theta_4$$

$$\Delta = \cos^2\theta_r \left(E_4 \cos\theta_4 - p_4 \cos\theta_r \right)^2$$

$$p_4 = \left(-A \cos\theta_4 \pm \cos\theta_r A \right) / \left(\cos^2\theta_4 - \cos^2\theta_r \right)$$

$$= \begin{bmatrix} p_4 & \text{upper sign} \\[2ex] \dfrac{-2 E_4 \cos\theta_4 \cos\theta_r + p_4 \left(\cos^2\theta_4 + \cos^2\theta_r \right)}{\cos^2\theta_4 - \cos^2\theta_r} & \begin{array}{l}\text{lower} \\ \text{sign}\end{array} \end{bmatrix}$$

This shows that the root with the lower sign is not a solution of (A.1). The complete solution of (A.1) is

$$p_4 = \begin{bmatrix} \dfrac{-\left(A^2 - m^2 \cos^2\theta_r \right)}{2 A \cos\theta_4} & \text{for} \quad \cos^2\theta_r = \cos^2\theta_4 \\[3ex] \dfrac{-A \cos\theta_4 + \cos\theta_r \left[A^2 + m^2 \left(\cos^2\theta_4 - \cos^2\theta_r \right) \right]^{\frac{1}{2}}}{\cos^2\theta_4 - \cos^2\theta_r} & \\[2ex] & \text{for} \quad \cos^2\theta_r \neq \cos^2\theta_4 \end{bmatrix}$$

$$\text{(A.6)}$$

Appendix B

It is shown here that, in coplanar geometry, when

$$\frac{P_1}{m} \cdot \frac{1}{\sin(\theta_3 + \theta_4)} \ll 1 \qquad (B.1)$$

the kinematical locus in the $T_3 - T_4$ plane is an ellipse.

Condition (B.1) implies that we may use non-relativistic kinematics:

$$P_3 = \frac{1}{\sin\theta_s} \left(p_1 \sin\theta_4 - k \sin\theta_{4\gamma} \right) \qquad (B.2)$$

$$P_4 = \frac{1}{\sin\theta_s} \left(p_1 \sin\theta_3 - k \sin\theta_{3\gamma} \right) \qquad (B.3)$$

$$k = \left(p_1^2 - p_3^2 - p_4^2 \right) / (2m) \qquad (B.4)$$

where $\theta_s = \theta_3 + \theta_4$, $\theta_{3\gamma} = \theta_3 - \theta_\gamma$

$$\theta_{4\gamma} = \theta_4 + \theta_\gamma$$

Eq. (B.4) implies $k < p_1 \dfrac{p_1}{m} \ll p_1$

Therefore as a first approximation we may set k to zero, and get an improved solution by iterating eqs. (B.2) to (B.4)

i.e. $\qquad k^{(0)} = 0 \qquad (B.5)$

$$P_3^{(0)} = \frac{1}{\sin\theta_s} \, p_1 \sin\theta_4 \qquad (B.6)$$

$$P_4^{(0)} = \frac{1}{\sin\theta_s} \, p_1 \sin\theta_3 \qquad (B.7)$$

127

$$k^{(1)} = \frac{P_1^2}{2m}\left(1 - \frac{\sin^2\theta_3 + \sin^2\theta_4}{\sin^2\theta_5}\right) = T_1 A \qquad (B.8)$$

where
$$A = 1 - \frac{\sin^2\theta_3 + \sin^2\theta_4}{\sin^2\theta_5}$$

$$P_3^{(1)} = \frac{1}{\sin\theta_5}\left(p_1\sin\theta_4 - T_1 A \sin\theta_{4r}\right) \qquad (B.9)$$

$$= P_1\left(\frac{\sin\theta_4}{\sin\theta_5} - \frac{P_1}{m}\frac{1}{\sin\theta_5}\frac{A}{2}\sin\theta_{4r}\right)$$

$$P_4^{(1)} = P_1\left(\frac{\sin\theta_3}{\sin\theta_5} - \frac{P_1}{m}\frac{1}{\sin\theta_5}\frac{A}{2}\sin\theta_{3r}\right) \qquad (B.10)$$

$$k^{(2)} = \frac{P_1^2}{2m}\left\{1 - \frac{1}{\sin^2\theta_5}\left[\sin^2\theta_3 + \sin^2\theta_4\right.\right.$$

$$- \frac{P_1}{m}A\left(\sin\theta_3\sin\theta_{3r} + \sin\theta_4\sin\theta_{4r}\right)\Big]$$

$$+ \frac{P_1^2}{4m^2}A^2\left(\sin^2\theta_{3r} + \sin^2\theta_{4r}\right)\Bigg\}$$

$$= \frac{P_1^2}{2m}\left[A + \frac{P_1}{m}\frac{1}{\sin\theta_5}AB - \frac{P_1^2}{m^2}\frac{A^2}{4}C\right] \qquad (B.11)$$

where
$$B = \left(\sin\theta_3\sin\theta_{3r} + \sin\theta_4\sin\theta_{4r}\right)/\sin\theta_5$$

$$C = \left(\sin^2\theta_{3r} + \sin^2\theta_{4r}\right)/\sin^2\theta_5$$

$$P_3^{(2)} = P_1\left[\frac{\sin\theta_4}{\sin\theta_5} - \frac{P_1}{m}\frac{1}{\sin\theta_5}\frac{A}{2}\sin\theta_{4r}\right.$$

$$\left. - \frac{P_1^2}{m^2}\frac{1}{\sin^2\theta_5}\frac{AB\sin\theta_{4r}}{2} + O\left(\frac{P_1^3}{m^3}\right)\right] \qquad (B.12)$$

$$P_4^{(2)} = P_1 \left[\frac{\sin\theta_3}{\sin\theta_s} - \frac{P_1}{m} \frac{1}{\sin\theta_s} \frac{A\sin\theta_{3\gamma}}{2} \right.$$

$$\left. - \frac{P_1^2}{m^2} \frac{1}{\sin^2\theta_s} \frac{AB\sin\theta_{3\gamma}}{2} + O\left(\frac{P_1^3}{m^3}\right) \right] \tag{B.13}$$

$$k^{(3)} = \frac{P_1^2}{2m} A \left\{ 1 + \frac{P_1}{m} \frac{1}{\sin\theta_s} B + \frac{P_1^2}{m^2} \frac{1}{\sin^2\theta_s} \right.$$

$$\left. \times \left[B^2 - (\sin^2\theta_{3\gamma} + \sin^2\theta_{4\gamma}) \frac{A}{4} \right] + O\left(\frac{P_1^3}{m^3} \frac{1}{\sin^3\theta_s}\right) \right\} \tag{B.14}$$

The iteration evidently generates a power-series expansion in $\frac{P_1}{m} \frac{1}{\sin\theta_s}$ for p_3, p_4, k^*. Therefore, when condition (B.1) is satisfied the iteration is convergent. Equations (B.12), (B.13), (B.14) give the first three terms in the expansions. The kinetic energies T_3, T_4 are:

$$T_3 = \frac{p_3^2}{2m} = \frac{P_1^2}{2m} \left[\frac{\sin^2\theta_4}{\sin^2\theta_s} - \frac{P_1}{m} \frac{1}{\sin\theta_s} \frac{A\sin\theta_4 \sin\theta_{4\gamma}}{\sin\theta_s} \right.$$

$$\left. + O\left(\frac{P_1^2}{m^2} \frac{1}{\sin^2\theta_s}\right) \right] \tag{B.15}$$

$$T_4 = \frac{P_1^2}{2m} \left[\frac{\sin^2\theta_3}{\sin^2\theta_s} - \frac{P_1}{m} \frac{1}{\sin\theta_s} \frac{A\sin\theta_3 \sin\theta_{3\gamma}}{\sin\theta_s} \right.$$

$$\left. + O\left(\frac{P_1^2}{m^2} \frac{1}{\sin^2\theta_s}\right) \right] \tag{B.16}$$

---

*The term $\frac{1}{\sin\theta_s}$ is included in the expansion parameter because for small θ_s high-order terms can become large, even though $\frac{P_1}{m}$ is small.

Keeping the first two terms in the expansions B.15, B.16 the

locus $T_3 = T_3(\theta_\gamma)$

$T_4 = T_4(\theta_\gamma)$ is now shown to be an ellipse by expressing

it in the standard form $\dfrac{x^2}{a^2} + \dfrac{y^2}{b^2} = 1$.

Let

$$y = T_3 - T_3^{(0)} = -D \sin\theta_4 \sin\theta_{4\gamma} \qquad (B.17)$$

$$x = T_4 - T_4^{(0)} = -D \sin\theta_3 \sin\theta_{3\gamma} \qquad (B.18)$$

where $D = \dfrac{P_1^2}{2m} \quad \dfrac{P_1}{m} \quad \dfrac{A}{\sin^2\theta_s}$

$$y = -D\left(\sin^2\theta_4 \cos\theta_\gamma + \sin\theta_4 \cos\theta_4 \sin\theta_\gamma\right) \qquad (B.17)$$

$$x = -D\left(\sin^2\theta_3 \cos\theta_\gamma - \sin\theta_3 \cos\theta_3 \sin\theta_\gamma\right) \qquad (B.18)$$

$$\therefore \quad \sin^2\theta_3\, y - \sin^2\theta_4\, x = -D\sin\theta_\gamma\left(\sin^2\theta_3 \sin\theta_4 \cos\theta_4 \right.$$
$$\left. + \sin^2\theta_4 \sin\theta_3 \cos\theta_3\right) \qquad (B.19)$$
$$= -D \sin\theta_\gamma \sin\theta_3 \sin\theta_4 \sin\theta_s$$

$$\sin\theta_3 \cos\theta_3\, y + \sin\theta_4 \cos\theta_4\, x$$
$$= -D\cos\theta_\gamma\left(\sin\theta_3 \cos\theta_3 \sin^2\theta_4 + \sin\theta_4 \cos\theta_4 \sin^2\theta_3\right) \qquad (B.20)$$
$$= -D\cos\theta_\gamma \sin\theta_3 \sin\theta_4 \sin\theta_s$$

Therefore from (B.19):
$$\cos^2\theta_\gamma = 1 - \frac{(\sin^2\theta_3\, y - \sin^2\theta_4\, x)}{D^2 \sin^2\theta_3 \sin^2\theta_4 \sin^2\theta_s}$$

and

$$\left(\sin\theta_3 \cos\theta_3\, y + \sin\theta_4 \cos\theta_4\, x\right)^2 = D^2 \sin^2\theta_3 \sin^2\theta_4 \sin^2\theta_s$$
$$- \left(\sin^2\theta_3\, y - \sin^2\theta_4\, x\right)^2$$

$$\therefore x^2 (\sin^2\theta_4 \cos^2\theta_4 + \sin^4\theta_4) + y^2(\sin^2\theta_3 \cos^2\theta_3 + \sin^4\theta_3)$$

$$+ 2xy(\sin\theta_3 \cos\theta_3 \sin\theta_4 \cos\theta_4 - \sin^2\theta_3 \sin^2\theta_4)$$

$$= D^2 \sin^2\theta_3 \sin^2\theta_4 \sin^2\theta_5$$

OR

$$x^2 \sin^2\theta_4 + y^2 \sin^2\theta_3 + 2xy \sin\theta_3 \sin\theta_4 \cos\theta_5$$
$$= D^2 \sin^2\theta_3 \sin^2\theta_4 \sin^2\theta_5$$

$$(B.21)$$

define rotated coordinates x', y'

$$x = x' \cos\delta - y' \sin\delta$$

$$y = x' \sin\delta + y' \cos\delta$$
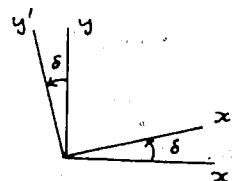
and choose the angle δ so that the coefficient of x'y' is zero.

$$\therefore \quad -2 \cos\delta \sin\delta \sin^2\theta_4 + 2 \sin\delta \cos\delta \sin^2\theta_3$$
$$+ 2(\cos^2\delta - \sin^2\delta)\sin\theta_3 \sin\theta_4 \cos\theta_5 = 0$$

i.e.

$$\cot 2\delta = (\sin^2\theta_4 - \sin^2\theta_3)/(2 \sin\theta_3 \sin\theta_4 \cos\theta_5) \quad (B.22)$$

In the rotated system the locus is

$$x'^2 (\cos^2\delta \sin^2\theta_4 + \sin^2\delta \sin^2\theta_3 + \sin 2\delta \sin\theta_3 \sin\theta_4 \cos\theta_5)$$
$$+ y'^2 (\cos^2\delta \sin^2\theta_3 + \sin^2\delta \sin^2\theta_4 - \sin 2\delta \sin\theta_3 \sin\theta_4 \cos\theta_5)$$
$$= D^2 \sin^2\theta_3 \sin^2\theta_4 \sin^2\theta_5 \quad (B.23)$$

Therefore, the ellipse is centred at $T_4^{(o)}$, $T_3^{(o)}$; is rotated by angle δ given by (B.22); and has semi-major, semi-minor axes:

$$a = \frac{D \sin\theta_3 \sin\theta_4 \sin\theta_5}{(\cos^2\delta \sin^2\theta_4 + \sin^2\delta \sin^2\theta_3 + \sin 2\delta \sin\theta_3 \sin\theta_4 \cos\theta_5)^{1/2}} \quad (B.24)$$

$$b = \frac{D \sin \theta_3 \sin \theta_4 \sin \theta_5}{(\cos^2 \delta \sin^2 \theta_3 + \sin^2 \delta \sin^2 \theta_4 - \sin 2\delta \sin \theta_3 \sin \theta_4 \cos \theta_5)^{1/2}} \qquad (B.25)$$

respectively. Note that as $\theta_s \to \frac{\pi}{2}$ (elastic limit) the eccentricity goes to zero; when $\theta_s = \frac{\pi}{2}$, $a = b = 0$. If we want $a > b$, then (B.24) and (B.25) imply that

$$\pi \leq 2\delta \leq 0 \qquad (B.26)$$

This defines the branch of the cot function in (B.22)*.

For the symmetric case, $\theta_3 = \theta_4 = \theta$, we have

$$A = \frac{\cos 2\theta}{2 \cos^2 \theta} \qquad D \sin \theta_3 \sin \theta_4 \sin \theta_5 = \frac{T_1}{4} \frac{p_1}{m} \frac{\cos 2\theta}{\cos^2 \theta} \qquad (B.27)$$

$$a = \frac{T_1}{2\sqrt{2}} \frac{p_1}{m} \frac{\cot 2\theta}{\sin \theta \cos \theta} \qquad (B.28)$$

$$b = \frac{T_1}{2\sqrt{2}} \frac{p_1}{m} \frac{\cot 2\theta}{\cos^2 \theta} \qquad (B.29)$$

$$b/a = \tan \theta \qquad (B.30)$$

i.e. the eccentricity increases as the opening angle θ decreases; for θ near $\frac{\pi}{4}$ the ellipse is nearly a circle (as noted before), and as $\theta \to 0$ (subject to condition B.1) the ellipse degenerates to a line segment.

---

*The other distinct solution of (B.22) is a $90°$ rotation with respect to this solution.

Appendix C

A Summary of the OBE Model of N-N Scattering of

Erkelenz, Holinde, Machleidt /347

EHM take the Feynman amplitude corresponding to the exchange of a number of mesons as the Born approximation to the full T matrix. Specifically, if $\vec{P}, \vec{P}'$ is the initial, final CM momentum of the nucleons, $V_{OBE}(\vec{P}', \vec{P})$ is the relativistic OBE amplitude, and $V(\vec{P}', \vec{P})$ the p-space potential, then the authors set

$$V(\vec{P}', \vec{P}) = \left(\frac{m}{E_{P'}}\right)^{1/2} V_{OBE}(\vec{P}', \vec{P}) \left(\frac{m}{E_P}\right)^{1/2} \tag{C.1}$$

The T matrix is obtained by putting $V(\vec{P}', \vec{P})$ into the Lippmann-Schwinger equation (LSE):

$$T(\vec{P}', \vec{P}) = V(\vec{P}', \vec{P}) - \frac{m}{(2\pi)^3} \int d^3q \, V(\vec{P}', \vec{q}) \frac{1}{\vec{q}^2 - \vec{P}^2 - i\epsilon} T(\vec{q}, \vec{P}) \tag{C.2}$$

In elastic scattering $\vec{P}'^2 = \vec{P}^2 = \frac{1}{4} s$

The LSE is solved in the helicity representation, $|JM\lambda_1\lambda_2\rangle$, then transformed to the $|JMLS\rangle$ representation. The phase shifts are then obtained from elastic unitarity.

The model parameters are determined to give the correct deutron binding energy and a best fit to the nucleon phase-shift analysis up to 330 MeV. The authors list the predicted phase shifts, low energy and deutron parameters, and nuclear-matter parameters. With the exception of the deutron D-state probability, which is about a factor of 2 too large, the agreement with experiment is good.

The meson-nucleon couplings used by EHM (in writing down V_{OBE}) are, for scalar, pseudo-scalar and vector mesons respectively

$$\mathcal{L}_s = g_s \, \overline{\psi} \psi \, \phi^{(s)}$$

$$\mathcal{L}_{ps} = g_{ps} \, \overline{\psi} \, i\gamma_5 \psi \, \phi^{(ps)} \tag{C.3}$$

$$\mathcal{L}_v = g_v \, \overline{\psi} \gamma^\mu \psi \, \phi^{(v)}_\mu + \frac{f_v}{4m} \overline{\psi} \, \sigma^{\mu\nu} \psi \, (\partial_\mu \phi^{(v)}_\nu - \partial_\nu \phi^{(v)}_\mu)$$

For isovector mesons the fields ϕ are replaced by the isovector $\vec{\phi}$ and the isovector $\vec{\tau}$ is sandwiched between the nucleon fields $\overline{\psi}$ and ψ. $V_{OBE}(\vec{p}',\vec{p})$ is formed by summing the Lorentz-invariant amplitudes of the various one-boson-exchange diagrams; i.e.,

$$\langle s_3 \, p_3 \, s_4 \, p_4 | V_{OBE} | s_1 \, p_1 \, s_2 \, p_2 \rangle = \sum_\alpha \begin{array}{c} ^3 \quad ^4 \\ | \!-\!\bar{\alpha}\!-\! | \\ ^1 \quad ^2 \end{array}$$

$$= \sum_{\alpha=s} \left[g^2_{(\alpha)} (\overline{u}_3 u_1)(\overline{u}_4 u_2) \frac{1}{g^s g_s - m^2_{(\alpha)}} \right]$$

$$+ \sum_{\alpha=ps} \left[-g^2_{(\alpha)} (\overline{u}_3 \gamma_5 u_1)(\overline{u}_4 \gamma_5 u_2) \frac{1}{g^s g_s - m^2_{(\alpha)}} \right] \tag{C.4}$$

$$+ \sum_{\alpha=v} \left[g^2_{(\alpha)} \, \overline{u}_3 (\gamma^\mu + i\sigma^{\mu\rho} \frac{f_{(\alpha)}}{g_{(\alpha)}} \frac{1}{2m} g_\rho) u_1 \right.$$

$$\times \overline{u}_4 (\gamma^\nu - i\sigma^{\nu\sigma} \frac{f_{(\alpha)}}{g_{(\alpha)}} \frac{1}{2m} g_\sigma) u_2$$

$$\left. \times (-g_{\mu\nu})/(g^s g_s - m^2_{(\alpha)}) \right]$$

where $q^{\Sigma} = p_4^{\Sigma} - p_3^{\Sigma} = -(p_3^{\Sigma} - p_1^{\Sigma})$

and the subscript on the spinor denotes both the spin projection and momentum.

From the theory of integral equations it is known that in order that the Born series from (C.2) converge, the equation must be of the Fredholm type; i.e., the kernel

$$K(\vec{p}', \vec{q}) = -\frac{m}{(2\pi)^3} V(\vec{p}', \vec{q}) \frac{1}{\vec{q}^2 - \vec{p}^2 - i\epsilon}$$

must satisfy the condition

$$\int d^3p' \, d^3q \; |K(\vec{p}', \vec{q})|^2 < \infty$$

This requirement is satisfied in the model through the use of form factors: $g_{(\alpha)}$ is replaced by $g_{(\alpha)} F_{(\alpha)} (q^{\mu} q_{\mu})$. The "coupling constant" is then defined as

$$g_{0(\alpha)} = g_{(\alpha)} F_{(\alpha)} (m_{\alpha}^2) \tag{C.5}$$

The exchanged mesons, their masses, coupling strengths $g_{(\alpha)}$, $g_{0(\alpha)}$, and form factors as used in the EHM model are listed in Table C.1 below.

Meson	J^P	T	$[F_{(\omega)}(g^\mu g_\mu)]^2$	Λ (MeV)	Λ_v (MeV)	$\frac{g^2}{4\pi}$	$\frac{g_0^2}{4\pi} = \frac{g^2}{4\pi}[F_{(\omega)}(m_\omega)]^2$	f/g
π	0^-	1	$\dfrac{\Lambda^2}{\Lambda^2 - g^\mu g_\mu}$	2500		14	14.2	
η	0^-	0		2500		2	2.2	
σ	0^+	0		2000		5.04	5.8	
δ	0^+	1		2500		6.12	8.4	
ρ	1^-	1	$\dfrac{\Lambda^2}{\Lambda^2 - g^\mu g_\mu}\left[\dfrac{\Lambda_v^2 - m_\omega^2}{\Lambda_v^2 - g^\mu g_\mu}\right]$	1300	2500	0.7	1.7	4.5
3	1^-	0		1300	2500	9.8	24.0	0
φ	1^-	1		1300	2500	4.9	33.2	0

Meson	Masses (MeV)
π	138.5
η	548.5
σ	500
δ	960
ρ	763
3	782.8
φ	1020

The nucleon mass was taken as 938.9 MeV.

Table D.1. Parameters of the EHM model.

Appendix D

Phase Shifts from Geometric Unitarization

The partial-wave projections, α, are defined in terms of the scattering matrix S by

$$S = 1 + 2i\alpha \qquad \text{(D.1)}$$

These are the α's of SYM $\underline{/40\underline{}7}$ divided by 2i. For uncoupled states the singlet and triplet amplitudes are α_j and α_{jj} (i.e. $\alpha_{\ell j}$ with $l = j$) respectively. For coupled states

$$\|\alpha_j\| = \begin{pmatrix} \alpha_{j-1,j} & \alpha^j \\ \alpha^j & \alpha_{j+1,j} \end{pmatrix}$$

the unitarity condition $SS^{-1} = 1$ reads

$$\mathfrak{Im}\,\alpha_j = (Re\,\alpha_j)^2 + (\mathfrak{Im}\,\alpha_j)^2$$

$$\mathfrak{Im}\,\alpha_{jj} = (Re\,\alpha_{jj})^2 + (\mathfrak{Im}\,\alpha_{jj})^2$$

$$\mathfrak{Im}\,\|\alpha_j\| = (\mathfrak{Im}\,\|\alpha_j\|)^2 + (Re\,\|\alpha_j\|)^2 \qquad \text{(D.2)}$$

or

$$\alpha_j = exp(i\,\delta_j)\,\sin\delta_j$$

$$\alpha_{jj} = exp(i\,\delta_{jj})\,\sin\delta_{jj}$$

$$\alpha_{\ell j} = (2i)^{-1}\,[\,\cos2\,\epsilon_j\,exp(2i\,\delta_{\ell j}) - 1\,] \qquad \ell = j \pm 1 \qquad \text{(D.3)}$$

$$\alpha^j = \tfrac{1}{2}\,\sin2\epsilon_j\,exp(i\,\delta_{j-1,j} + i\,\delta_{j+1,j})$$

The (real) Born amplitudes as given by the meson-pole model are denoted by B's, with the indices defined as for the α's. We unitarize by taking the model amplitude, B, as the real part of

the unitary amplitude α ; the imaginary part of α can then be obtained either from (D.2) or (D.3). Thus

$$B_j = \cos\delta_j \sin\delta_j = \tfrac{1}{2}\sin\delta_j \tag{D.4a}$$

$$B_{jj} = \tfrac{1}{2}\sin\delta_{jj} \tag{D.4b}$$

$$B_{j-1,j} = \tfrac{1}{2}\cos 2\epsilon_j \sin 2\delta_{j-1,j} \tag{D.4c}$$

$$B_{j+1,j} = \tfrac{1}{2}\cos 2\epsilon_j \sin 2\delta_{j+1,j} \tag{D.4d}$$

$$B^j = \tfrac{1}{2}\sin 2\epsilon_j \cos\Delta_j \tag{D.4e}$$

where $\Delta_j = \delta_{j-1,j} + \delta_{j+1,j}$

Obtaining the phase shifts for the coupled states requires the solution of the simultaneous non-linear equations (D.4c) to (D.4e) for $\delta_{j-1,j}$, $\delta_{j+1,j}$, and ϵ_j . We used the Newton-Raphson method for this: define

$$x = \delta_{j-1,j}$$

$$y = \delta_{j+1,j}$$

$$z = \epsilon_j$$

$$f_1(x,y,z) = \tfrac{1}{2}\cos 2z \sin 2x - B_{j-1,j}$$

$$f_2(x,y,z) = \tfrac{1}{2}\cos 2z \sin 2y - B_{j+1,j} \tag{D.5}$$

$$f_3(x,y,z) = \tfrac{1}{2}\sin 2z \cos(x+y)$$

For the zeroth approximation we take $\epsilon_j = 0$, decoupling the states:

$$B_{j-1,j} = \tfrac{1}{2}\sin 2x_0$$

$$B_{j+1,j} = \tfrac{1}{2}\sin 2y_0 \tag{D.6}$$

$$z_0 = 0$$

let (x_i, y_i, z_i) denote the zero of (D.5) after i iterations.

By the Newton-Raphson method

$$
\begin{bmatrix}
f_{1,x} & f_{1,y} & f_{1,z} \\
f_{2,x} & f_{2,y} & f_{2,z} \\
f_{3,x} & f_{3,y} & f_{3,z}
\end{bmatrix}
\begin{bmatrix}
\delta x \\
\delta y \\
\delta z
\end{bmatrix}
= -
\begin{bmatrix}
f_1 \\
f_2 \\
f_3
\end{bmatrix}
\tag{D.7}
$$

where $x_{i+1} = x_i + \delta x, \quad y_{i+1} = y_i + \delta y, \quad z_{i+1} = z_i + \delta z$

The derivative matrix on the left-hand side of (D.7) is

$$
\begin{bmatrix}
\cos 2z \cos 2x & 0 & -\sin 2z \sin 2x \\
0 & \cos 2z \cos 2y & -\sin 2z \sin 2y \\
-\frac{1}{2} \sin 2z \sin(x+y) & -\frac{1}{2} \sin 2z \sin(x+y) & \cos 2z \cos(x+y)
\end{bmatrix}
$$

Appendix E

Quark-Model Constraint on g*

The purpose of this exercise is to relate the sign of the $\Delta N \pi$ vertex to that of the $NN\pi$ vertex in the (Δ, π) diagram through the quark model.

Consider the $NN\pi$ derivative coupling:

$$\mathcal{L}_{\pi NN} = \frac{f_{\pi NN}}{m_\pi}\left[\overline{\psi}\gamma_5\gamma^i\psi\,\vec{\tau}\,\partial_i\vec{\phi} + \overline{\psi}\gamma_5\gamma^0\vec{\tau}\psi\,\partial_0\vec{\phi}\right] \qquad (E.1)$$

with

$$\gamma^i = \begin{pmatrix} 0 & \sigma^i \\ -\sigma^i & 0 \end{pmatrix} \qquad \gamma^0 = \begin{pmatrix} 1 & 0 \\ 0 & -1 \end{pmatrix}$$

$$\gamma_5 = \begin{pmatrix} 0 & 1 \\ 1 & 0 \end{pmatrix} \qquad \gamma_5\gamma^i = \begin{pmatrix} -\sigma_i & 0 \\ 0 & \sigma_i \end{pmatrix} \qquad \gamma_5\gamma^0 = \begin{pmatrix} 0 & -1 \\ 1 & 0 \end{pmatrix} \qquad (E.2)$$

Reducing non-relativistically:

$$\psi = \sqrt{\frac{E+m}{2m}}\begin{pmatrix} \chi \\ \frac{\vec{\sigma}\cdot\vec{p}}{E+m}\chi \end{pmatrix} \xrightarrow{n.r.} \begin{pmatrix} \chi \\ \frac{\vec{\sigma}\cdot\vec{p}}{2m}\chi \end{pmatrix}$$

$$\mathcal{L}_{\pi NN} \xrightarrow{n.r.} \frac{f_{\pi NN}}{m_\pi}\overline{\psi}\gamma_5\gamma^i\vec{\tau}\psi\,\partial_i\phi_\pi$$

$$= \frac{f_{\pi NN}}{m_\pi}\left(\chi^+, \; -\chi^+\frac{\vec{\sigma}\cdot\vec{p}}{2m}\right)\begin{pmatrix} -\sigma^i & 0 \\ 0 & \sigma^i \end{pmatrix}\vec{\tau}\begin{pmatrix} \chi \\ \frac{\vec{\sigma}\cdot\vec{p}}{2m} \end{pmatrix}\partial_i\vec{\phi}_\pi \quad (E.3)$$

$$\simeq -\frac{f_{\pi NN}}{m_\pi}\chi^+\sigma^i\vec{\tau}\chi\,\partial_i\vec{\phi}_\pi$$

By analogy we take the non relativistic $\overline{q}q\pi$ coupling to be

$$\mathcal{L}_{\pi qq} = -\frac{f_{\pi qq}}{m_\pi}\chi_q^+\vec{\tau}\sigma^i\chi_q\,\partial_i\vec{\phi}_\pi \qquad (E.4)$$

In particular consider matrix element of the $p\pi p$ vertex with the pion momentum $\vec{k} = \vec{p}' - \vec{p}$ along the z direction, and proton spin

140

up

$$T = -i \frac{f_{\pi NN}}{m_\pi} \chi_\uparrow^+ \tau_3 \sigma_3 \chi_\uparrow \, i k^3 = \frac{f_{\pi NN}}{m_\pi} k_z \qquad \text{(E.5)}$$

We use the labels p, n, λ for the three quarks with

$$\langle p | \tau_3 | p \rangle = 1 \, , \qquad \langle n | \tau_3 | n \rangle = -1 \, , \qquad \langle \lambda | \tau_3 | \lambda \rangle = 0 \, ,$$

and make use of the quarks structure of the proton with spin up:

$$|\text{proton} \uparrow \rangle = \frac{1}{3\sqrt{2}} \Big[2 | p\uparrow \, p\uparrow \, n\downarrow \rangle - | p\uparrow \, p\downarrow \, n\uparrow \rangle - | p\downarrow \, p\uparrow \, n\uparrow \rangle$$

$$+ 2 | p\uparrow \, n\downarrow \, p\uparrow \rangle - | p\uparrow \, n\downarrow \, p\downarrow \rangle - | p\downarrow \, n\uparrow \, p\uparrow \rangle \qquad \text{(E.6)}$$

$$+ 2 | n\downarrow \, p\uparrow \, p\uparrow \rangle - | n\uparrow \, p\uparrow \, p\downarrow \rangle - | n\uparrow \, p\downarrow \, p\uparrow \rangle \Big]$$

The matrix element in the quark model (impulse approximation with interaction given by (E.4)) is

$$T = -i \frac{f_{\pi gg}}{m_\pi} \langle \text{proton} \uparrow | \sum_{i=1}^{3} \sigma_3^{(i)} \tau_3^{(i)} | \text{proton} \uparrow \rangle \, (i k_z) \qquad \text{(E.7)}$$

Only diagonal terms contribute to (E.7); furthermore the three permutations in (E.6) contribute equally. Thus

$$T = \frac{f_{\pi gg}}{m_\pi} k_z \frac{5}{3} \qquad \text{(E.8)}$$

Comparing (E.5) and (E.8) we have

$$f_{\pi NN} = \frac{5}{3} f_{\pi gg} \qquad \text{(E.9)}$$

Now consider the $\Delta N \pi$ coupling given in (6.9). To relate g^* to $f_{\pi gg}$ we again concentrate on a vertex with simple

quark and spin structure; we choose the $\Delta^{++} p \pi^+$ vertex with

$$S_z(\Delta^{++}) = +3/2, \quad S_z(\text{proton}) = +1/2 \,.$$

Using the identity

$$A_i \, B_i = A_+ B_- + A_- B_+^* + A_3 B_3 \tag{E.10}$$

where

$$A_\pm = (A_1 \pm i A_2)/\sqrt{2}$$

$$B_\pm = (B_1 \pm i B_2)/\sqrt{2}$$

with

$$\pi_+ = -(\phi_1 - i \phi_2)/\sqrt{2} = -\phi_-$$

$$\pi_- = (\phi_1 + i \phi_2)/\sqrt{2} = \phi_+$$

we get from (6.9)

$$\mathcal{L}_{\Delta N \pi^+} = -g^* \, \overline{N}^{*\,\mu}_{(+)} \, N \, \partial_\mu \pi^+$$

where

$$\overline{N}^*_{(+)} = (\overline{N}^*_1 + i \overline{N}^*_2)/\sqrt{2}$$

$$= \frac{1}{2}\left[\begin{pmatrix} \overline{\Delta}^{++} - \overline{\Delta}^0/\sqrt{3} \\ \overline{\Delta}^+/\sqrt{3} - \overline{\Delta}^- \end{pmatrix} + \begin{pmatrix} \overline{\Delta}^{++} + \overline{\Delta}^0/\sqrt{3} \\ \overline{\Delta}^+/\sqrt{3} + \overline{\Delta}^- \end{pmatrix} \right]$$

$$= \begin{pmatrix} \overline{\Delta}^{++} \\ \overline{\Delta}^+/\sqrt{3} \end{pmatrix}$$

In particular

$$\mathcal{L}_{\Delta^{++} p \pi^+} = -g^* \, \overline{\Delta}^{++\,\mu} \, p \, \partial_\mu \pi^+ \tag{E.11}$$

The matrix element of the vertex in fig. 39_I (with the pion four momentum $= k^\mu$) is then

$$T = -g^* \, \overline{u}^\mu(p^*) \, u(p) \, (-i k_\mu) \tag{E.12}$$

For $\quad S_z = +3/2 \quad \overline{u}^\mu(p^*) = \overline{u}(\uparrow) \, \epsilon^{*\mu}(+1)$

with $\quad \vec{\epsilon}(+1) = \frac{-1}{\sqrt{2}}(1, i, 0) \quad$ and $\quad u(\uparrow) \xrightarrow{n.r.} \begin{pmatrix} \chi_\uparrow \\ \frac{\vec{\sigma} \cdot \vec{p}}{2 m_\Delta} \chi_\uparrow \end{pmatrix}$

Non-relativistically

$$T \simeq -i g^* (\vec{\varepsilon}^* \cdot \vec{k}) \left(\chi_\uparrow^+ , \ -\chi_\uparrow^+ \frac{\vec{\sigma} \cdot \vec{p}^{\,\prime}}{2 m_\Delta} \right) \begin{pmatrix} \chi_\uparrow \\ \frac{\vec{\sigma} \cdot \vec{p}}{2m} \chi_\uparrow \end{pmatrix} \qquad \text{(E.13)}$$

$$\simeq \ i g^* (k_x - i k_y)/\sqrt{2}$$

Now we compute the same amplitude in the quark model:

$$|\Delta^{++} \ S_z = +\tfrac{3}{2}\rangle = |p\uparrow \ p\uparrow \ p\uparrow \rangle \qquad \text{(E.14)}$$

$$\mathcal{L}_{\pi^+ \delta \delta} = \frac{f_{\pi \delta \delta}}{m_\pi} \chi_\delta^+ \, \tau_+ \, \vec{\sigma} \, \chi_\delta \, \vec{\nabla} \phi_{\pi^+} \qquad (\tau_+ = (\tau_1 + i \tau_2)/\sqrt{2})$$

$$T = \frac{f_{\pi \delta \delta}}{m_\pi} \ \langle \Delta^{++} \ S_z = \tfrac{3}{2} | \sum_{i=1}^{3} \tau_+^{(i)} \vec{\sigma}^{(i)} \, i \vec{k} | \, \text{proton} \uparrow \rangle \qquad \text{(E.15)}$$

Only the terms $\sqrt{2} \, \sigma_+^{(i)} \, i \, k_{(-)}$ (where $k_{(-)} = \frac{k_x - i k_y}{\sqrt{2}}$, $\sigma_+ = \frac{\sigma_x + i \sigma_y}{\sqrt{2}}$) contribute to (E.15). Therefore

$$T = i \, \frac{f_{\pi \delta \delta}}{m_\pi} \ k_{(-)} \ \langle \Delta^{++} \ S_z = +\tfrac{3}{2} | \sum_{i=1}^{3} \tau_+^{(i)} \, \sigma_+^{(i)} | \, \text{proton} \uparrow \rangle$$

$$= 2 i \, \frac{f_{\pi \delta \delta}}{m_\pi} \ k_{(-)} \ \sqrt{2} \qquad \text{(E.16)}$$

Comparing (E.13) with (E.16) we get

$$g^* = 2\sqrt{2} \, \frac{f_{\pi \delta \delta}}{m_\pi} = \frac{6}{5} \sqrt{2} \, \frac{f_{\pi NN}}{m_\pi} \qquad \text{(E.17)}$$

In the present case the two nucleon fields are on shell and the interaction (E.1) can be rewritten as

$$\mathcal{L}_{\pi NN} = -g_\pi \, \overline{\Psi} \, i \gamma_5 \Psi \, \phi_\pi \tag{E.18}$$

where $\quad g_\pi = -\dfrac{2m}{m_\pi} \, f_{\pi NN}$

(E.17) and (E.18) relate g^* to g_π :

$$g^* = -\frac{6}{5\sqrt{2}} \frac{1}{m} g_\pi \tag{E.19}$$

With $\dfrac{g_\pi}{4\pi} = 14$ (E.19) gives $\dfrac{g^*}{4\pi} \simeq 1.14 \times 10^{-5}$ MeV^{-2}, however we use the value of g^{*2} as obtained from the width of the decay $\Delta \rightarrow N + \pi$: $\dfrac{g^*}{4\pi} = 1.875 \times 10^{-5}$ MeV^{-2}.

Δ Width and the Value of g^*

In this appendix the width corresponding to the process of fig. 50 is derived from the $\Delta^{++} p \pi^+$ interaction given by

$$\mathcal{L} = g^* \bar{\Psi} \gamma^\mu \partial_\mu \phi_\pi \, ..$$

To within a phase

$$S = g^* \bar{u} u^\mu g_\mu \left[\frac{1}{V^3} \frac{m}{E} \frac{m_\Delta}{W} \frac{1}{2\omega} \right]^{\frac{1}{2}} (2\pi)^4 \delta^{(4)}(p^* - p - g) \qquad (F.1)$$

the sum over the Δ and nucleon spins are done with the closure properties:

$$\sum_{spin} u_\mu \bar{u}_\nu = \frac{1}{6 m_\Delta} (\not{p}^* + m_\Delta) \left(\frac{2}{m_\Delta^2} p_\mu^* p_\nu^* - g_{\mu\nu} \right.$$
$$\left. - \gamma_\mu \gamma_\nu - \frac{1}{m_\Delta} (\gamma_\mu p_\nu^* - \gamma_\nu p_\mu^*) \right)$$

and

$$\sum_{spin} u \bar{u} = (\not{p} + m)/2m \qquad\qquad\qquad\qquad (F.2)$$

$$\therefore \sum_{spins} \bar{u} u_\mu \bar{u}_\nu u = \frac{1}{12 \, m \, m_\Delta} tr \left[(\not{p}^* + m_\Delta) \left(\frac{2}{m_\Delta^2} p_\mu^* p_\nu^* \right. \right.$$
$$\left. \left. - g_{\mu\nu} - \gamma_\mu \gamma_\nu - \frac{1}{m_\Delta} (\gamma_\mu p_\nu^* - \gamma_\nu p_\mu^*) \right) (\not{p} + m) \right] \qquad (F.3)$$

Trace calculation:

$$tr \, \not{p}^* \left(\frac{2}{m_\Delta^2} p_\mu^* p_\nu^* - g_{\mu\nu} - \gamma_\mu \gamma_\nu \right) \not{p}$$
$$= p_\mu^* p_\nu^* \frac{8}{m_\Delta^2} p \cdot p^* - g_{\mu\nu} 8 p^* \cdot p - 4(p_\mu^* p_\nu - p_\nu^* p_\mu)$$

$$\text{tr } \not{p}^* \left(-\frac{1}{m_\Delta} (\gamma_\mu p_\nu^* - \gamma_\nu p_\mu^*) m \right) = 0$$

$$\text{tr } m_\Delta \left(\frac{2}{m_\Delta^2} p_\mu^* p_\nu^* - g_{\mu\nu} - \gamma_\mu \gamma_\nu \right) m \tag{F.4}$$

$$= p_\mu^* p_\nu^* \, 8 \frac{m}{m_\Delta} - 8 \, m \, m_\Delta \, g_{\mu\nu}$$

$$\text{tr } m_\Delta \left(-\frac{1}{m_\Delta} (\gamma_\mu p_\nu^* - \gamma_\nu p_\mu^*) \not{p} \right) = -4 \left(p_\mu p_\nu^* - p_\nu p_\mu^* \right)$$

$$\therefore \frac{1}{4} \sum_{spins} \bar{u} \, u_\mu \, \bar{u}_\nu u = \frac{2}{12 \, m \, m_\Delta} \left(\frac{p \cdot p^*}{m_\Delta} + m \right) \left(\frac{p_\nu^* p_\nu}{m_\Delta} - g_{\mu\nu} m_\Delta \right) \tag{F.5}$$

The factor ¼ in (F.5) comes from averaging over the initial four
Δ spin states.

Decay probability $= \dfrac{1}{4} \displaystyle\sum_{spins} \sum_{\vec{q}, \vec{p}} S S^\dagger$

$$= \sum_{\vec{q}, \vec{p}} g^* \frac{m m_\Delta}{V^3 E W 2\omega} (2\pi)^4 \delta^{(4)}(p^* - p - q) VT$$

$$\times 2 \left(\frac{p \cdot p^*}{m_\Delta} + m \right) \left[\frac{(p^* q)^2}{m_\Delta} - q^2 m_\Delta \right] \frac{1}{12 \, m \, m_\Delta}$$

Replace $\displaystyle\sum_{\vec{q}, \vec{p}} \longrightarrow \frac{V^2}{(2\pi)^6} d^3q \, d^3p$

Decay rate $= \Gamma = \dfrac{V^2}{(2\pi)^6} g^{*2} \dfrac{1}{V^3} \displaystyle\int d^3q \, d^3p \, \frac{m m_\Delta}{E W 2\omega} \frac{(2\pi)^4 \delta^{(4)}(p^* - p - q)}{12 \, m \, m_\Delta}$

$$\times V 2 \left(\frac{p \cdot p^*}{m_\Delta} + m \right) \left[\frac{(p^* q)^2}{m} - q^2 m_\Delta \right]$$

In the rest frame of the Δ

$$W = m_\Delta, \qquad \vec{p} = -\vec{q}, \qquad \vec{p}^* = 0 \quad \text{and}$$

$$\Gamma = \frac{g^{*2}}{4\pi} \frac{1}{12\pi} \int d^3q \frac{1}{E\omega} \delta(m_\Delta - E - \omega)(E+m)\vec{q}^{\,2}$$

Define $\qquad E_f = E + \omega$

$$\therefore \quad \frac{dE_f}{dq} = \frac{d}{dq}\left(\sqrt{q^2+m^2} + \sqrt{q^2+m_\pi^2}\right)$$

$$= \frac{q}{E} + \frac{q}{\omega}$$

and

$$q\,dq = \frac{E\omega}{E_f}\,dE_f$$

$$\Gamma = \frac{g^{*2}}{4\pi} \frac{1}{12\pi} 4\pi \int q \frac{E\omega}{E_f} dE_f \frac{1}{E\omega} \delta(m_\Delta - E_f)(E+m)q^2$$

$$= \frac{g^{*2}}{4\pi} \frac{E+m}{3\,m_\Delta} |\vec{p}|^3 \tag{F.6}$$

From $\qquad m_\Delta - (\vec{p}^{\,2}+m^2)^{\frac{1}{2}} = (\vec{q}^{\,2}+m_\pi^2)^{\frac{1}{2}}$

we get $\qquad E = (m_\Delta^2 + m^2 - m_\pi^2)/(2m_\Delta)$

With $\qquad \Gamma = 114.3 \text{ MeV } [62]$, $m_\Delta = 1232 \text{ MeV}$, $m = 938.9 \text{ MeV}$,

and $\qquad m_\pi = 137 \text{ MeV}$

we get $\qquad \dfrac{g^*}{4\pi} = 18.75 \times 10^{-6} \text{ MeV}^{-2}$, $\tag{F.7}$

the value used in our calculation.

Appendix G

Quark-Model Constraint on C

We write the non-relativistic amplitude for the process of fig. 40_{I} with the interaction $\mathcal{L}_{I} = -e\sqrt{\frac{2}{3}} C \bar{\Psi} \gamma^{\nu} i \gamma_5 \Psi^{\mu} F_{\mu\nu}$ and in the quark model. For simplicity we assume the Δ to have spin $S_z = +\frac{3}{2}$ and the proton to have spin $+\frac{1}{2}$. From (6.14) (T_I) we have (with $\vec{\epsilon}(+1) = -\frac{1}{\sqrt{2}} (1, i, 0) = -\epsilon_+$)

$$T = eC\sqrt{\frac{2}{3}} \, \bar{u}_{\uparrow}(p) \left(\epsilon_{(r)\nu} k_{\mu} - k_{\nu} \epsilon_{(r)\mu} \right) \gamma^{\nu} \gamma_5 \, u_{\uparrow}(p^*) \, \epsilon^{\mu}(+1)$$

$$\simeq -eC\sqrt{\frac{2}{3}} \, \bar{u}_{\uparrow}(p) \left(\vec{\epsilon}_{(r)} k_+ - \vec{k} \, \epsilon_{(r)+} \right) \begin{pmatrix} \vec{\sigma} & 0 \\ 0 & -\vec{\sigma} \end{pmatrix} u_{\uparrow}(p^*)$$

$$= -eC\sqrt{\frac{2}{3}} \, \chi_{\uparrow}^{\dagger} \left(\vec{\epsilon}_{(r)} k_+ - \vec{k} \, \epsilon_{(r)+} \right) \cdot \vec{\sigma} \, \chi_{\uparrow} \qquad (G.1)$$

$$= -eC\sqrt{\frac{2}{3}} \left(\epsilon_{(r)z} k_+ - k_z \, \epsilon_{(r)+} \right)$$

Now we calculate the amplitude from the quark model.

$$| \Delta^+ \, S_z = +3/2 \rangle = \frac{1}{\sqrt{3}} \left[\, | p\uparrow \, p\uparrow \, n\uparrow \rangle \right.$$

$$\left. + | p\uparrow \, n\uparrow \, p\uparrow \rangle + | n\uparrow \, p\uparrow \, p\uparrow \rangle \right] \qquad (G.2)$$

$| \text{proton} \uparrow \rangle$ is given in (E.6).

With the quark-γ interaction

$$\mathcal{L}_{qq\gamma} = -e_q \, \mu_P \, \chi^{\dagger} i \vec{\sigma} \cdot (\vec{k} \times \vec{\epsilon}_{(r)}) \chi \qquad (G.3)$$

where $e_q = \frac{2}{3}$ for the p quark

$\qquad -\frac{1}{3}$ for the n quark

148

and $\mu_P = 2.79 \dfrac{e}{2m}$

The matrix element corresponding to fig. 40_I is

$$T = -i\mu_P \sum_i \langle \text{proton} \uparrow | e_i \, \vec{\sigma} \cdot (\vec{k} \times \vec{\epsilon}_{(\gamma)}) | \Delta^+ \, s_z = +\tfrac{3}{2} \rangle$$

$$= -i\mu_P \sum_i \langle \text{proton} \uparrow | e_i \, \sigma_- \, (\vec{k} \times \vec{\epsilon}_{(\gamma)})_+ | \Delta^+ \, s_z = +\tfrac{3}{2} \rangle$$

$$= \frac{2i}{\sqrt{3}} \mu_P \, (\vec{k} \times \vec{\epsilon}_{(\gamma)})_+$$

$$= -\sqrt{\frac{2}{3}} \mu_P \left[(\vec{k} \times \vec{\epsilon}_{(\gamma)})_y - i (\vec{k} \times \vec{\epsilon}_{(\gamma)})_x \right]$$

$$= -\sqrt{\frac{2}{3}} \mu_P \left[k_z \epsilon_{(\gamma)x} - k_x \epsilon_{(\gamma)z} - i k_y \epsilon_{(\gamma)z} + i k_z \epsilon_{(\gamma)y} \right]$$

$$= \frac{2}{\sqrt{3}} \mu_P \left[\epsilon_{(\gamma)z} k_+ - k_z \epsilon_{(\gamma)+} \right] \qquad (G.4)$$

Comparing (G.4) with (G.1) we have

$$C \simeq -\frac{2.79}{2m} \sqrt{2}$$

$$= -2.10 \times 10^{-3} \, \text{MeV}^{-1} \qquad (G.5)$$

This compares with $C = -2.31 \times 10^{-3}$ MeV^{-1} – the value used in our calculation.